# RESOURCE RECOVERY AND VALUE-ADDED PRODUCTS FROM AGRICULTURAL WASTE

Thesis

Submitted in partial fulfilment of the requirements for the degree of

DOCTOR OF PHILOSOPHY

By

**ADHIRASHREE V**

(Roll. No. 177070CV001)



**DEPARTMENT OF CIVIL ENGINEERING**
**NATIONAL INSTITUTE OF TECHNOLOGY KARNATAKA,**
**SURATHKAL, MANGALORE-575025**
**JANUARY 2022**

# RESOURCE RECOVERY AND VALUE-ADDED PRODUCTS FROM AGRICULTURAL WASTE

Thesis

Submitted in partial fulfilment of the requirements for the degree of

DOCTOR OF PHILOSOPHY

By

**ADHIRASHREE V**

(Roll. No. 177070CV001)

Under the guidance of

**Dr. ARUN KUMAR THALLA**



**DEPARTMENT OF CIVIL ENGINEERING**
**NATIONAL INSTITUTE OF TECHNOLOGY KARNATAKA,**
**SURATHKAL, MANGALORE-575025**
**JANUARY 2022**

# D E C L A R A T I O N

I hereby *declare* that the Thesis entitled "**RESOURCE RECOVERY AND VALUE-ADDED PRODUCTS FROM AGRICULTURAL WASTE",** which is being submitted to the **National Institute of Technology Karnataka**, **Surathkal,** in partial fulfilment of the requirements for the award of the **Degree of Doctor of Philosophy** in the **Department of Civil Engineering** is *a bonafide report of the research work carried out by me*. The material contained in this Thesis has not been submitted to any University or Institution for the award of any degree.

ADHIRASHREE V

(177070CV001)

Department of Civil Engineering

Place: NITK-Surathkal

Date: 04-01-2022

# CERTIFICATE

This is to *certify* that the Research Thesis entitled "**Resource recovery and value-added products from agricultural waste**" submitted by **Ms. ADHIRSHREE V (177070CV001)** as the record of the research work carried out by her, is *accepted as the Research Thesis submission* in partial fulfilment of the requirements for the award of degree of **Doctor of Philosophy**.
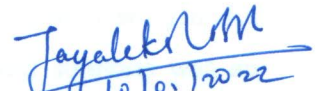
10|01|2022

**Dr. Arun Kumar Thalla**

Research guide

Department of Civil Engineering

(Signature with date and seal)

10|01|2022

**Prof. B.R Jayalekshmi**

Chairperson-DRPC

(Signature with date and seal)

Chairman (DRPC)
Department of Civil Engineering
National Institute of Technology Karnataka, Surathkal
Mangalore - 575 025, Karnataka, INDIA

# ACKNOWLEDGEMENT

**NITK Surathkal**                                                                                    **Adhirashree. V**

**ABSTRACT**

Lignocellulosic biomass resources such as agri-wastes are utilized as suitable feedstock to produce bioenergy and value-added products. In the present study, the Arecanut husk (AH) (*Areca catechu*) was selected as the feedstock to recover and produce value-added products. The study was carried out in three phases, (i) evaluation and ranking of various pretreatments methods using *multiple attribute decision-making* (MADM) approach, (ii) pretreatment and co-digestion of AH for biogas yield, and (iii) synthesis of AH derived lignin-carbon material for oil-water separation.

In phase I, the objective is to evaluate and rank different pretreatment methods and select the best pretreatment method using MADM approaches to facilitate the increased biogas yield. The evaluation was done using *Technique for Order Preference by Similarity to Ideal Solution* (TOPSIS) and integrated *Design of Experiments* (DoE) - TOPSIS. Seven alternatives with five relevant attributes were adopted for this study. Based on the above decision-making framework, the alkaline pretreatment (NaOH (8%)) option was ranked first, followed by $Ca(OH)_2$ and $NH_3.H_2O$ (10%) pretreatment as second and third options. The integrated DoE - TOPSIS method has reduced the uncertainty in results by considering different weights and replications. The model portrayed the best pretreatment method employed in anaerobic digestion; thus, minimizing the experiments done during the downstream pretreatment process aided anaerobic digestion.

Phase II of the study aims to evaluate the reduction of the recalcitrance of the AH by two approaches, (i) applying various pretreatment methods to access the cellulosic content and (ii) co-digesting it with food waste for the biogas production. The study evaluates the feasibility of utilizing chemically pretreated AH for biogas production. The effects of various pretreatment methods on the material solubilization to enhance biogas production from AH were checked. The AH was pretreated by four methods viz., acidic ($H_2SO_4$), alkaline (NaOH), oxidative ($H_2O_2$), and organosolv (ethanol in 1% $H_2SO_4$). The dosing of chemicals in acidic, alkaline, and oxidative pretreatments were 2, 4, 6, 8, and 10% (w/v), whereas, in organosolv, the dosage was varied from 25%, 50%, 75%, and 100% (v) for the batch hydrolysis. The batch hydrolysis trials were conducted at two different temperatures, i.e., 25ºC and 90ºC, and solids/liquid ratio of 1:10 ratio for 24 hours. The obtained experimental data from the

solubilization study were analyzed using the TOPSIS technique, which showed that alkaline pretreatment at a temperature of 90ºC had favoured the material solubilization among the four pretreatment methods. The pretreated AH was carried further for anaerobic digestion maintained at mesophilic condition. A maximum biogas yield of 683.89mL/gVS was obtained with 2.3 times more when compared with raw AH. Four kinetic models viz., First-order exponential, Logistic, Transference function, and Modified Gompertz model, were used to fit the experimental cumulative biogas production data. The Modified Gompertz model and logistic model (correlation coefficient > 0.99) were obtained as best fit to the cumulative biogas curve. The overall process performance is represented by the kinetic parameters obtained from these models. Furthermore, a multiple linear regression equation for the biodegradability index (BI) is formulated as a technical tool to predetermine biomethane production. It is depicted as a function of biomass compositions (cellulose, hemicellulose, and lignin) with a high correlation (> 0.95). The suitability of AH as the co-substrate with food waste (FW) for biogas production was examined in this research. The substrate mix ratio (AH: FW) was varied as 0:1, 1:3, 1:1, 3:1 and 1:0 in terms of volatile solids (VS) for a batch mode enclosed reactor (1L) at mesophilic (35ºC) condition for 34 days. The 1:1 mix ratio, which yielded the highest biogas (321.12mL/gVS), is fixed for further experiment for optimizing the S/I ratio.

The phase III lignin extracted from AH was used as an additive in lignin-carbon foam synthesis as a potential adsorbent for the oil-water separation. The lignin yield from the AH increased as the husk fibre size reduced. The extracted lignin and lignin-carbon foam were characterized by morphological, structural, compositional, and thermal degradation examinations. The synthesized carbon foam exhibited ultralight weight (density=0.0294 g/cm3), excellent hydrophobicity (water contact angle from 110°~132°), mesoporous structure (3D cell-like), good fire-retarding capacity and thermally stability due to lignin addition. The foam showed an excellent sorption capacity for different oils, and the highest sorption was observed for diesel oil (7842.71mg/g). The optimization of contact time, carbon foam dosage, and initial oil concentration were done for the diesel oil sorption. The isotherm study and kinetic model evaluation were done for the diesel adsorption on the lignin-carbon foam. Temkin model was found the best fit for the adsorption isotherm. The adsorption kinetics of the lignin-carbon foam

for diesel oil was best described by pseudo-second-order kinetics. The thermodynamic parameters showed that the adsorption was endothermic and spontaneous ($\Delta H°=+4926.46$ J/mol and $\Delta S°= 25.249$ J/mol/K). The proposed mechanism depicts that the adsorption primarily influenced H-bonding and n-$\pi$ interactions. The enduring adsorption of oil into the lignin-carbon foam within few seconds shows the material oleophilicity and confirms their application prospect in oil spill clean-ups.

**Keywords:** *Decision making; Arecanut husk; Pretreatment; Co-digestion; Biogas potential; Biodegradability index; Lignin-Carbon foam; Oil-water separation*

# CONTENTS

# LIST OF TABLES

# LIST OF FIGURES

# NOMENCLATURE

| | |
|---|---|
| AD | Anaerobic Digestion |
| AH | Arecanut Husk |
| AHP | Analytical Hierarchical Process |
| ANOVA | Analysis of variance |
| BET | Brunauer–Emmett–Teller |
| BI | Biodegradability Index |
| BJH | Barrett-Joyner-Halenda |
| BMP | Biomethane potential |
| BT | Biogas technology |
| CC | Cellulose Content |
| CI | Consistency Index |
| C/N | Carbon/Nitrogen |
| CNT | Carbon nanotube |
| CP | Compromise programming |
| CR | Consistency Ratio |
| COD | Chemical oxygen demand |
| DM | Decision matrix |
| DoE | Design of experiments |
| DTA | Differential Thermal Analysis |
| EDAX | Energy dispersive x-ray |
| ELECTRE | Elimination and Choice Translation Reality |
| FESEM | Field emission scanning electron microscope |
| FOE | First Order Exponential |
| FTIR | Fourier transform-infrared spectra |
| FW | Food waste |
| GC | Gas Chromatography |
| GHG | Greenhouse gas |
| GP | Goal programming |
| HC | Hemicellulose Content |
| HHV | High heating value |

| HRT | Hydraulic retention time |
| LC | Lignin Content |
| LCF | Lignin carbon foam |
| LFM | Logistic Function Model |
| LPU | Lignin-polyurethane |
| LS | Lignin sample |
| MADM | Multi-attribute decision-making |
| MAUT | Multiple Attribute Utility Theory |
| MCDM | Multi-Criteria Decision Making |
| NDM | Normalized Decision Matrix |
| NMR | Nuclear Magnetic Resonance |
| NSM | Negative Separation Measure |
| ODA | Octadecyl Amine |
| OFMSW | Organic Fraction of Municipal Solid Waste |
| PROMETHEE | Preference Ranking Organization Method for Enrichment Evaluation |
| PSM | Positive Separation Measure |
| rGO | Reduced Graphene Oxide |
| RSS | Residual Sum of Squares |
| SAW | Simple Additive Weight |
| sCOD | Soluble Chemical Oxygen Demand |
| SEM | Scanning Electron Microscopy |
| SMP | Specific Methane Potential |
| SS-AD | Solid-state- Anaerobic digestion |
| TAPPI | Technical Association of Paper and Pulp Industry |
| TC | Total Carbon |
| TCD | Thermal Conductivity Detector |
| TGA | Thermogravimetric Analysis |
| TKN | Total Kjeldahl Nitrogen |
| TMP | Theoretical Methane Potential |
| TOPSIS | Technique for Order Preference by Similarity to Ideal Solution |

| TPC | Total Phenolic Content |
| TRS | Total reduced sugars |
| UASBR | Up-flow Aerobic Sequential Batch Reactor |
| UV | Ultra-violet |
| VFA | Volatile Fatty Acids |
| VS | Volatile Solids |
| WCA | Water Contact Angle |
| WNM | Weighted Normalized Decision matrix |
| WPM | Weighted Product Method |
| XRD | X-Ray Diffractometer |

# CHAPTER 1

# INTRODUCTION

## 1.1 Background

Major global problems in the 21$^{st}$ century include the energy crisis, environmental pollution, and solid waste generation. The ever-increasing human population and the industrial revolution have exposed a ravenous appetite for fossil fuels. Thus, an alternative solution for the existing depleting energy source is becoming necessary to tackle the future energy crisis. It is also challenging that the alternative energy source should be renewable and eco-friendly. Similarly, oil pollution is gaining more attention as they pose a significant risk to the environment. A significant contribution to oil pollution includes the accidental release of the oil either due to oil spillage or the release of wastewater from petroleum industries/refineries. Onshore activities such as household and industrial activities generating oily wastewater, oil reception from the oil terminals, and docked oil carrying ship cleaning also cause oil pollution.

## 1.2 Energy supply and demand

A rapid growth in the global populace has led to the rapid consumption of fossil fuel resources, thereby generating ample waste that destroys the environment day by day. Continuous emissions of $CO_2$, $CH_4$ and other greenhouse gases (GHG) from fossil fuel burning has led to the environmental crisis worldwide. A substitute for the conventional energy source is becoming necessary because of a decline in existing fossil fuel reserves, higher energy demand, and environmental concerns. According to the British Petroleum Company (2020), the primary energy consumption growth averaged 1.3% in 2019, less than half the growth rate in 2018 (2.8%). Carbon emissions increased at a slower pace in 2019 than the previous year, when primary energy demand fell, and renewables and natural gas replaced coal in the energy supply. Renewables contribute about 36% to the increase in energy demand in 2020 (Figure 1.1). The entire world today is focusing on switching its total electricity generation to renewable. This global inclination is owing to the utilization of clean, alternate and reusable energy sources. It is essential to explore many other sustainable energy sources. For a developing nation like India, the energy crisis, the severity of global warming, air pollution leading to serious health issues,

and fluctuating conventional fuel prices have promoted new technologies in renewable energy sources.
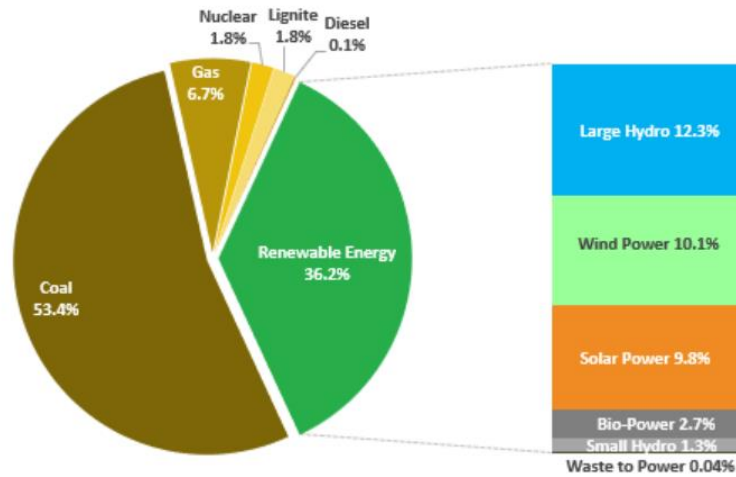


**Figure 1.1 Cumulative installed power capacity in the energy mix in India as of 31 March 2020 (Central electricity authority 2020)**

Renewable energy sources include solar, wind, hydroelectric, tidal, biofuels, and others at the transition mode for a sustainable and low carbon-intensive energy system. In this context, an increase of 5% in biofuel production in a global aspect has been estimated in the year 2019. Biomass energy was used in two forms; 1) traditional uses and 2) modern uses. The burning of biomass to fire for heating and cooking belongs to traditional uses, whereas bioethanol, biogas, and other biofuels from biomass belong to everyday use. Ethanol, biogas, biodiesel, and electricity produced by renewable energy sources are the commercially available renewable vehicle fuels. Biogas is a green energy supply that can be upgraded to be used as an automotive fuel, electricity and heat generation. Many industrial processes follow waste to the energy concept to produce biomethane to tackle waste disposal problems. Biomass energy consumption is in practice in India since ancient time. Biogas plants are being motivated by the Indian Govt. They produce no smoke, i.e., pollution-free. Many subsidies are provided for the establishment of the biogas plant (Kumar et al. 2015a). Lignocellulosic biomass, mainly agricultural residues, energy crops and other municipal wastes, can be utilized as a substrate for the most extensive conversion using the anaerobic digestion process (Liew

et al. 2011). Moreover, its ample availability in low cost and renewable nature accounts for these wastes as a potential raw material for energy generation.

## 1.3 Agri-waste for resource recovery

Lignocellulosic biomass is widely available all over the world. Biomass is a renewable energy source that contains a complex mix of carbon, nitrogen, hydrogen and oxygen. Biomass of this content is obtained from living or dead plants, a by-product of crop production, wood and agri-based industry. Lignocellulosic materials suitable for anaerobic digestion can be classified as either cultivated feedstocks, in which the plant is solely devoted to energy production or lignocelluloses, which are formed as residuals. The residuals have the advantage of not competing with food and feed demand for land. Since India has such a large agricultural land area, it produces much residue. Because of the residue content, biomass qualifies to be a potential feedstock for energy production (Prasad et al. 2007).

Agricultural residue refers to all organic materials produced as a by-product of the processing harvesting of crops. There are two types of agricultural residues: primary and secondary residues. The farm-based or primary residue is collected in the field at the time of yield, while the manufacturing-based or secondary residue is assembled during manufacturing. Rice straw, sugar cane tops, and other primary residues are primary residues, while rice husk and bagasse are secondary. Animal feed, fertilizers, and other products are made from primary residues. As a result, its energy application potential is limited.

On the other hand, secondary residues are abundant at the yielding site and can be restricted as an energy source (Astiaso et al. 2015). The significant components of lignocelluloses are cellulose, hemicelluloses, and lignin. In lignocellulosic plants, these polymers have distinct functions and chemistry. After judging biomass potential, technology also implemented the biological and thermochemical conversion to produce fuel gases. These fuel gases can be used for power generation. These carbohydrate-rich materials can be used for anaerobic digestion, and biomass-based power generation is now considered on the rising trend.

## 1.4 Arecanut husk (AH): A potential Agri-waste

Areca tends to be a promising material among all lignocellulosic fibres because of its variety, perenniality, and low cost. Areca is a member of the Arecaceae family and is thought to have originated in Malaysia or the Philippines. It can be found in most of the tropical Pacific, Asia, and East Africa. Arecanut (Figure 1.2) cultivation is growing on a large scale in India, especially in the southern part of the country, to achieve self-sufficiency in paint, medicine, and other value-added products (Nagaraja et al. 2014; Sadasivuni et al. 2016). The kernel of an arecanut comes from the fruit of the areca palm tree, and India harvests over 0.833 million tonnes of the fruit per year. The amount of AH collected from an arecanut garden is approximately 5.5 - 6 metric tonnes/hectare/year, which poses a significant disposal challenge (Ministry of Agriculture & Farmers Welfare 2019). The fruit's husk is cut, and there is no other conventional use for it. AH accounts for 60-80 percent of the fresh fruit's overall weight and volume. It is also an inconvenience to the producer/processor as it is left in piles to dry. AH is a waste product mainly used as a source of energy to produce areca nuts. Areca husk in the plantation that goes unnoticed produces a foul odour and other decay-related problems. Due to combustion, fire, termite attack, and the spread of pests and diseases, direct dumping of these wastes causes environmental problems. Pollution of the air and water is caused by improper treatment and disposal of organic wastes. Burning causes a wide range of environmental issues, including carbon deposits and global warming. The phenols from heaped leaf wastes can leach into the soil during the rainy season, resulting in soil pollution.
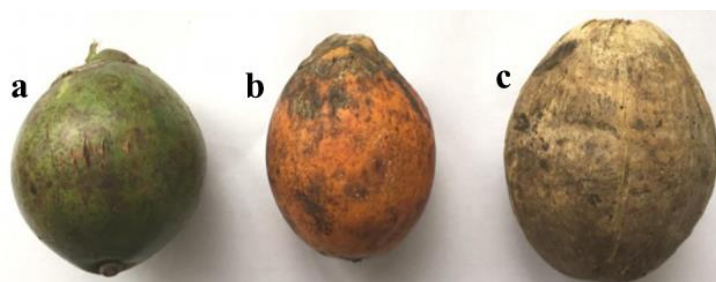


**Figure 1.2 Digital images of (a) unripe arecanut, (b) ripe arecanut and (c) dried arecanut**

AH comprises cellulose, hemicelluloses, lignin, and extractives and is fibrous (hard and soft fibres). Hemicelluloses and lignin are amorphous, whereas cellulose has many

crystalline regions (Julie Chandra et al. 2016). Carbohydrate components fermentable after hydrolysis, such as cellulose and hemicellulose, make them a suitable feedstock for biofuels. Biodegradation by enzymes and microbes is difficult for lignocellulosic biomass because of its structural and chemical properties.

## 1.5 Oil pollution

Rapid industrial development results in emissions and other environmental threats. A significant problem faced by the various stages in the oil production and transportation sector is the oil spillage/leakage. Moreover, the oil spill in aqueous environments is a catastrophic scale problem that has grabbed attention from the scientific community in the last decade. Furthermore, spillage of oil from tankers during their transit, such as the Exxon Valdex in 1987 (11 million gallons) and the Deep Horizon in 2010 (4.9 million barrels), were listed as the worst environmental disasters (Brody et al. 2012; Carson et al. 2003). Petroleum/oil pollution is a common ecological threat that has negative consequences for all marine living species. It directly impacts sea animals, but it also poses a threat to human health, food, protection, and the environment. With the expansion of petroleum operations, the value of oil emissions problems grows in lockstep (Broje and Keller 2006). This is because oil emissions can come from various causes, including oil leaks from onshore infrastructure and oil tanker spills during transportation. In a marine climate, leaked oil is exposed to the weathering process, which causes the oil to scatter and move on the sea's surface due to wind and currents. Temperature, salinity, and waves all contribute to faster oil dispersion and weathering. The oil can undergo a variety of chemical and physical changes as a result of this movement (Sarbatly et al. 2016).

Booms, skimming, and burning the oil on the water's surface are some of the current strategies for handling oil leaks (Figure 1.3). These methods are expensive in terms of time and resources, and they pollute the environment while using much energy to extract the oil. Owing to the ability for oil to scatter in seawater, the use of booms and the skimming process may not be possible offshore where turbulent conditions remain. Burning the oil is the most cost-effective way of getting rid of it, but the longer it takes to burn the oil will allow it to disperse depending on the wind direction, and

burning the oil emits a lot of $CO_2$. As a result, developing materials that can effectively remove oil from contaminated seawater and commercial and domestic wastewater is crucial. In general, there are three methods of isolation of oil or water from an oil/water mixture: water removal, oil removal, and controllable separation of oil or water.
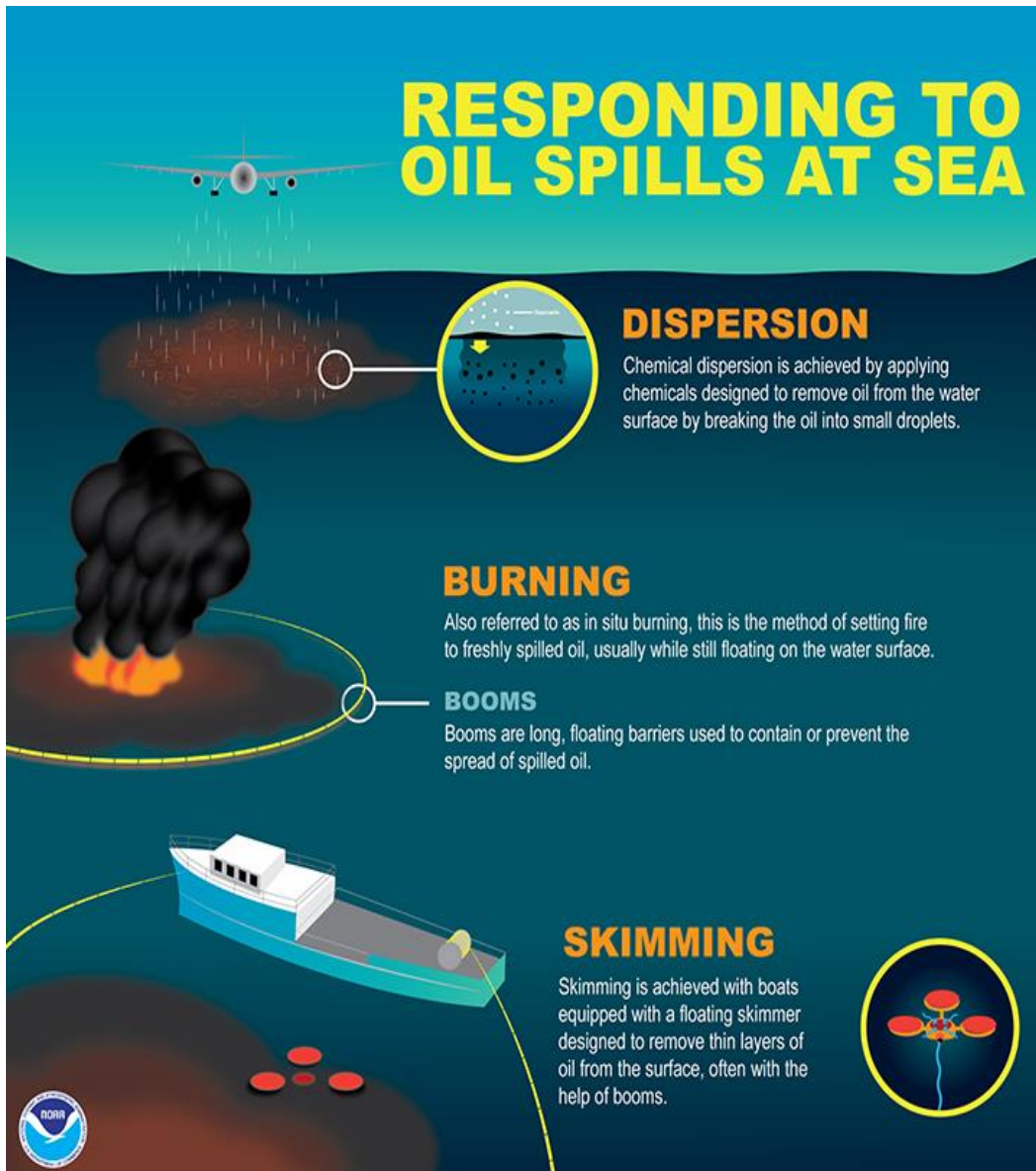


**Figure 1.3 Traditional method of oil spill clean-up**

(*https://response.restoration.noaa.gov*)

## 1.6 Oil spill treatment methods

Physical/mechanical, chemical, and biological approaches are used to handle oil spills. Booms, which are rigid floating structures that block the oil slick from moving, are one example of physical/mechanical solutions. The use of high-temperature booms allows for in-situ oil burning. Skimmers are floating and emulsified oil removal systems that may be fixed or mobile. For improved oil recovery, hydrophobic meshes that repel water but allow oil to move through can be used in skimmers. Dispersants sprayed on the spilled oil to break it into tiny droplets are one kind of chemical process.

Furthermore, sorbent materials can also be used to clean up small-scale oil leaks. (Broje and Keller 2006; Zhang et al. 2020). The incorporation of microbes, nutrients, and oxygen to promote bacterial growth and, as a result, biodegradation of the spilled oil, are examples of biological approaches (Azubuike et al. 2016).

## 1.7 Framework of thesis

The thesis includes a systematic study carried out concerning the above objectives. A brief skeletal structure of the thesis is given below.

**Chapter 1** gives a general introduction and discusses the objectives and outline of the thesis.

**Chapter 2** presents the literature reviews on sources of AH, decision-making modelling, recent advancements in anaerobic digestion (AD), and materials used for oil-water separation.

**Chapter 3** depicts the decision-making modelling for selecting the best pretreatment method for biogas production with an illustrative example.

**Chapter 4** presents the materials and methods used for the experimental studies on anaerobic digestion and oil-water separation.

**Chapter 5** describes the results and discussion on

      (a) anaerobic digestion of pretreated AH with due emphasis on its biomethane potential,

      (b) the effect of substrate mix ratio in batch mode anaerobic co-digester for biogas production

(c) extraction of lignin from AH and to synthesis a novel lignin-based carbon material for oil-water separation.

**Chapter 6** outlines the conclusions obtained and possible future scope.

## CHAPTER 2

## LITERATURE REVIEW

A review of previous studies helps analyze theoretical and methodological problems significant for the research potentiality and consistency. This chapter aims to examine the relevant research on the areas and to relate to this thesis.

### 2.1 General

Nowadays, conventional fossil fuels are replaced by renewable energy sources due to several drawbacks such as emissions that cause global warming, fuel depletion, and other severe environmental impacts. In response to the rise in global energy demand, Biogas Technology (BT) has widely attracted researchers' attention abided by green energy sources. Lignocellulosic biomass, mainly agricultural residues, energy crops, and other municipal wastes, can be utilized as a substrate for the most effective energy conversion using the anaerobic digestion process (Liew et al. 2011). Moreover, its renewability, low cost and ample availability account for these wastes to be a potential raw material for energy generation.

### 2.2 Fundamentals of anaerobic digestion (AD)

Anaerobic Digestion (AD) process decreases overall waste mass, creates solid or liquid fertilizer, and produces fuel (Figure 2.1). It is the breakdown of the organic matter to produce biogas with a diverse group of microorganisms. Biogas has a composition of methane (55–65%), carbon dioxide (35–45%), $CO_2$, and traces of other gases. The microbial consortium carries out different activity from the hydrolysis phase to the methanogenesis phase during the biogas conversion. Anaerobic digestion completes in a series of four metabolic phases; (I) hydrolysis, (II) acidogenesis, (III) acetogenesis, and (IV) methanogenesis. In phase I, the complex organic matter disintegrates into simpler monomers by hydrolysis and microorganism starts their microbial activity after this stage. In phase II, Volatile Fatty Acids (VFA) was formed from the monomer units by fermentative bacteria called the acidogenesis stage. Later, in phase III of Acetogenesis, VFA's are converted to acetic acid, $H_2$, and $CO_2$ by acetogens. Finally, in phase IV of the methanogenesis stage, conversion to methane and $CO_2$ takes place

by methanogens. This method scores the best option for all other environmental balance methods (Vasco-correa et al. 2018).
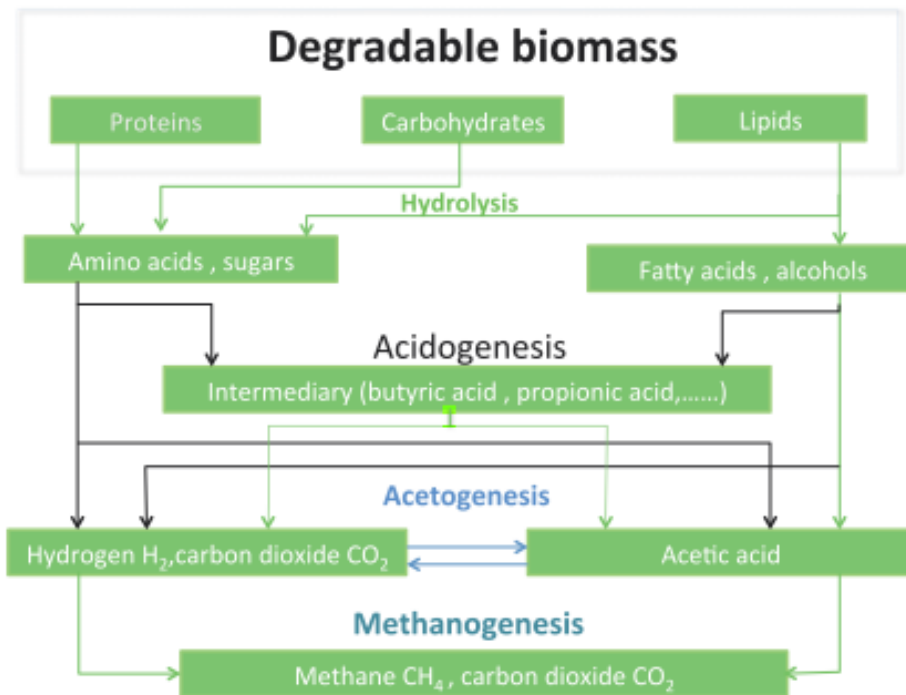


**Figure 2.1 Schematic diagram of anaerobic digestion process (Li et al. 2014)**

## 2.2.1 Steps involved in AD

### 2.2.1.1 Hydrolysis

The first phase of anaerobic digestion is hydrolysis. Macromolecules like polysaccharides, proteins, and fats are converted into monomers like carbohydrates, amino acids, and fatty acids during this process (Sayara and Sánchez 2019). Extracellular hydrolytic enzymes are responsible for this since they use water to cut the polymer covalent bonds. Cellulases, hemicellulase, amylases, lipases, and proteases are examples of hydrolytic enzymes involved in the process. Exoenzyme complexes, also called cellulosomes, are found in many cellulose-degrading species. These complexes bind to the cellular wall and the substrate simultaneously, allowing for more efficient degradation (Misi and Forster 2001). Complex materials, such as lignocelluloses, can take weeks to hydrolyze, and the degradation is also incomplete. As a result, the rate-

limiting step is hydrolysis, while the rate-limiting step for readily accessible substrates is Methanogenesis (Gonzalez-estrella et al. 2017).

### 2.2.1.2 Acidogenesis

Fermentative bacteria degrade the monomers formed in the hydrolysis process into short-chain organic acids with 1 to 5 carbons (valeric acid, butyric acid, propionic acid, acetic acid, and formic acid), ammonia, alcohols, $H_2$, and $CO_2$ in the second phase. The significant compounds produced by fermentative bacteria in a stable phase with a low partial pressure of hydrogen are acetate, carbon dioxide, and hydrogen. More intermediates, such as volatile fatty acids and alcohols, are formed when the partial pressure of hydrogen is high (Appressi 2014).

### 2.2.1.3 Acetogenesis

The methanogens will use some of the degradation products from the acidogenesis process directly. However, in the acetogenic process, fatty acids with more than 2 C atoms, alcohols with more than 1 C atom, and branched chained are converted to fatty acids. Aromatic fatty acids are further degraded into acetic acid, hydrogen, and carbon dioxide. The acetogenic microorganisms are necessary $H_2$ producers, and they require a low partial hydrogen pressure for the degradation to proceed thermodynamically. As a result, acetogens coexist with hydrogen-consuming methanogens, ensuring that the partial hydrogen pressure remains low enough for acetogenic microorganisms to develop (Mata-alvarez et al. 2011). If hydrogen concentrations are too high, concentrations of butyric, caprionic, propionic, and valeric acids and ethanol increase, making methanogens poisonous. Homoacetogenic microorganisms reduce hydrogen and carbon dioxide into acetic acid parallel with acetic acid synthesis from short-chain organic acids (López González et al. 2013).

### 2.2.1.4 Methanogenesis

Methanogenesis is the final phase of the anaerobic digestion process, and the methanogenic microorganisms operate in an anaerobic environment. Methanogens, which belong to the archaea community, are different from those in the anaerobic reactor. As it comes to environmental threats in the reactor, such as pH or toxic

chemicals like heavy metals or various toxic organic materials, archaea are more vulnerable than bacteria. Methanogens produce methane mostly from acetate, carbon dioxide, and hydrogen and methylamines, alcohols, and formate. Around 70% of methane supply comes from acetate, with the remaining 30% coming from hydrogen and carbon dioxide. Methanogens are the microorganisms in the reactor with the most prolonged generation periods (2-25 days), making this process the most time-consuming for readily hydrolyzed materials (Gonzalez-estrella et al. 2017; Stamatelatou et al. 2014).

## 2.2.2 Digester configurations

Bioenergy recovery from solid wastes is achieved in different reactor configurations. Batch and continuous reactors, one-stage and two-stage reactors, and solid-state anaerobic reactors are among them. The performance of the methane production process is dependent on the process configuration.

Wastes are fed into a batch reactor, and all decay phases are allowed to proceed as planned. The conventional digestion method is single-stage digestion. All reactions occur concurrently in a single reactor producing methane, ammonia, and other gaseous materials from polymeric compounds such as sugars, protein, and fat. The acidogenic and methanogenic phases of the single-stage process occur in the same reactor, depending on whether the solids are low or high. The current trend is to use wet or dry processes, with dry digestion (solids range of 20-40%) being preferred more to wet digestion (Liew et al. 2011). Multistage reactors (two-stage) use two separate reactor systems based on acidogenesis and methanogenesis phase separations. The multistage system is divided into hydrolysis and acidogenesis in one reactor and Methanogenesis in another. The first reactor performs hydrolysis and fermentative acidification, while stage two is designed for Methanogenesis, and hydrolysis is rate restricted with complex carbohydrates. Methanogenic bacteria prefer a pH of 6.5 to 8.5, whereas acidogenic microorganisms need a low pH and diluted organic acids at this level. As a result, the best conditions for each step and the average reaction rate were retained (Elsayed et al. 2021).

The digesters can be used in batch or semi-continuous digestion systems. Batch digesters are accessible, efficient, and have a number of advantages, including low

maintenance, low energy loss, and low capital costs. However, a lower loading rate and waste collection at the bottom of the reactor lower the biogas yield and create a concern during reactor unloading. In a batch method, total solids are usually held between 20 and 40%. (Kalyani et al. 2017). The fresh feedstock used for digestion for each batch reaction in a batch method. Single-stage, sequential, and upflow anaerobic sludge reactors are the three types of batch reactors. In mesophilic and thermophilic environments, single-stage batch digesters were used. Continuous reactors have a continuous flow of reactors by preserving equilibrium conditions, whereas batch reactors have distinct phases. Both reactions occur in a steady state, with stable feedstock input and consistent biogas output (Appressi 2014; Guo et al. 2014).

The solids content can be divided into two categories: low-rate digestion and high-rate digestion. Solids in the digester had a negligible effect on the volume and operation of the digester. Low solids with less than 10% solids require the most water, determined by reactor volume and post-treatment technologies. Low solids were used for anaerobic digestion in the 1980s, but the pattern has recently shifted to high solids content feedstock. Solid-state anaerobic digestion, on the other hand, has many benefits over liquid anaerobic digestion in terms of reactor volume settings, content and water needs, and so on.(André et al. 2018; Liew et al. 2011).

**2.2.3 Process parameters**

Different factors, such as the feedstock type used and operational variables such as temperature, pH, alkalinity, substrate and nutrients, hydraulic retention time, and inhibitors, may influence the biogas process.

*2.2.3.1 Substrate and nutrients*

Biogas generation from different organic materials are found in the environment. Currently, sewage sludge, wastewater, slaughterhouse waste, the organic fraction of urban solid waste (OFMSW), various commercial food sources, fertilizer, and energy crops are used in anaerobic digesters. A suitable nutrient is needed to achieve adequate microorganism growth and increase biogas output. For their life, microorganisms need an energy supply, which is chemical compounds like proteins, fats, or carbohydrates in

the biogas phase (Nozari and Mirmohamadsadeghi 2018). They will need an electron acceptor, which in the case of the anaerobic digester is $CO_2$. The energy supply is oxidized, and electrons/protons are passed through various intermediates before finally arriving at the electron acceptor, where energy is stored. The type of substrate specifically influences the biogas yield; for example, fat digestion produces more methane than protein or carbohydrate digestion. The substrate is often measured in total volatile solids (VS) or chemical oxygen demand (COD), which specifies the fraction of organic material and is simple to do in a laboratory environment (Sayara and Sánchez 2019). The carbon/nitrogen ratio, in addition to the organic content of the substrate, is considered a significant factor in the biogas process. For the digester to operate at its maximum capacity, the C/N ratio should be between 10 and 30, with an optimal ratio ranging between 25 and 30. There is a chance of ammonia inhibition at lower C/N levels, with methanogens being the most vulnerable. As a result, an aggregation of volatile fatty acids will occur, resulting in a drop in pH and reactor failure. Higher ratios may result in lower methane yields due to a lack of nitrogen available for cell growth (Chakraborty and Venkata Mohan 2019; Dinh et al. 2018).

### 2.2.3.2 Temperature

AD can be maintained at different temperature conditions such as

- ❖ Psychrophilic conditions (12–16°C)
- ❖ Mesophilic conditions (35–37°C)
- ❖ Thermophilic conditions (55–60°C)

Microorganisms are estimated to have a 25-50% higher activity at thermophilic temperatures relative to mesophilic temperatures, resulting in higher methane productivity. The decreased process stability and lowered dewatering properties of the fermented sludge, and the need for significant quantities of energy for heating are disadvantages of thermophilic anaerobic fermentation. Simultaneously, the thermal degradation of pathogenic bacteria at elevated temperatures is considered a significant benefit (Molino et al. 2013). Mesophilic systems are more stable but have a slower reaction time. The thermophilic temperature has fewer species than the mesophilic

temperature, suggesting that mesophilic microorganism diversity can help stabilize the process (Kumar et al. 2015b).

### 2.2.3.3 pH and alkalinity

The microorganisms in the anaerobic digester are pH sensitive and have varying pH optimal conditions. The optimal pH of methanogens is between 6.5 and 8.0, while the for acetogens is between 5.0 and 8.5. Anaerobic digesters should be operated at a pH of 7.0-8.5; operating outside of this range will result in process imbalances (Mata-alvarez et al. 2011; Ware and Power 2017).

High and stable alkalinity is needed to maintain a neutral and stable pH in the reactor. The quantity of essential compounds in the reactor is measured by alkalinity. The higher the alkalinity, the greater the buffer potential and the greater the probability of achieving a stable pH. Carbonate ($CO_3^{2-}$) in equilibrium with dissolved $CO_2$ is the principal source of alkalinity. However, as proteins-rich substrates are degraded, ammonia is released, contributing to the alkalinity (Kumar et al. 2020).

### 2.2.3.4 Volatile fatty acids

The $C_2$-$C_7$ monocarboxylic aliphatic acids found in organic wastes are known as volatile fatty acids (VFA). VFAs are an essential intermediate in the anaerobic digestion metabolic pathway. The VFA accumulation produced by acidogenic and acetogenic bacteria causes the degradation of acid producers and consumers. When the VFA concentrations were high, the pH in the system was lowered (Kumar et al. 2015b). VFA present in higher concentrations can cause microbial stress, and a drop in pH may result in the digestion process failure. Acetic, propionic, butyric, valeric, and i-forms of butyric and valeric acids, and hexanoic acid, were the intermediates formed. The main compounds released during digestion are acetic and butyric acids, which signify the performance of the digestive system (Sayara and Sánchez 2019).

### 2.2.3.5 Hydraulic retention time

The time it takes to convert all the substrate in a reactor is known as hydraulic retention time (HRT). Typically, the loading rate exceeds the rate at which the

substrate degrades into methane and carbon dioxide, implying that none of the content is degraded. Since a portion of the substrate has gasified, the density of the substrate is greater than the mass of the residues. The residues are made up of non-degradable organic material and inorganic and inert materials, biomass from microorganisms, salts, and water. Anaerobic digesters' HRT is usually 10 to 25 days or longer. The materials containing cellulose which are slowly degradable, need a longer HRT than quickly degraded materials, such as dissolved sugars (Kafle et al. 2013; Kumar et al. 2015b).

### 2.2.3.6 Presence of inhibitors

In the anaerobic digester, there are a variety of compounds that could serve as inhibitors. Methanogens are widely believed to be the most sensitive of the microorganisms found in the digester. Toxic compounds may come from the substrate or as a by-product of one of the digester's degradation stages. In certain circumstances, microorganisms can adapt to the environment in which toxic compound-tolerant microorganisms emerge, and in later stages of the digester, they can dominate in the reactor. Ammonia is the most critical inhibitor in the anaerobic process. Ammonia accumulation is caused by protein or urea degradation or by soluble ammonia in the wastewater. Since it may diffuse through the cell wall and induce a proton imbalance and a potassium shortage, non-ionized ammonia is considered the most toxic type. The concentration of VFA is caused by the inhibition of ammonia on methanogens. VFAs are formed by acetogens and ingested by methanogens, so if methanogens are inhibited, there would be an accumulation of VFAs. The aggregation of VFA causes a pH decrease, which can cause the entire digester to stop functioning. Both dissociated ($H^+$ and $R^-$) and undissociated ($H^+$ and $R^-$) forms of volatile fatty acids exist in the reactor. This is based on pH, with lower pH resulting in higher concentrations of undissociated VFAs. Since VFAs can diffuse through the cell wall in their undissociated state, they have an inhibitory effect.

## 2.3 Lignocellulosic biomass

Food waste, urban solid waste, and manure were among the organic materials used as feedstock for anaerobic digestion. The feedstock was chosen based on regional availability. Furthermore, the properties of biomass are favorable to digestion. Lignocellulosic biomass has recently received recognition as a potential feedstock for AD.

Plant biomass residues obtained as a by-product from agricultural and industrial process serve as a sustainable carbon pool for bioenergy production. Plant biomass mainly consists of polymers such as cellulose (40-50%), hemicellulose (20-30%), lignin (10-25%) and traces of extractives, as shown in figure 2.2 (S. Kim and Dale 2004). Cellulose forms the inner core and hemicellulose and lignin act as the encrusting material (Anwar et al. 2014; Saini et al. 2015). After hydrolysis, the sugar components such as cellulose and hemicellulose are readily fermentable, making them a better feedstock for biogas production. Cellulose is a polysaccharide polymer of glucose disaccharides, strongly linked with $\beta$-1,4 glycosidic bond and attached with hydroxyl groups forming a linear structure. Within the structure, they differ in their orientation, leading to different crystallinity levels. At a high crystallinity level, the degradation rate of the cellulose reduces (Dulermo et al. 2016). Hemicellulose is a branched and amorphous kind of substance that is readily susceptible to thermal, chemical and biological hydrolysis. Lignin is the most complex, hydrophobic, aromatic and amorphous heteropolymer found in biomass. It is made up of sinapyl and coniferyl alcohols forming a firm 3-D structure of cell wall (Guo et al. 2014; Zheng et al. 2014). The lignin hinders the hydrolysis process accounting for the rate-limiting step in the anaerobic digestion process. This hindrance necessitates the application of pretreatment for the lignocellulosic biomass before the AD. The pretreatment causes lignin degradation and uncovers the hemicellulose and cellulose for the microbial attack to increase the biogas yield. Softwood contains higher lignin content than hardwood and agricultural residues. So, the softwood resists the bioenergy conversion even after pretreatment (Olusola and Omojola 2013).
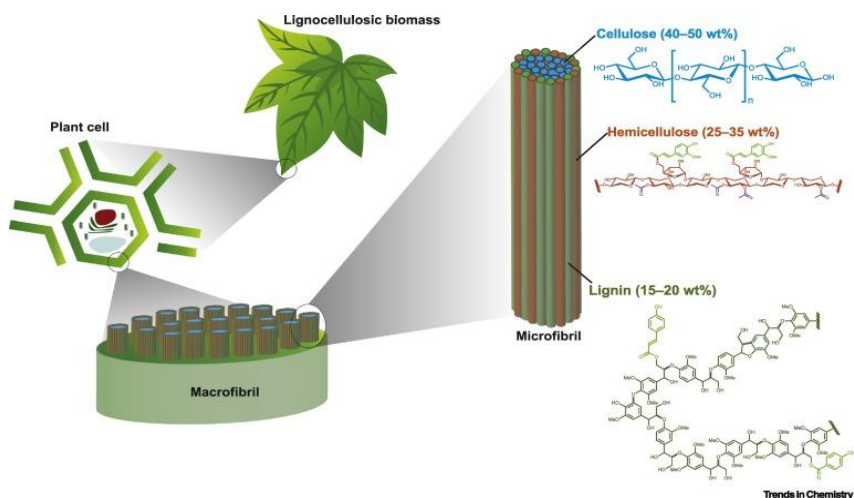
**Figure 2.2 Overview of the lignocellulosic biomass structure (Bertella and Luterbacher 2020)**

## 2.4 Pretreatment methods for biogas production

Over the last decade, different pretreatment methods have been investigated to improve the anaerobic digestion technology. They may be broadly categorized as physical, chemical, biological pretreatment and even their combinations. Some of the recent literature on various biomass used for pretreatment aided biogas production are depicted in table 2.1. The application of pretreatment such as physical, chemical, biological, enzymatic, thermal and their combination on various lignocellulosic biomass helps them overcome the inhibitions through structural and chemical changes during hydrolysis.

Physical pretreatment comprises mechanical (milling and grinding), hydrothermal (liquid or gaseous), irradiation and extrusion processes (Amin et al. 2017). The hydrothermal treatment (liquid hot water) of sugar beet pulp at 160ºC yielded four times more free glucose than at 120ºC. This glucose yield increased the methane yield by 76% compared with the raw sugar beet pulp (Zieminski et al. 2014). The chemical pretreatment method is a promising and effective method of degrading complex organic substrates using different chemicals. They can be roughly grouped into alkaline, dilute acid, organosolv (Mancini et al. 2018), oxidizing agents, etc. The reagents involved are sodium hydroxide (NaOH), sodium carbonate ($Na_2CO_3$), sodium bicarbonate ($NaHCO_3$), calcium hydroxide, Sulfuric acid ($H_2SO_4$), acetic acid, citric acid, hydrogen

peroxide ($H_2O_2$), acetone, ethanol, ammonia, etc. Sodium chloride (NaCl), calcium chloride ($CaCl_2$), and other inorganic salts are also utilized in chemical pretreatments of lignocellulosic materials (Achkar et al. 2018; Kaur and Phutela 2016a; Pellera and Gidarakos 2017).

The rigid lignocellulosic cell wall is ruptured by bacterial and fungal action during biological pretreatment. Only if a sufficient variety of microbes (bacterial strain) is done does this approach account for low cost, inhibition-free, and environmentally safe with no chemical input. The most significant disadvantage is that it takes longer than most recovery options (Barua et al. 2018). The recent advent of the advanced oxidation method of biomass pretreatment with UV irradiation has ushered in new possibilities for its integrated applications. According to the findings, during pretreatment, lignin undergoes oxidative fractionation, and the by-products generated have no impact on the anaerobic digestion process (Alvarado-Morales et al. 2016). Researchers are increasingly involved in combining different pretreatments, such as physicochemical, thermochemical, and other methods (Alexandropoulou et al. 2016; Ethaib et al. 2018; Kaur and Phutela 2016a). Pérez-rodríguez et al. (2016) conducted a comprehensive analysis on the use of enzymes, ultrasounds, and their variations to improve digestibility. They discovered that ultrasound pretreatment decreased methane emission while enzymatic hydrolysis increased it positively. The lignin relocation creates a barrier over the substrate degradation, which was the primary cause of their negative impact.

**Table 2.1 Review of the feedstocks used in an anaerobic digester**

| Feedstock | Pretreatment | | AD conditions | Biogas production | References |
|---|---|---|---|---|---|
| | **Method** | **Condition** | | | |
| Maize straw | Alkaline pretreatment and Fe dosing | Combining NaOH (6%) pretreatment and Fe dosage (200–1000 mg/L) | Batch, Mesophilic, 48 days | 472.9 mL $CH_4$/gVS | (Khatri et al. 2015) |
| Wheat straw | Advanced oxidation process combining UV 16 irradiations in the presence of the photocatalyst titanium dioxide (TiO2) | 1.5% (w/w) $TiO_2$/straw at 3 hours of UV light | Batch, thermophilic conditions | $333.25 \pm 276$ 15.02 $NmLCH_4$/gVS$_{added}$ | (Alvarado-morales et al. 2016) |
| Water hyacinth | Lignocellulose degrading bacterial strains isolated from<br>➤ Soil (*Bordetella muralis* VKVVG5) (UN3d2),<br>➤ Gut of silverfish (*Citrobacter werkmanii* VKVVG4) (SFa2)<br>➤ Millipede (*Paenibacillus sp.* VKVVG1) (BrB2) | the optimum dosage of 109 CFU/mL and time of 4 days- solubilization of 33.3% | Batch, Mesophilic for 50 days | Cumulative 393 biogas production of $3737\pm21$ mL | (Barua et al. 2018) |

| Sugarcane bagasse | Combined Hydrothermal & Ca(OH)$_2$ | 180°C+8.5% | Batch, Mesophilic for 35 days | 318 mL/g Volatile Solids | (Mustafa et al. 2018) |
|---|---|---|---|---|---|
| wheat and pearl millet straw | Lime, Ca(OH)$_2$ | 60% (w/w) loading for 8 h at ambient temperature | working volume of 400 mL, Mesophilic, 45 days. | 518 mL/g VS | (Kumar et al. 2019) |
| Giant reed stems (*Arundo Donax*) & wheat straw | Two stages dry milling device | Working capacity 1-2 t h$^{-1}$ | Batch reactors under mesophilic conditions for 28 days | 212 Nm$^3$ t$^{-1}$ of VS & 250.3 Nm$^3$ t$^{-1}$ of VS | (Dell'Omo and Spena 2020) |

**2.5 Efficacy of pretreatment method and its issues**

The effective pretreatment of biomass involves many vital features. The pretreatment option adopted should be low cost both in capital and operational aspects. It should be applicable in a wide range and have to be effective in recovering most of the biomass components in an amenable form. It should not produce any inhibitory compounds that inhibit the fermentative microorganism growth or hydrolytic enzymes' action and should be energy efficient (Hendriks and Zeeman 2009). In addition to that, lignocellulosic biomass in a bulk quantity requires a severe pretreatment (alkali, acidic, thermal, and thermochemical) method(Amin et al. 2017; Costa et al. 2014; Ward-Doria et al. 2016). However, improper implementations of these pretreatments can show a negative influence on anaerobic digestion. Various pretreatment methods have both advantages and disadvantages, but process cost and energy consumption play a crucial role in selecting process upscaling applications. Thus, economic feasibility with the derived benefits in waste minimization, biogas production and digestate as biofertilizers should be the watchword for selecting the pretreatment method (Noonari et al. 2017). Research on the pretreatment methods is still going on, and these parameters should balance against the entire cost involved and steps in the down streaming process. It is complicated to evaluate and compare various pretreatment methods as they include total processing (upstream and downstream) cost, initial investment, recycling of chemicals and treatment systems for wastes. This calls for the need for decision making in the pretreatment method selection for the given feedstock from the various methods available so that methane yield can be maximized.

Before anaerobic digestion, the emerging pretreatment technologies have become more prominent to enhance the digestibility of substrate added with the increased production rate of biomethane. Due to the resistant and recalcitrant nature of lignocellulose content, biodegradation is hindered and forms a significant barrier in bioconversions for biofuel production. Lignocellulosic biomass's compositional and structural properties hold the cellulose and hemicellulose together due to their sturdy and adhesive properties covered by lignin to form a rigid three-dimensional structure. This makes the hydrolysis step a bottleneck for the anaerobic digestion, forming a rate-limiting step.

## 2.6 Co-digestion for biogas production

The digestion of solid-state- Anaerobic digestion (SS-AD) could be increased by adding one or more substrates (i.e., co-digestion). As an initiative, SS-AD's efficiency was evaluated based on operational characteristics such as C/N ratio and food to inoculum ratio. The anaerobic digestion of several substrates co-digested with food waste used for biogas production is shown in Table 2.2. Co-digestion aims to increase methane production by balancing nutrient C/N ratios, diluting inhibitors/toxic compounds, and balancing macro and micronutrients.

**Table 2.2 Anaerobic digestion performance of multiple substrates**

| Feedstock | Temperature, °C | Mode of operation | Methane / Biogas yield, L/kg VS | Reference |
|---|---|---|---|---|
| Corn stover and chicken manure | Mesophilic | semi-continuous | 300-700 | (Yu et al. 2021) |
| Food waste, cow dung, and sludge solution waste | Mesophilic 37±1°C | - | 143.1-181.4 | (Deheri and Acharya 2021) |
| Food waste: Wheat straw and chicken manure | Mesophilic | semi-continuous | 351 | (Karki et al. 2021) |
| Fallen leaves, grass and primary sludge | Mesophilic | semi-continuous | 221.8-351.2 | (Elsayed et al. 2021) |
| Food waste: 50% fruits, 20% vegetables, 20% starchy food and 10% meat + Waste active sludge | Mesophilic | batch | 214 | (Zan and Hao 2020) |
| Food waste: vegetables (30.2%), rice (58.4%), and meat (11.4%) (w/w) + | Mesophilic | Continuous and intermittent | 212 | (Chan et al. 2018) |

| domestic wastewater | | | | |
|---|---|---|---|---|
| Food waste and horse manure | Mesophilic | Semi-continuous | 370 | (Zhang et al. 2017) |
| Food waste: carbohydrate, lipid, and protein | Mesophilic | Semi-continuous | 375.9–506.3 | (Zhang et al. 2015) |

**2.7 Lignin for value-added products**

**2.7.1 lignin and its structure**

Lignin is a significant source of carbon that is both green and bio-based. Fractionation allows lignin, as well as all other components of lignocellulosic biomass, to join valorizable streams. Lignin is the second most prevalent biopolymer and could be a critical factor in producing vast quantities of biomass-derived "green chemicals." Lignin acts as a resin in plant cell walls, filling the spaces between cellulose and hemicellulose and holding the lignocellulose matrix together. The mechanism gains resilience and rigidity by crosslinking with carbohydrate polymers (Zakzeski et al. 2010). Lignin is a complex aromatic-based chemical structure that accounts for 15–35 % of the over-dry mass of lignocellulosic biomass. It is generally recognized that the distribution of lignin and its quality in biomass differ between plant groups, botanical organisms, and also between trees and their morphological sections. In softwood, for example, lignin accounts for 30% of the weight, while in hardwood, it accounts for 20%–25% of the weight. Grass lignin accounts for just 10–15% of the overall plant mass (Li et al. 2015a).

Lignins are insoluble plant polymers with diverse and variable structures that have a high molecular weight. They are primarily made up of methoxylated benzene derivatives (phenylpropanoid alcohols, also known as monolignols), especially coniferyl, sinapyl, and coumaryl alcohols. Ether and C–C bonds connect these structural units (Rashid et al. 2018b). The critical function of lignin is to provide structural protection, impermeability, and tolerance to microbial attack and oxidative stress to plants. Since the amorphous heteropolymer is non-water soluble and optically inert, lignin degradation is complex. (Hendriks and Zeeman 2009).

## 2.7.2 Sources of Lignin

One way to unleash lignin's ability is to convert it into valuable items. Lignins can be used in various forms as raw materials that can be used in a variety of transformation processes. These "bulk" lignins come from the existing industry (mostly from paper and pulp delignification processes). However, they may also come in more significant quantities in the future from second-generation bioenergy whose aim is to valorize all the flows of matter derived from lignocellulosic biomass (cellulose, hemicellulose and lignins) (Beisl et al. 2017; Ojala et al. 2018). Technical lignins have been extensively described and can be considered a potentially crucial raw material since they are manufactured in lignocellulosic material treatment processes. Many technical lignins, such as those derived from the paper industry, are readily available in vast quantities (kraft lignin, lignosulphonates and soda lignin) (Arni 2018).

## 2.7.3 Lignin extraction process

Lignin is present in various ways and can be extracted using a variety of techniques, including mechanical, physical, chemical, and enzymatic methods. A hydrolytic treatment of alkali solutions such as ammonium, sodium, and calcium hydroxide, among others, is known as the soda method. Different temperatures, soda concentrations, and reaction times are used in this pretreatment (Carvajal et al. 2016). The Organosolv method has some benefits over the Kraft and sulphite processes. Lignin can be easily extracted from the lignocellulosic matrix, and the solvent can be recovered through various routes (precipitation and distillation) with fewer environmental effects. The Organosolv method has some benefits over the Kraft and sulphite processes. Lignin can be easily extracted from the lignocellulosic matrix, and the solvent can be recovered through various routes (precipitation and distillation) with less environmental effects.

On the other hand, Kraft pulping process is the most used in the world to produce cellulose pulp with approximately 85 percent (Ahuja et al. 2017; Arni 2018). Due to the increased demand for bio-based and bio-active nanomaterial fillers for biodegradable composites, nano-lignin has recently gained interest. However, lignin is used as a filler to make natural rubber vulcanization more resistant to thermo-oxidative oxidation in the air. (Beisl et al. 2017).

## 2.8 Oil-water separation methods

### 2.8.1 Theoretical aspects for surface wettability

The chemical composition and topographical structure of solid surfaces decide their wettability; thus, surfaces with different wettability (including hydrophobicity and oleophilicity) can be obtained by modifying these two variables. The contact angle ($\theta$) is a standard way of describing the degree of wettability of liquid droplets on a solid surface. Based on the water contact angle (WCA), surface wettability behaviour is classified into four distinct regimes. The hydrophilic and hydrophobic surfaces are described using WCAs of 10° to 90° and 90° to 150°, respectively. In comparison, the superhydrophilic (0° < WCA < 10°) and superhydrophobic surface (150° < WCA < 180°) have drawn more attention because of the extreme wetting behaviour of a water droplet on the surface of the material, which imparts the high oil−water selectivity.

The surface wettability of a liquid droplet on a static and smooth solid surface (Figure 2.3) is defined by the solid surface's surface free energy, which is represented by Young's equation:

$$\gamma_{sv} = \gamma_{sl} + \gamma_{lv} Cos\theta \tag{2.1}$$

where $\gamma_{sv}$, $\gamma_{sl}$, and $\gamma_{lv}$ are the vapor-solid, liquid-solid, and vapor-liquid interfaces interfacial surface tensions, respectively.

$$Cos\theta = 2\varphi \sqrt{\gamma_{sv}/\gamma_{lv}} - 1 \tag{2.2}$$

where the $\varphi$ of is an intermolecular interaction correction factor. According to the equation (2.2), a reduction in the vapor solid interface free energy ($\gamma_{sv}$) corresponds to an increase in the contact angle. However, this does not imply that the value $\theta$ will continue to rise forever.
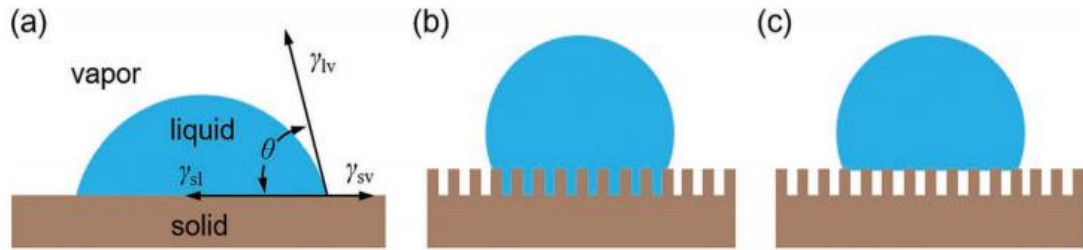
**Figure 2.3 Schematic diagram of a liquid droplet on a solid surface with and without roughness. a) Young's model, b) Wenzel's model, and c) Cassie's model (Ge et al. 2016)**

The equation (2.1) is valid for the flat smooth surface, and the principle has to be improved when it comes to a rough surface. Wenzel (equation (2.2)) and Cassie (equation (2.3)) suggested two classical models for explaining the wettability caused by roughness. The Wenzel model, the Cassie model, or the transition condition can both be used to explain the wetting behaviour of a liquid droplet on a rugged solid surface.

### 2.8.2 Global status of oil clean-up methods

Several methods have been employed to recover oil from the water or to enhance the oil-water separation. Traditionally, clean-up methods include centrifugation, bioremediation, in-situ burning, sedimentation, and electrochemical process, have many demerits in terms of lower efficiency in extensive scale application (Broje and Keller 2006). Among the various strategies for oil clean-up, highly efficient sorbents are more focused in recent years. However, conventional sorbents still show some drawbacks related to environmental incompatibility, low sorption and less chance for recyclability (Chen et al. 2018). The selective wettability of super wetting materials to oil and water are promising and effective methods to separate oil-water emulsions. Based on the selective wettability, materials are broadly classified into oil-sorbing and water-sorbing. In the former type, material exhibit super-hydrophobicity and super-oleophilicity by spreading the oil and flow through the material surface. The later type exhibited super hydrophilicity and superoleophobicity by blocking oil entry into the surface (Liu et al. 2018; Zhang et al. 2013). Wide varieties of sorbents are developed based on the nature of materials, i.e., (a) inorganic, (b) natural organic and (c) synthetic. Several studies are done on the oil sorption by the inorganic and synthetic sorbents,

which are hydrophobic and oleophilic in nature. However, certain drawbacks make them inefficient for pilot-scale or industrial applications (Al-Majed et al. 2012). Synthetic sorbent materials are sometimes expensive and non-eco-friendly.

Moreover, they can even be hazardous after the oil sorption and can harm the aquatic species on prolonged exposure. Besides, the inorganic metal sorbents possibly leach the oil into the water due to their lower retention capacity (Al-Majed et al. 2012; Qi et al. 2013; Teas et al. 2001). Most of the natural organic-based sorbents are made up of cellulosic material from agricultural waste. The agricultural wastes include cotton (Cao et al. 2017), kapok (Dong et al. 2015), rice husk (Kenes et al. 2012), sawdust (Mojžiš et al. 2019), wheat straw (Ermeng et al. 2017), pistia leaves and roots (Sánchez-Galván et al. 2013), etc. They exhibit lower oil sorption capacity, slower sorption rate and lower reusability, but they are cheap and environmentally friendly. As a result, the production of cost-effective sorbent materials with improved oil spill clean-up properties is needed.

Similarly, the presence of lignin in the biomass decreases water permeability across plant cell walls. This property of lignin can be used to develop a hydrophobic substance material to clean-up oil spills. Additionally, lignin is a cost-effective substitute for some chemicals used in developing oil sorbents (Cinelli et al. 2013). Using a hydrophobic Lignin-polyurethane (LPU) substrate coated with adhesive polydopamine-reduced graphene oxide (rGO), Oribayo et al. (2017) developed a superhydrophobic and superoleophilic absorbent for oil spill clean-up. However, polyurethane (PU) is a synthetic material that is a non-biodegradable synthetic material, and after a few cycles of reuse cycles, it may add up as a secondary pollutant. Long hydrophobic $-CH_2$ chains and alkyl groups from octadecyl amine (ODA) molecules are incorporated into LPU foam using polydopamine rGO as an adhesive. The specific wettability of the resulting LPU-rGO-ODA foam sorbent to oil was due to the $-CH_2$ long strings, which have a high affinity for oil and a lower surface free energy than water. Ahamad et al. (2019) reported that lignin-based bio-waste date palm pits powder (Phoenix dactylifera L.), modified with magnetic $Fe_3O_4$ nanocrystals, was an efficient, porous, and oil/organic solvent sorption magnetic material. Ma et al. (2021) used the photothermal effect to heat crude oil and significantly reduced their viscosities to accomplish a fast oil clean-up. A carbon nanotube (CNT) modified lignin-based polyurethane foam with excellent

adsorption capability for heavy oil was manufactured. The heavy oil viscosity was effectively reduced due to solar heating, allowing the improved foam to absorb more than six times its weight in crude oil in just six minutes.

### 2.8.3 National Status of oil clean-up methods

In the Indian context, a limited number of researches can be seen on the oil spill clean-up using natural sorbents. Teli et al. (2017) aim to increase the oleophilicity of coir fibre and thus the oil absorption potential. As a result, the fibres are grafted with butyl acrylate monomer in the presence of a cross-linker, causing the butyl acrylate monomer to react with the hydroxyl group in the cellulose and form esters. The weight percent gain of graft add-on imparted high hydrophobicity to the fibres and have enhanced the oil sorption. During the reaction, the weight percentage increase (graft add-on) in the synthetic graft polymer chain was maintained optimum for economical and improved fibre biodegradability. Dashairya et al. (2018) synthesized a superhydrophobic and superoleophilic reduced graphene oxide-coated cotton by a facile single-step hydrothermal method for oil-water separation. The absorption capacity for 1 gm of the material was around 30-40g, indicating an excellent oil sorption capacity. Negi and Singh (2020) reviewed the chemical modifications of the use of lignin that find applications in petroleum exploration, product formulation, biofuel production and in the field of oil herding (oil separation from water). The literature says that by various interactions such as hydrophobic interaction and van der Waals interaction, lignin NP has an outstanding ability to reduce the interfacial tension between water and oil interfaces, forming a monolayer between water and oil. The monolayer prevents oil from flowing into the water and needs to be separated mechanically, which is again separated mechanically, which is laborious work.

### 2.8.4 Agri-waste/bio-based material for oil/water separation.

Cinelli et al. (2013) describe an advanced, sustainable, and environmentally friendly soft foam synthesis using Kraft lignin. The research centred on using and valorizing forest resources, such as lignin as a by-product of the wood industry and bioethanol processing. Foams represent the essential commercialized products of Polyurethanes. These foams are commonly classified as flexible, semi-rigid, or rigid, depending on

their mechanical performance and core densities (Oribayo et al. 2017). Many studies have approached the development of new materials for application in the remediation of impacted areas by oil spills, particularly those that have large sorption capacity as shown in figure 2.4. Some examples of materials used for the sorption of crude oil and derivatives include sugarcane bagasse, vegetable fibres, clays, and polyurethane foams. Particularly for oil sorption, polyurethane foams are attractive materials, mainly due to the combination of porous structure with a hydrophobic polymer matrix (Santos et al. 2017).
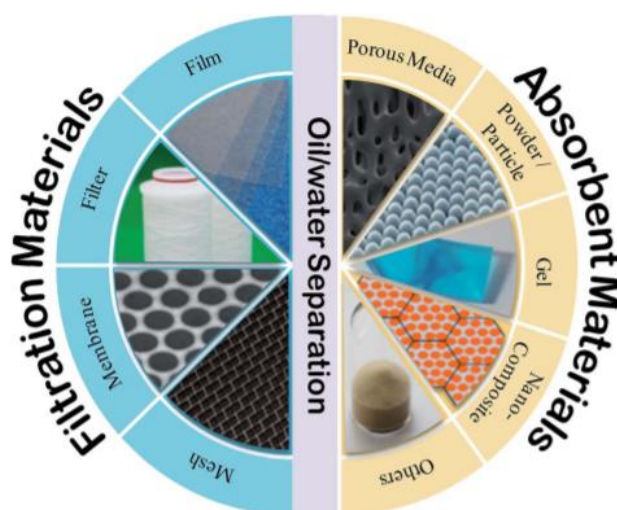


**Figure 2.4 Different materials used for the oil-water separation**

In recent times, superhydrophobic materials have been synthesized for oil-water separation. Recently, the studies related to 3D porous materials (Chen et al., 2015; Du et al., 2015; Gui et al., 2010; Kayvani Fard et al., 2016; Nguyen et al., 2012; Zhao et al., 2012), commercially available materials like foams or sponges (Liu et al., 2015), metal-based sponges (Qiu et al., 2015) have been investigated for the single pollutant, i.e., either dye or oil removal. Besides, superhydrophobic and super oleophilic materials were fabricated and successfully applied for the oil/water separation (Wang et al., 2009), (Wu et al., 2015). However, in most cases, such materials are unable to remove dissolved organic contaminants, specifically dyes. The materials capable of removing insoluble oil and soluble dyes in water media are rarely investigated (Li et al., 2014; Zhang et al., 2015).

## 2.9 Summary of the literature review

Lignocellulosic biomass, animal manure, and agricultural residues are abundant in a country like India. In anaerobic digestion, these residues were converted to methane-rich biogas, which provided merits for producing biogas while also improving the digestate condition for their landfills. SS-AD has a higher organic loading rate, less volume, lower energy consumption, and the highest volumetric methane emission rate than traditional anaerobic digestion. The mismatch of nutrients and insufficient buffering capability make single substrate digestion difficult. The efficient way to digest various raw materials for co-digestion is to balance the nutrients and eliminate toxic compounds, which improves biogas efficiency. It acts as a nitrogen source, provides buffering space, and is rich in micronutrients needed for optimal microbial growth. However, to increase performance, feedstock selection of different mix ratios for anaerobic digestion must be optimized for different characteristics.

Additionally, the open-source literature survey found that the use of porous materials as sorbents allows more effective and safe oil-water separation with lower environmental effect than conventional clean-up approaches. Carbon foams are emerging types of materials that come under the group of 3D porous material and offer a wide variety of pore structure. Carbon foam has certain properties such as large specific surface area, higher thermal stability, ultra-lightweight, good reusability, etc. The thermal and electrical properties may tend to change the structure of carbon foams to amorphous nature. These materials pose a higher tolerance rate by altering the bulk properties than other carbon materials (Gupta and Tai 2016). The current methods deploy commercially available porous sorbents in various forms and shapes such as booms, rolls, mops, pillows, pads, etc. (Felix et al. 2016; Harikishore Kumar Reddy et al. 2017).

Furthermore, the recovery of oil from sorbent is conventionally executed through batch mode squeezing, making them complicated and laborious. Sorbent regeneration is also achieved by heating and burning, which could lead to highly hazardous airborne emissions. Besides, these techniques reduce the product recycling ability, which indicates that a larger supply of sorbent materials is needed. As a result, time-consuming separation procedures, sorbent regeneration, recycling, disposal, and oil

recovery processes are significant hurdles to sorbent materials scalability that is reliable, sustainable, and cost-effective. Despite the incredible development of efficient porous sorbent materials for oil sorption, their implementation on the industrial scale is limited.

## 2.10 Research objectives

- To prioritize the best pretreatment method for enhanced biogas yield using MADM techniques.
- To investigate the anaerobic digestion of pretreated AH with due emphasis on its biogas potential.
- To evaluate the effect of substrate mix ratio in batch mode anaerobic co-digester for biogas production.
- To extract the Lignin from AH and to synthesis a novel lignin-based carbon material for oil-water separation.

# CHAPTER 3

## MULTI-ATTRIBUTE DECISION-MAKING APPROACH

### 3.1 General

The multi-Attribute Decision Making (MADM) system is a flourished and well-established decision system that evaluates the systems among the existing options under conflicting criteria. MADM approach enables the laborious task of selecting the ideal choice in a more effortless manner where the simultaneous application of several criteria occurs. MADM is one among the divisions of Multi-Criteria Decision Making (MCDM). MADM can be defined as the best possible decisions for various alternatives based on attributes which can be quantitative or qualitative. Several methods were employed in this decision-making model: outranking, priority, distance, and mixed methods. The methods adopted can be fuzzy, deterministic, or stochastic or even a combination of the above. Each method differed in its characteristics and systematized into a single decision-making method or a grouped one. In the MADM model, the alternatives were customized from a particular pool of objective functions rather than taking it explicitly. These alternatives were assessed against the set of attributes, and the best from the various alternatives were chosen with respect to the attributes (Pohekar and Ramachandran 2004).

### 3.2 Techniques in MADM

The available primary techniques in MADM modelling is Simple Additive Weight (SAW) method, Weighted Product Method (WPM), Compromise and Goal Programming (CP and GP), Technique for Order Preference by Similarity to Ideal Solution (TOPSIS), Analytical Hierarchical Process (AHP), Elimination and Choice Translation Reality (ELECTRE), Preference Ranking Organisation Method for Enrichment Evaluation (PROMETHEE) (Ameri et al. 2018; Dhanisetty et al. 2017; Mousavi-nasab and Sotoudeh-Anvari 2018; Zaman et al. 2018) and Multiple Attribute Utility Theory (MAUT) (Pohekar and Ramachandran 2004). Among the different approaches, TOPSIS and AHP were extensively used for logical decision making. MADM model has found applications in science and technology to select the best choice from many alternatives. This modelling makes the subtle task of selection easier

and simpler (Ashby 2000). Rao and Davim (2008) assessed the selection of material by evaluating and ranking the various materials using TOPSIS and AHP technique of MADM model.

TOPSIS approach is based on selecting alternatives that have the least Euclidean distance from an ideal solution. The ideal solution can be hypothetically best or hypothetically worst from the attribute value in the given database, assimilating maximum and minimum values, respectively. The choice of alternatives was close enough to hypothetical best and far enough to hypothetical worst. In a decision-making process, tangible and intangible attributes were considered by prioritizing those attributes by comparing them one by one. Now, AHP plays a crucial role in the comparison by reducing the difficulty level and making the decision process flexible and forming the relative importance of each parameter (Tan et al. 2013). The expert's choice of weights played a significant role in the decision-making process, and the weights can be given by a single expert or a group of experts. In the real-time application of MADM, uniqueness in the expert's preferences makes them reluctant to assign the specific numerical values for the relative importance matrix. In this regard, the results from MADM techniques were meant to be sensitive to each attribute's relative importance (dominance weights) (Devatha and Thalla 2017). Hence, it is necessary to ascertain unique weights, which is very important to make the decision-making process accurate.

## 3.3 Need for MADM approach in pretreatment and AD process

The anaerobic digestion process is complex in view of operational conditions, maintenance, biogas quality and quantity, feedstock characteristics and pretreatment, performance time, and digestate quality. The emerging pretreatment technologies prior to anaerobic digestion has become more prominent, to enhance digestibility of substrate added with the increased rate of production of biomethane. Due to the resistant and recalcitrant nature of lignocellulose content, biodegradation is hindered and forms major barrier in bioconversions for biofuel production. The structural and compositional properties of lignocellulosic biomass hold the cellulose and hemicellulose together due to their sturdy and adhesive properties encrusted by lignin to form a rigid three-dimensional structure. This makes the hydrolysis step as bottleneck

for the anaerobic digestion, forming a rate-limiting step. Over the last decade, different pretreatment methods have been investigated to improve the anaerobic digestion technology. They may be broadly categorized as physical, chemical, biological pretreatment and even their combinations. The factors involved in the pretreatment and parameters checked prior and after the pretreatment are enlisted in the tables 3.1, 3.2, and 3.3. It is evident that a huge mapping and to optimize the pretreatment method and parameters involved to maximize the biomethane yield is a tedious laboratorial work. Thus, decision making plays a crucial role in this aspect.

Longer digester stability time, pH maintenance by alkali addition, sensitivity towards water content, sludge post-treatment, etc., pose the disadvantages of the anaerobic digestion system. To overcome these limitations, digester has to be designed accordingly by considering these critical aspects. So, it is imperative to critically review the factors and parameters to design the digester configurations to yield maximum biogas (Rao and Baral 2011). For a pretreatment aided anaerobic digestion, the pretreatment method's evaluation and selection for a particular feedstock is a must to ease the further down streaming process. Thus, the pretreatments direct selection can be made without actually performing the anaerobic digestion experiment for the entire digestion period, saving time and energy. The methodology proposed helps the biogas unit operators select the best pretreatment option for the particular feedstock based on the parameters and factors involved to maximize energy yield. This makes the process economically feasible.

The varied and complex chemical structure of biomass resists the degradation process. The optimization of the pretreatment method depends upon the type of lignocellulosic material. The compositional and structural properties include lignin content, hemicellulose content, silica content, crystallinity index, surface area, the degree of acetylation, and cellulose polymerization (Zheng et al. 2014). The attributes can be classified as general, physical and chemical attributes. The physical attributes include Colour, odour, temperature, moisture content, total solids and volatile solids.
Similarly, chemical attributes include pH, alkalinity, Volatile Fatty Acids (VFA), Carbon/Nitrogen ratio (C/N), chemical oxygen demand, biochemical oxygen demand, sulfates, phosphates, lignin content, silica content, dissolved carbohydrates, lignin

/cellulose ratio, uronic acids, heavy metals, inhibitory by-products (such as hydroxymethylfurfural (HMF), furfural, etc.), Ammonia, etc. Other general attributes comprise the feedstock's nature, source, price, seasonal availability and production rate, feedstock age, biogas productivity, methane composition, and mode of transport. In the attributes mentioned earlier, most of them are interdependent. Any variation in one attribute affects the other (Cioabla et al. 2012). These attributes are critical in the case of pretreated lignocellulosic materials for anaerobic digestion and are shown in table 3.1, 3.2, and 3.3. The attributes can be mentioned in two ways, i.e., either quantitative or qualitative. Quantitative measurements of attributes are value-based, whereas the qualitative measurements include very poor, poor, average, good, excellent, etc. The conversion of these qualities into some values was done by using a set of scales ranging from 1-9 (Rao and Baral 2011).

Decision making tool to rank various pretreatment options for highest biogas yield was not developed to our knowledge till date. Now, researchers are focusing on time saving approaches in order to ease their experimental work. This kind of mathematical approach helps the researchers to reduce the hurdles (time, cost, and work) in the anaerobic digestion process (for e.g. actual performance & maintenance of the digester till their complete digestion period). From the solubilization results obtained after the pretreatment, evaluation and ranking of the pretreatment methods can be done without doing actual anaerobic digestion study which longs for days together. In our present study, we have tried to showcase how the decision making can be implemented for the pretreatment selection for a particular feedstock. So, our study involved only 7 pretreatment options/ alternatives from Song et al., (2014) with 5 attributes to check the feasibility of the proposed idea of implementing decision making for the pretreatment method selection.

**Table 3.1 Parameters involved in pretreatment methods** (Choong et al. 2018; Matsakas et al. 2017; Veluchamy and Kalamdhad 2017)

| | Pretreatment method | Particle size reduction | Moisture content | Cost | Temperature | Pressure | Time | Chemical addition | pH | Mixing | Type of biomass | Source of biomass | Energy requirement | Chemical dosage | Solids loading | Additives added |
|---|---|---|---|---|---|---|---|---|---|---|---|---|---|---|---|---|
| Physical | Comminution (milling & grinding) | ○ | ● | ● | X | X | X | X | X | X | ● | ● | ● | X | | X |
| | Steam explosion | X | X | ● | ● | ● | ● | X | ○ | ○ | ● | ● | ○ | X | ● | X |
| | Liquid hot water | X | ● | ● | ● | ● | ● | X | ○ | ○ | ● | ● | ● | X | ● | X |
| | Extrusion | ● | ○ | ○ | ○ | ● | ● | X | X | ● | ● | ● | ○ | X | ● | X |
| | Ultrasound/ Microwave irradiation | X | ○ | ● | ○ | ● | ● | X | ○ | ○ | ● | ● | ● | X | ● | ● |
| Chemical | Alkaline | X | ○ | ● | ● | ○ | ● | ● | ● | ● | ● | ● | X | ● | ● | X |
| | Acidic | X | ○ | ● | ● | ○ | ● | ● | ● | ● | ● | ● | X | ● | ● | X |
| | Organosolv | X | ○ | ● | ● | ● | ● | ● | ○ | ● | ● | ● | X | ● | ● | ● |
| | Oxidative | X | ● | ● | ● | ● | ● | ● | ● | ● | ● | ● | X | ● | ● | ● |
| | Wet explosion | X | ● | ● | ● | ● | ● | ● | ● | ● | ● | ● | ● | ● | ● | ● |
| | Saline | X | ○ | ○ | X | X | ● | ● | ● | ● | ● | ● | X | ● | ● | X |
| | Ionic liquids | X | ○ | ● | X | ● | ● | ● | ● | ● | ● | ● | ● | ● | ● | X |
| Biological | Fungus | ● | ● | ● | ○ | X | ● | X | ○ | X | ● | ● | X | X | X | X |
| | Bacteria | ● | ● | ● | ○ | X | ● | X | ○ | X | ● | ● | X | X | X | X |
| | Ensiling | ● | ● | ● | ○ | X | ● | X | ○ | ○ | ● | ● | ○ | X | X | X |

●: Major role; ○: Minor role; **X**: No role

**Table 3.2 Influence of factors involved in pretreatment methods** (Elliott and Mahmood 2007; Hu et al. 2016; Jain et al. 2015; Jiao et al. 2012; Kim et al. 2018; Yunqin et al. 2010)

| Pretreatment method | | Factors affecting | | | | | | | | | | | |
|---|---|---|---|---|---|---|---|---|---|---|---|---|---|
| | | Cellulose solubilization | Hemicellulose solubilization | Lignin solubilization | Crystallinity | Inhibitory compounds | Surface area | Total Carbon | Total reduced sugars | sCOD | VS/TS ratio | Degree of depolymerization | C/N ratio |
| Physical | Comminution (milling & grinding) | X | X | X | X | X | ● | X | X | X | X | ● | X |
| | Steam explosion | ● | ● | ● | ● | ● | ● | X | ● | ● | ● | ● | ● |
| | Liquid hot water | ○ | ○ | ○ | ● | ● | ● | ○ | ○ | ● | ● | ● | ○ |
| | Extrusion | X | X | X | ○ | X | ● | X | X | X | X | ○ | X |
| | Ultrasound irradiation | ○ | ○ | ○ | ○ | ● | ● | X | X | X | ● | ● | X |
| Chemical | Alkaline | ○ | ○ | ● | ● | ● | ● | ● | ● | ● | ● | ● | ● |
| | Acidic | ● | ● | ○ | ○ | ● | ● | ● | ● | ○ | ● | ○ | ○ |
| | Organosolv | ○ | ● | ● | ○ | ○ | ○ | ○ | ○ | ● | ● | ○ | ○ |
| | Oxidative | ● | ● | ● | ● | ● | ● | ● | ● | ● | ● | ● | ● |
| | Wet explosion | ● | ● | ● | ● | ● | ● | ● | ● | ● | ● | ● | ● |
| | Saline | X | ● | ● | ● | ○ | ● | ● | ● | ● | ● | ● | ○ |
| | Ionic liquids | X | ● | ● | ● | ● | ● | ● | ● | ● | ● | ● | ● |
| Biological | Fungus | ● | ● | ● | ● | X | ○ | ○ | ● | X | ● | ● | ○ |
| | Bacteria | ● | ● | ● | ● | X | ○ | ○ | ● | X | ● | ● | ○ |
| | Ensiling | ● | ● | ○ | ○ | X | ○ | ○ | ● | X | ● | ● | ○ |

**Table 3.3 Influence of factors involved in pretreatment methods (continued)** (Achkar et al. 2018; Alexandropoulou et al. 2016; Amin et al. 2017; Baruah et al. 2018; Borand and Karaosmanoğlu 2018; Dutra et al. 2018; Krishania et al. 2013; Laghari et al. 2016; Patowary and Baruah 2018; Perendeci et al. 2018; Tsapekos et al. 2016; Vasmara et al. 2017; Venturin et al. 2018; Ward-Doria et al. 2016)

| | Pretreatment method | Factors affecting | | | | | |
|---|---|---|---|---|---|---|---|
| | | Porosity | Total solids | Calorific value | CHNSO elements | Volatile fatty acids | Protein content |
| Physical | Comminution (milling & grinding) | ● | ● | ○ | ○ | **X** | **X** |
| | Steam explosion | ● | ● | ● | ● | ○ | ○ |
| | Liquid hot water | ● | ● | ● | ● | ○ | ○ |
| | Extrusion | ● | ● | ○ | ○ | **X** | **X** |
| | Ultrasound irradiation | ● | ● | ● | ● | ○ | ○ |
| Chemical | Alkaline | ● | ● | ● | ● | ● | ● |
| | Acidic | ● | ● | ● | ● | ● | ● |
| | Organosolv | ○ | ● | ● | ● | ● | ● |
| | Oxidative | ● | ● | ● | ● | ● | ● |
| | Wet explosion | ● | ● | ● | ● | ● | ● |
| | Saline | ○ | ● | ● | ● | ● | ● |
| | Ionic liquid | ○ | ● | ● | ● | ● | ● |
| Biological | Fungus | ○ | ● | ○ | ○ | ○ | ● |
| | Bacteria | ○ | ● | ○ | ○ | ○ | ● |
| | Ensiling | ○ | ● | ○ | ○ | ○ | ● |

●: Major role; ○: Minor role; **X**: No role

In this phase I, predetermination of the best pretreatment method for biogas generation before the anaerobic digestion was done. The study includes the integration of Design of Experiments (DoE) with the TOPSIS approach to tackling the difficulty in assigning weights during the selection process. A comparison in the ranks between integrated DoE-TOPSIS and TOPSIS was accomplished along with this research. According to the previous studies, the DoE-TOPSIS features weights, making them less sensitive to frame the relative importance or dominance of weights (Sabaghi et al. 2015; Tansel 2012; Tansel Yusuf 2014; Wang et al. 2013). The selection of the best pretreatment method was made based on the prioritization results from both techniques. The direct selection of the pretreatment method can be employed without performing the actual set of AD experiments. Thus, limiting the digesters count to one single digester without compromising the maximum biogas yield.

## 3.4 Phase I: To prioritize the best pretreatment method for lignocellulosic biomass for enhanced biogas yield using MADM techniques.

### 3.4.1 TOPSIS approach

TOPSIS method is a widely accepted technique known for its simplicity and user-friendly approach for ranking the alternatives according to the ranking score. It is also well known for its easy computational practice, and it can be grouped with other MADM approaches to solve complex problems in a structured and easy manner. The advantage of TOPSIS over other methods is interpreted data can be given directly as input by not considering the past mathematical calculations (Tansel 2014; Tansel and Ergun 2011). Here, the methodology was used to evaluate and rank the pretreatment method for the lignocellulosic biomass with due emphasis on attributes. The methodology is as follows, 1) selection of pertinent attribute, 2) TOPSIS analysis 3) selection from the priority list (Bhangale et al. 2004; A. Kumar and Agrawal 2009).

Phase 1: Selection of pertinent attribute

The application-specific attributes were selected from the pool of attributes considered for the pretreated substrate anaerobic digestion. The irrelevant attributes were eliminated.

Phase 2: TOPSIS analysis

The analysis using TOPSIS was done, as explained below in steps 1-8.

Step 1: Decision matrix (DM) development:

The decision matrix contains the attribute values corresponding to the alternatives. The attributes were arranged in a column, whereas alternatives along the row to form matrix as given in Eq. 3.1:

$$D= [xij]_{mxn,} \qquad (3.1)$$

Where, i = 1, 2, 3… m and j = 1, 2, 3… n;

      m is the number of attributes,

      n is the number of alternatives

Step 2: Normalized Decision Matrix (NDM) development

The computationally efficient and symmetric vector normalization of the decision matrix values brings all values to the same dimensionality (Vafaei et al. 2015; Yang et al. 2017). This transformation process helps in comparing the input data on a common scale and done using the Eq. 3.2:

$$r_{ij} \;=\; \frac{X_{ij}}{\sqrt{\sum_{u=1}^{m} X_{uj}{}^2}}, \qquad (3.2)$$

The $r_{ij}$ matrix denotes the normalized decision matrix.

Step 3: Relative Importance Matrix (RIM) development

The field experts frame the RIM by judging the importance of one attribute to another attribute concerning the problem statement. The scale of judgment was based on the Analytical Hierarchical Process (AHP) by Saaty (2008).

Step 4: Formation of Eigenvalues

The Eigenvalues calculation and the weights associated with each attribute were obtained using MATLAB code. The procedure to find the weights for each criterion was developed by Saaty (2008) and represented as a matrix $w_{ij}$. The determination of Consistency Index (CI) and Consistency Ratio (CR) were checked to check the

consistency of the judgement. If the CR value is lesser or equal to 0.1, the considered judgemental matrix is consistent in nature (Alonso and Lamata 2006; Kolios et al. 2016).

Step 5: Development of a Weighted Normalized Matrix (WNM)

These weights were incorporated into the normalized decision matrix to obtain the weighted normalized matrix. Thus, the values attained for each attribute can be structured to a comparable form and denoted as given in Eq. 3.3:

$$\text{WNM}, a_{ij} = w_{ij} \times r_{ij}, \tag{3.3}$$

Step 6: Estimation of ideal best and ideal worst solution

Let $I^+$ and $I^-$ be the ideal best and ideal worst solution for the given attributes. The ideal best and the ideal worst solutions were found by considering maximum and minimum values from the alternatives for each attribute. If the $j^{th}$ attribute is a beneficial factor and follows, as mentioned in Eq. 3.4 and 3.5:

$$I^+ = \max\{a_{ij}, i = 1, 2, 3 \ldots, m\}, \tag{3.4}$$

$$I^- = \min\{a_{ij}, i = 1, 2, 3 \ldots, m\}, \tag{3.5}$$

If the attribute is non-beneficial, consider the Eq. 3.6 and 3.7:

$$I^+ = \min\{a_{ij}, i = 1, 2, 3 \ldots, m\}, \tag{3.6}$$

$$I^- = \max\{a_{ij}, i = 1, 2, 3 \ldots, m\}, \tag{3.7}$$

Step 7: Calculation of separation measures

The distance between each attribute and its corresponding ideal positive solution ($I^+$) is called a Positive Separation Measures (PSM). Similarly, the distance between the attributes and the ideal negative solution ($I^-$) is called a Negative Separation Measure (NSM). The PSM and NSM calculation for each alternative is as mentioned below in Eq. 3.8 & 3.9,

$$S^{i+} = \sqrt{(a_{i1} - I^+{}_1) + (a_{i2} - I^+{}_2) + \cdots + (a_{in} - I^+{}_n)} \tag{3.8}$$

$$S^{i\text{-}} = \sqrt{(a_{i1} - I^-_1) + (a_{i2} - I^-_2) + \cdots + (a_{in} - I^-_n)} \tag{3.9}$$

Step 8: Calculation of TOPSIS score or relative closeness of a particular alternative

The TOPSIS score or relative closeness of each alternative to its ideal solution can be found using the Eq. 3.10:

$$\text{TOPSIS scores} = \frac{S^-}{S^+ + S^-} \tag{3.10}$$

Phase 3: Selection from the priority list

According to the decreasing order of the TOPSIS scores, a ranking list of the alternatives was provided. The alternatives having identical TOPSIS scores have assigned the same rank. The first rank alternative was selected as the best alternative or the best pretreatment method.

### 3.4.2 Integrated TOPSIS-DOE approach

Design of experiments (DoE) is a statistical method applied to evaluate the effect of various factors simultaneously. The changes in input variables (independent variables) are made to determine their effects on the output variable (dependent variables). In this study, the complete factorial design ($2^k$) illustrates the variation in the TOPSIS scores with the attributes. The 'k' denotes the number of attributes considered in the model. The upper and lower levels of attributes selected for the factorial design is the maximum and minimum values that an attribute can accept. Generally, in the DoE, the critical attributes are determined by fitting the data related to the problem statement in a multiple linear regression analysis (Tansel 2014). In this design, we try to examine the linear effects of attributes on TOPSIS scores. Figure 3.1 below shows the steps in the integrated TOPSIS- DoE approach.

**MADM problem** → **Decision Matrix (DM)** → **Normalised Decision Matrix (NDM)**

Levels of attributes (Upper/Lower)

$2^k$ factorial design ← **Design expert 10 software**

Decision matrix set

Normalised Decision Matrix (NDM)

Determination of weights

Formation of Relative Importance Matrix

Scaling of relative importance (1-10)

3 Replications

Analytical Hierarchy Process (AHP)

Normalised Decision Matrix (NDM)

TOPSIS scores (3 replications)

$2^k$ factorial design analysis

$2^k$ factorial design analysis

Assign ranks for the alternative

DoE

**Figure 3.1 Application steps of the integrated TOPSIS-DoE approach**

*3.4.3 Illustrative example*

For the analysis i.e., to screen the best pretreatment method by TOPSIS and Integrated TOPSIS-DoE method, the base date i.e., composition of biomass (cellulose, Hemicellulose, Lignin, Total Carbon and C/N ratio) and the yield of biogas, corresponding to pretreatment (seven) methods were adopted from Song et al. (2014). The biomass used in the study was the corn straw, and they have examined the effect of seven pretreatment methods in biogas production under batch mode and on the mesophilic condition, as shown below. The corn straw and AH have similar biomass compositions as shown in Table 3.4, so used in this study (Rocha-Meneses et al. 2017; Wojcieszak et al. 2020).

**Table 3.4 Comparison of biomass compositions between corn stalk and AH**

| Feedstock | Cellulose (%) | Hemicellulose (%) | Lignin (%) |
|---|---|---|---|
| Corn stalks | 39-48.7 | 24-35.8 | 7.6-20.1 |
| Arecanut husk | 48.1 | 24.6 | 22.1 |

The data for the analysis of the model and to select the best pretreatment method to yield maximum biogas (Song et al. 2014) can be referred from Table 3.5 along with their notations. They have examined the effect of seven pretreatment methods in biogas production under batch mode and on the mesophilic condition. The pretreatments applied were $H_2SO_4$(2%), HCl(2%), $CH_3COOH$(4%), $H_2O_2$(3%), NaOH(8%), $Ca(OH)_2$(8%), and $NH_3.H_2O$(10%).

**Table 3.5 Data considered for modelling (Song et al. 2014)**

| Pretreatment method | Decision matrix | | | | |
|---|---|---|---|---|---|
| | Cellulose (%) | Hemicellulose (%) | Lignin (%) | Total carbon (%) | C/N ratio |
| 2% $H_2SO_4$ | 41.3 | 22.5 | 7.3 | 30.6 | 38.7 |
| 2% HCl | 40.4 | 22.2 | 7.2 | 32.4 | 39.5 |
| 4% $CH_3COOH$ | 30.4 | 15.1 | 6.7 | 26.4 | 32.2 |
| 3% $H_2O_2$ | 30.8 | 14.3 | 5.7 | 25.1 | 30.6 |
| 8% $Ca(OH)_2$ | 46.7 | 16.2 | 4.6 | 33.7 | 42.1 |
| 8%NaOH | 46.3 | 16.4 | 5.4 | 29.4 | 38.7 |
| 10% $NH_3.H_2O$ | 45.1 | 17.8 | 5.5 | 30.7 | 37.4 |

*3.4.3.1 TOPSIS model*

Phase 1: Selection of pertinent attribute

The main aim of the present decision making is to maximize the biogas generation. Attributes that are highly influencing methane generation can be considered. The pretreatment option mainly facilitates the reduction in lignin inhibitions and enhances methane production. The pretreatment helps in the reduction of lignin content can increase the accessibility to cellulose and hemicellulose. From the various attributes considered for pretreatment options, some are interdependent. For example, any reduction in the cellulose, hemicellulose and lignin content forms the degradation compounds inhibitory in nature.

Moreover, lignin content shows a negative correlation with methane production, as studied by (Monlau et al. 2012) So, cellulose hemicellulose and lignin content can be

considered an essential attribute responsible for methane production. The total Carbon (TC) and C/N ratio analysis affirmed that on pretreatment, the TC decreases, and the C/N ratio drops down to a range of 20-30, which is crucial for an efficient anaerobic digester performance (Song et al. 2014). Hence, the present study's selected pertinent attributes were cellulose, hemicellulose, lignin content, TC and C/N ratio. The study's database was obtained from the batch mode digestion study done by (Song et al. 2014) on corn stalks. The importance is given to select attributes as beneficial and non-beneficial attributes (Bhangale et al. 2004). In this research, the attribute values were considered after pretreatment with cellulose, hemicellulose, total carbon, and C/N ratio as the beneficial attributes and lignin content as the non-beneficial attribute. The selection of the pertinent attributes from the list of attributes primarily depends on the designer's choice by considering economic feasibility, technical difficulty, field conditions and viability (Rao and Baral 2011).

Phase 2: TOPSIS analysis

The explanation for the analysis of TOPSIS is given below.

Step 1: Decision matrix (DM) development:

The matrix contains the attribute values (column-wise) corresponding to the alternatives (row-wise). The attributes were denoted as 'A' and alternatives as 'P'. This illustrative example; forms a 7x5 decision matrix, and the decision matrix (D) is shown below in Eq. 3.11:

$$
D = \begin{bmatrix}
Cellulose & Hemicellulose & Lignin & TC & C/N \\
41.3 & 22.5 & 7.3 & 30.6 & 38.7 \\
40.4 & 22.2 & 7.2 & 32.4 & 39.5 \\
30.4 & 15.1 & 6.7 & 26.4 & 32.2 \\
30.8 & 14.3 & 5.7 & 25.1 & 30.6 \\
46.7 & 16.2 & 4.6 & 33.7 & 42.1 \\
46.3 & 16.4 & 5.4 & 29.4 & 38.7 \\
45.1 & 17.8 & 5.5 & 30.7 & 37.4
\end{bmatrix} \tag{3.11}
$$

Step 2: Normalized decision matrix (NDM) development

Vector normalization was done and have made into single dimensionality with values less than 1. The NDM was developed as shown in Eq. 3.12:

$$\text{NDM} = \begin{bmatrix} 0.3839 & 0.4712 & 0.4501 & 0.3869 & 0.3929 \\ 0.3756 & 0.4649 & 0.4439 & 0.4096 & 0.4010 \\ 0.2826 & 0.3162 & 0.4131 & 0.3338 & 0.3269 \\ 0.2863 & 0.2995 & 0.3514 & 0.3173 & 0.3107 \\ 0.4304 & 0.3435 & 0.3329 & 0.3717 & 0.3929 \\ 0.4342 & 0.3393 & 0.2836 & 0.4261 & 0.4275 \\ 0.4193 & 0.3727 & 0.3391 & 0.3881 & 0.3797 \end{bmatrix} \quad (3.12)$$

Step 3: Relative Importance Matrix development

The group of experts decides the Relative Importance Matrix (RIM) by scaling the judgment from 1-9 (Saaty 2008) and is depicted as shown in Eq. 3.13:

$$\text{RIM} = \begin{bmatrix} 1.0000 & 5.0000 & 7.0000 & 0.2000 & 0.1100 \\ 0.2000 & 1.0000 & 3.0000 & 4.0000 & 7.0000 \\ 0.1400 & 0.3300 & 1.0000 & 0.2000 & 0.1100 \\ 5.0000 & 0.2500 & 5.0000 & 1.0000 & 0.1400 \\ 9.0000 & 0.1400 & 9.0000 & 7.0000 & 1.0000 \end{bmatrix} \quad (3.13)$$

Step 4: Determination of weights

The Eigenvalues for the weight determination was calculated from the Eigenvectors of relative importance matrix Eigenvalues using MATLAB code. The procedure to find the weights for each criterion was developed by Saaty (2008). The weights for each attribute is shown as given in Eqn. 3.14. The CI and CR values for the judgment set were calculated as 0.077 and 0.068, respectively, less than 0.1, showing better consistency and reliability.

$$w = [0.1902 \quad 0.1311 \quad 0.4132 \quad 0.1491 \quad 0.1164] \quad (3.14)$$

Step 5: Development of a weighted normalized matrix (WNM)

The normalized decision matrix multiplied to the attribute weight matrix gives a weighted normalized matrix as detailed in Eq. 3.15:

$$\text{WNM} = \begin{bmatrix} 0.0730 & 0.0618 & 0.1860 & 0.0577 & 0.0457 \\ 0.0715 & 0.0609 & 0.1834 & 0.0611 & 0.0467 \\ 0.0538 & 0.0414 & 0.1707 & 0.0498 & 0.0380 \\ 0.0545 & 0.0392 & 0.1452 & 0.0473 & 0.0361 \\ 0.0819 & 0.0450 & 0.1376 & 0.0554 & 0.0457 \\ 0.0826 & 0.0445 & 0.1172 & 0.0635 & 0.0497 \\ 0.0798 & 0.0489 & 0.1401 & 0.0579 & 0.0442 \end{bmatrix} \quad (3.15)$$

Step 6: Estimation of ideal best and ideal worst solution

The maximum and minimum values of attributes account for the ideal best and the ideal

worst solution. The ideal best and worst solution for cellulose, hemicellulose, lignin content, TC and C/N ratio were tabulated in Table 3.6.

**Table 3.6 Ideal best and ideal worst solutions for the attributes.**

| Attribute | Cellulose | Hemicellulose | Lignin | TC | C/N ratio |
|---|---|---|---|---|---|
| Ideal best (+) | 0.0826 | 0.0618 | 0.1172 | 0.0473 | 0.0361 |
| Ideal worst (-) | 0.0537 | 0.0392 | 0.1859 | 0.0635 | 0.0497 |

Step 7: Separation measure determinations

The Euclidean distance between the alternative and its particular ideal solution gives the separation measure for each alternative. The positive separation measure and negative separation measure for each alternative were shown in Table 3.7.

Step 8: Calculation of TOPSIS score or relative closeness of a particular alternative

The TOPSIS scores calculated as per equation (Eq. 3.10) were depicted in Table 3.6 given below.

Phase 3: Selection from the priority list

The ranking of alternatives was in accordance with the decrease in the suitability index value. The alternative with the highest TOPSIS score has chosen as the best pretreatment method. The ranking for each alternative was shown in Table 3.7, along with separation measures and TOPSIS scores.

**Table 3.7 Positive and negative separation measures, TOPSIS scores and ranking of alternatives.**

| Alternatives | Positive separation measure | Negative separation measure | TOPSIS scores | Rank |
|---|---|---|---|---|
| P1 | 0.0708 | 0.0304 | 0.3007 | 5 |
| P2 | 0.0693 | 0.0283 | 0.2903 | 6 |
| P3 | 0.0641 | 0.0237 | 0.2703 | 7 |
| P4 | 0.0456 | 0.0459 | 0.5015 | 4 |
| P5 | 0.0292 | 0.0569 | 0.6611 | 2 |
| P6 | 0.0273 | 0.0747 | 0.7323 | 1 |
| P7 | 0.0295 | 0.0541 | 0.6466 | 3 |

*3.4.3.2 Integrated TOPSIS-DoE method*

Step 1: Factor level determination

As per Table 3.4, cellulose (A1) with a maximum level of 49.3 and a minimum level of 30.4, hemicellulose (A2) with a maximum level of 28.8 and a minimum level of 14.3, lignin (A3) with a maximum level of 7.5 and a minimum level of 4.6, TC (A4) with a maximum level of 42.3 and a minimum level of 25.1, and C/N ratio (A5) with a maximum level of 51.4 and a minimum level of 30.6, were determined as the levels of factors affecting the selection of best pretreatment method.

Step 2: Decision matrix development

The independent attribute variables (A1, A2, A3, A4 and A5) and their factor levels were used to obtain the TOPSIS scores, which forms the dependent output variables in the TOPSIS model. A 25 complete factorial design with 32 combinations were studied. Only minimum and maximum levels of each attribute were considered to perform the data collection using TOPSIS models.

Step 3: TOPSIS model replications

The replications were carried out by taking random weight sets, which follows independence for the set of combinations. Here, three replications performed accounts for 32 combinations using three sets of independent random attribute weights. The weights were determined using the 9 point scale (Sen and Yang 1998) and incorporated into the decision matrix. The $2^5$ full factorial design was based on five attributes, two levels, and three replications, as shown in Table 3.

## Table 3.8 2⁵ full factorial design results

| Run | Factor 1 Cellulose | Factor 2 Hemicellulose | Factor 3 Lignin | Factor 4 TC | Factor 5 C/N Ratio | Response 1 TOPSIS scores | Run | Factor 1 Cellulose | Factor 2 Hemicellulose | Factor 3 Lignin | Factor 4 TC | Factor 5 C/N Ratio | Response 1 TOPSIS scores |
|---|---|---|---|---|---|---|---|---|---|---|---|---|---|
| 1 | 49.3 | 28.8 | 7.5 | 25.1 | 30.6 | 5.872 | 49 | 49.3 | 14.3 | 4.6 | 25.1 | 30.6 | 87.999 |
| 2 | 49.3 | 28.8 | 4.6 | 25.1 | 30.6 | 2.234 | 50 | 30.4 | 14.3 | 7.5 | 25.1 | 51.4 | 98.337 |
| 3 | 49.3 | 14.3 | 7.5 | 25.1 | 51.4 | 98.882 | 51 | 49.3 | 14.3 | 7.5 | 25.1 | 30.6 | 15.116 |
| 4 | 49.3 | 28.8 | 4.6 | 42.3 | 30.6 | 94.036 | 52 | 49.3 | 28.8 | 4.6 | 25.1 | 30.6 | 98.775 |
| 5 | 49.3 | 14.3 | 4.6 | 25.1 | 30.6 | 15.968 | 53 | 30.4 | 14.3 | 7.5 | 25.1 | 30.6 | 8.751 |
| 6 | 30.4 | 14.3 | 4.6 | 25.1 | 30.6 | 100 | 54 | 49.3 | 14.3 | 7.5 | 42.3 | 30.6 | 11.85 |
| 7 | 30.4 | 14.3 | 4.6 | 25.1 | 30.6 | 100 | 55 | 49.3 | 14.3 | 4.6 | 25.1 | 51.4 | 80.056 |
| 8 | 30.4 | 28.8 | 7.5 | 25.1 | 30.6 | 0 | 56 | 49.3 | 14.3 | 7.5 | 25.1 | 51.4 | 100 |
| 9 | 30.4 | 28.8 | 4.6 | 42.3 | 30.6 | 74.018 | 57 | 49.3 | 28.8 | 4.6 | 42.3 | 30.6 | 0 |
| 10 | 49.3 | 28.8 | 4.6 | 42.3 | 51.4 | 81.791 | 58 | 49.3 | 28.8 | 7.5 | 42.3 | 30.6 | 15.004 |
| 11 | 30.4 | 14.3 | 7.5 | 42.3 | 30.6 | 2.507 | 59 | 49.3 | 14.3 | 7.5 | 25.1 | 30.6 | 94.622 |
| 12 | 30.4 | 14.3 | 7.5 | 25.1 | 51.4 | 94.258 | 60 | 30.4 | 14.3 | 7.5 | 42.3 | 51.4 | 6.113 |
| 13 | 30.4 | 28.8 | 7.5 | 25.1 | 30.6 | 17.256 | 61 | 49.3 | 14.3 | 7.5 | 42.3 | 30.6 | 13.218 |

| | | | | | | | | | | | | |
|---|---|---|---|---|---|---|---|---|---|---|---|---|
| 14 | 30.4 | 28.8 | 7.5 | 25.1 | 51.4 | 34.87 | 62 | 30.4 | 14.3 | 7.5 | 42.3 | 51.4 | 47.158 |
| 15 | 49.3 | 14.3 | 7.5 | 42.3 | 51.4 | 89.117 | 63 | 30.4 | 14.3 | 7.5 | 25.1 | 51.4 | 79.556 |
| 16 | 49.3 | 28.8 | 7.5 | 42.3 | 30.6 | 7.189 | 64 | 30.4 | 28.8 | 7.5 | 42.3 | 51.4 | 100 |
| 17 | 30.4 | 28.8 | 4.6 | 25.1 | 51.4 | 96.693 | 65 | 49.3 | 14.3 | 7.5 | 42.3 | 30.6 | 97.259 |
| 18 | 30.4 | 14.3 | 7.5 | 25.1 | 30.6 | 11.971 | 66 | 49.3 | 14.3 | 4.6 | 42.3 | 51.4 | 11.892 |
| 19 | 49.3 | 28.8 | 4.6 | 25.1 | 51.4 | 62.574 | 67 | 30.4 | 28.8 | 4.6 | 25.1 | 51.4 | 93.216 |
| 20 | 49.3 | 14.3 | 7.5 | 25.1 | 51.4 | 8.487 | 68 | 30.4 | 14.3 | 7.5 | 42.3 | 51.4 | 72.433 |
| 21 | 30.4 | 14.3 | 4.6 | 42.3 | 30.6 | 34.448 | 69 | 30.4 | 28.8 | 7.5 | 42.3 | 30.6 | 7.254 |
| 22 | 30.4 | 14.3 | 4.6 | 42.3 | 51.4 | 97.229 | 70 | 30.4 | 14.3 | 4.6 | 25.1 | 51.4 | 99.457 |
| 23 | 30.4 | 14.3 | 4.6 | 42.3 | 30.6 | 99.964 | 71 | 49.3 | 28.8 | 7.5 | 42.3 | 51.4 | 86.36 |
| 24 | 49.3 | 28.8 | 4.6 | 25.1 | 51.4 | 62.574 | 72 | 30.4 | 14.3 | 7.5 | 42.3 | 30.6 | 8.991 |
| 25 | 30.4 | 28.8 | 7.5 | 25.1 | 51.4 | 87.556 | 73 | 49.3 | 14.3 | 7.5 | 25.1 | 30.6 | 82.174 |
| 26 | 49.3 | 28.8 | 7.5 | 42.3 | 30.6 | 67.18 | 74 | 30.4 | 28.8 | 4.6 | 25.1 | 30.6 | 11.507 |
| 27 | 30.4 | 28.8 | 7.5 | 25.1 | 51.4 | 84.638 | 75 | 49.3 | 14.3 | 4.6 | 25.1 | 51.4 | 94.118 |
| 28 | 49.3 | 14.3 | 7.5 | 42.3 | 51.4 | 73.157 | 76 | 49.3 | 14.3 | 4.6 | 42.3 | 51.4 | 87.436 |
| 29 | 49.3 | 28.8 | 7.5 | 25.1 | 51.4 | 100 | 77 | 30.4 | 14.3 | 7.5 | 42.3 | 30.6 | 0 |
| 30 | 30.4 | 28.8 | 7.5 | 42.3 | 51.4 | 100 | 78 | 30.4 | 28.8 | 4.6 | 25.1 | 51.4 | 100 |
| 31 | 30.4 | 28.8 | 4.6 | 42.3 | 30.6 | 89.739 | 79 | 49.3 | 14.3 | 4.6 | 25.1 | 51.4 | 100 |
| 32 | 30.4 | 14.3 | 4.6 | 25.1 | 30.6 | 0 | 80 | 49.3 | 14.3 | 7.5 | 42.3 | 51.4 | 8.457 |
| 33 | 49.3 | 28.8 | 7.5 | 25.1 | 30.6 | 97.668 | 81 | 49.3 | 28.8 | 4.6 | 25.1 | 51.4 | 95.284 |
| 34 | 30.4 | 28.8 | 4.6 | 25.1 | 30.6 | 99.118 | 82 | 49.3 | 14.3 | 4.6 | 42.3 | 51.4 | 99.991 |

| 35 | 49.3 | 28.8 | 4.6 | 42.3 | 30.6 | 100 | 83 | 30.4 | 28.8 | 7.5 | 42.3 | 30.6 | 5.007 |
|---|---|---|---|---|---|---|---|---|---|---|---|---|---|
| 36 | 49.3 | 28.8 | 4.6 | 25.1 | 30.6 | 14.254 | 84 | 49.3 | 14.3 | 4.6 | 42.3 | 30.6 | 10.058 |
| 37 | 49.3 | 14.3 | 4.6 | 42.3 | 30.6 | 45.241 | 85 | 30.4 | 28.8 | 4.6 | 42.3 | 51.4 | 97.334 |
| 38 | 30.4 | 14.3 | 7.5 | 25.1 | 30.6 | 97.448 | 86 | 30.4 | 14.3 | 4.6 | 42.3 | 51.4 | 100 |
| 39 | 30.4 | 28.8 | 4.6 | 42.3 | 51.4 | 91.057 | 87 | 30.4 | 14.3 | 4.6 | 42.3 | 30.6 | 11.469 |
| 40 | 30.4 | 14.3 | 4.6 | 25.1 | 51.4 | 15.742 | 88 | 49.3 | 28.8 | 7.5 | 25.1 | 51.4 | 89.289 |
| 41 | 30.4 | 28.8 | 7.5 | 25.1 | 30.6 | 3.456 | 89 | 49.3 | 28.8 | 7.5 | 42.3 | 51.4 | 97.375 |
| 42 | 30.4 | 28.8 | 7.5 | 42.3 | 51.4 | 98.779 | 90 | 49.3 | 28.8 | 4.6 | 42.3 | 51.4 | 14.008 |
| 43 | 49.3 | 14.3 | 4.6 | 42.3 | 30.6 | 88.577 | 91 | 49.3 | 28.8 | 7.5 | 25.1 | 30.6 | 100 |
| 44 | 49.3 | 28.8 | 7.5 | 25.1 | 51.4 | 9.007 | 92 | 49.3 | 28.8 | 4.6 | 42.3 | 51.4 | 17.282 |
| 45 | 30.4 | 28.8 | 4.6 | 42.3 | 30.6 | 100 | 93 | 30.4 | 28.8 | 4.6 | 25.1 | 30.6 | 97.084 |
| 46 | 30.4 | 14.3 | 4.6 | 25.1 | 51.4 | 94.63 | 94 | 49.3 | 28.8 | 7.5 | 42.3 | 51.4 | 100 |
| 47 | 30.4 | 14.3 | 4.6 | 42.3 | 51.4 | 97.486 | 95 | 30.4 | 28.8 | 4.6 | 42.3 | 51.4 | 97.897 |
| 48 | 49.3 | 14.3 | 4.6 | 25.1 | 30.6 | 5.009 | 96 | 30.4 | 28.8 | 7.5 | 42.3 | 30.6 | 0 |

Step 4: Regression model determination

The evaluation of experimental results can be done using the ANOVA table, which summarizes the main effects and the interactions. The ANOVA (Analysis of Variance) with a five-factor interaction (5FI) effect analyses the DoE layout using the Design expert 10 software. The ANOVA results were shown in Table 3.9. The Fischer (F-value) of 4.33 for the model shows that the model was significant. The terms corresponding to p-value <0.05 indicates their significance with 95% of confidence. The significance of the attributes and their interactions can be studied using ANOVA. From Table 3.8, it is clear that lignin content and C/N ratio interactions were significant model terms (p-value <0.05) whereas, their two-factor, three-factor, four-factor and five-factor interactions were non-significant terms (p-value >0.05). So, the regression equation has only statistically significant terms as coded factors.

**Table 3.9 ANOVA results for the model**

| Source | Sum of Squares | df | Mean Square | F Value | p-value Prob > F | |
|---|---|---|---|---|---|---|
| Model | 30611.74 | 5 | 6122.35 | 4.33 | 0.0014 | significant |
| A-Cellulose | 170.63 | 1 | 170.63 | 0.12 | 0.7290 | |
| B-Hemicellulose | 448.95 | 1 | 448.95 | 0.32 | 0.5744 | |
| C-Lignin | 5606.28 | 1 | 5606.28 | 3.97 | 0.0494 | |
| D-TC | 876.92 | 1 | 876.92 | 0.62 | 0.4329 | |
| E-C/N ratio | 23508.96 | 1 | 23508.96 | 16.64 | < 0.0001 | |
| Residual | 1.272E+005 | 90 | 1412.98 | | | |
| Lack of Fit | 39050.02 | 26 | 1501.92 | 1.09 | 0.3780 | not significant |
| Pure Error | 88118.47 | 64 | 1376.85 | | | |
| Cor Total | 1.578E+005 | 95 | | | | |

The TOPSIS score obtained for the above model is represented in Eq. 3.16 given below,

TOPSIS score= 36.59904 + ((C/N ratio x 1.20851) -(5.27028 x lignin content)) (3.16)

Eq. 3.16 represents the linear regression relation between the C/N ratio, lignin content and the TOPSIS scores since no significant interactions among the attributes. The positive coefficient term indicates direct proportional, whereas a negative coefficient indicates inversely proportion to the response. Thus, we can confirm the lignin's

negative correlation and a positive correlation of C/N ratio with the considered response. The coefficient of determination ($R^2$) value of 0.95 shows that the significant factors model the response well.

Step 5: Prioritizing alternatives

Now, the regression can be used to find the TOPSIS scores for various alternatives. The decision makers were able to rank the alternatives according to the decreasing TOPSIS scores. Table 3.10 depicts the ranking of the alternatives obtained.

**Table 3.10 Comparison of ranking by TOPSIS and integrated TOPSIS-DoE method.**

| Alternatives | TOPSIS values | Rank | Integrated TOPSIS-DoE scores[*] | Rank | Difference between rank |
|---|---|---|---|---|---|
| P1 | 0.3007 | 5 | 44.8953 | 5 | 0 |
| P2 | 0.2903 | 6 | 46.3891 | 4 | 2 |
| P3 | 0.2703 | 7 | 40.2021 | 7 | 0 |
| P4 | 0.5015 | 4 | 43.5388 | 6 | -2 |
| P5 | 0.6611 | 2 | 54.9088 | 2 | 0 |
| P6 | 0.7323 | 1 | 63.2340 | 1 | 0 |
| P7 | 0.6466 | 3 | 52.8107 | 3 | 0 |

The best pretreatment method has been selected by analyzing the attributes using TOPSIS and integrated TOPSIS-DoE approaches. Seven pretreatment methods were taken into consideration in this study. The decreasing value of the TOPSIS score portrays the ranking of each alternative as given in table 3.10. The above studies observed that alkaline pretreatment has a higher rank than acidic pretreatment. As per the experimental study was done by Song et al. (2014), the highest methane yield was obtained for $Ca(OH)_2$ and $H_2O_2$ pretreatment followed by NaOH pretreatment. With due consideration of the cost, alkaline pretreatment was found to be efficient for biogas production. As per our statistical study, the results obtained matches well with the results of an experimental study done by Song et al. (2014). The results from TOPSIS

and TOPSIS-DoE analysis have a close resemblance. They can be adopted for decision-making in selecting the best pretreatment method for biogas production.

The selection of the best pretreatment method for enhanced biogas production from the lignocellulosic substrate is always a chaotic task. Pretreatment is essential in the case of lignocellulosic substrates as the lignin content cause hindrance to anaerobic digestion. The pretreatment method's prioritization was done using the MADM technique to figure out the best out of all.

There were many attributes concerned with the pretreatment aided anaerobic digestion. The selection of pertinent attributes can minimize the time taken for decision making. The increase in the number of pertinent attributes can raise the accuracy of the TOPSIS scores. The relative importance matrix varies with respect to the attributes and problem statement. The ideal best and worst solutions were calculated based on the attribute data for various alternatives. The ranking done for each alternative from the suitability index value gives the priority list. The weight sets reduce the sensitivity of the weights, and the regression equation was obtained using DoE. Further, the calculated TOPSIS scores from the regression equation were used for the ranking.

The best option obtained was the alkaline pretreatment both in terms of efficiency and economy. Similarly, the least preferred option was acidic pretreatment methods. The confirmation of the best pretreatment method obtained from the two techniques can be done using the experimental findings by the source. It was clear that alkaline pretreatment aided a rise in methane potential. It can be concluded that the model works well in prioritizing the pretreatment method for the sustainable conversion of lignocellulosic biomass to biogas.

# CHAPTER 4

# MATERIALS & METHODOLOGY

## 4.1 General

This chapter deals with the substrates and material selection, its characterization, and the experimental setup. Experimental work was carried out in three phases, as shown below.

Phase 1: To investigate the anaerobic digestion of pretreated AH with due emphasis on its biogas potential.

Phase 2: To evaluate the effect of mix ratio in batch mode anaerobic co-digester for biogas production.

Phase 3: To extract the lignin from AH and to synthesis a novel lignin-based material for oil-water separation.

Figure 4.1, shown below, depicts the experimental plan for the present research.
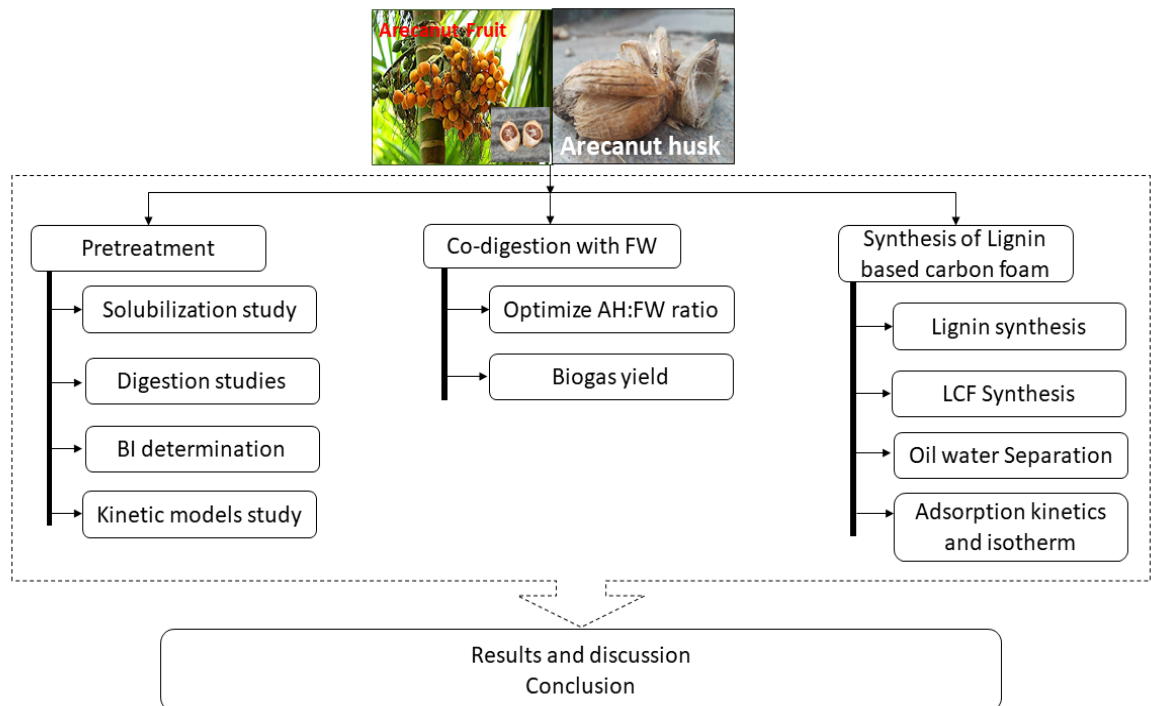


**Figure 4.1 Experimental plan for the present research**

## 4.2 Materials

### 4.2.1 Source of feedstock/substrate(s) and inoculum

The feedstock/substrate used in this research were AH, which belongs to agricultural waste, and food waste. AH was collected from north-western coastal areas of Kerala, India. The collected feedstock was cleaned for dirt removal, sun-dried for moisture free, and husk fibres were finely chopped to a size of 5 mm. The chopped AH was preserved at -11ºC in a zip-lock polythene bag until further use.

Food waste (FW) was collected from hostel canteens of National Institute of Technology Karnataka, India, which mainly contains leftover cooked foods, such as meats, rice, bread, roti and vegetables. The food waste was oven-dried and then crushed to a particle size of 1-2 mm by an electrical mixer grinder (*Bajaj twister grinder CL B*). Thawing of the AH at room temperature was done before using it for further analysis (Pellera et al. 2016).

The inoculum used was the anaerobic sludge obtained from the up-flow anaerobic sludge blanket reactor (UASBR), in a sewage treatment plant located at Kavoor, Mangalore, India. Before the usage, the preserved sludge was kept at room temperature (35ºC) to regain its microbial activity and allowed to get stabilized for later experiments.

### 4.2.2 Chemicals used

The chemical pretreatments for AH include, acidic, alkaline, oxidative and organosolv. $H_2SO_4$ (98%, w/w) was used for the acidic pretreatment whereas, NaOH pellets were used for alkaline pretreatment. Oxidative pretreatment was performed using $H_2O_2$ (standard grade of 30%) and organosolv by ethanol with 1% $H_2SO_4$. All the chemicals and reagents used for the study were of analytical grade, purchased from Sigma-Aldrich and Loba Chemie. The preparation of reagents was done using distilled water throughout the experiments. For oil-water separation experiments, 2T engine oil, petrol oil, and diesel oil were purchased from Indian petroleum lubricants, India. Crude sunflower oil was obtained from Anagha refineries, Baikampady, Karnataka, India. All other organic solvents such as toluene, petroleum ether, and n-hexane. The oils were

labelled with Sudan (III) dye for the visual identification were purchased from Loba Chemie, India.

## 4.3 Methodology

### 4.3.1 Characterization of substrate and inoculum

The initial characterization of raw AH, FW and inoculum includes pH using pH meter, total solids (TS) (NREL/TP-510-42621), and volatile solids (VS) (ASTM standard E872–82) in terms of TS (Laghari et al. 2016). Elemental (CHNSO) analysis was done using EuroEAElemental Analyzer, and higher heating value (HHV) was calculated from the CHNSO results (Awasthi et al. 2019). Biomass compositional analysis includes determining the percentage of cellulose, hemicellulose, and lignin after the removal of extractives from the AH. Extractive free residues were obtained by sequential Soxhlet extraction using various solvents such as distilled water, ethanol, and n-hexane (NREL/TP-510-42619), each at a solid loading of 1:50 ratio for 4 hours. Lignin (NREL/LAP), hemicellulose, and cellulose were determined by the Technical Association of Paper and Pulp Industry (TAPPI) method (Ayeni et al. 2015). The total reduced sugars (TRS) were determined by 3, 5-dinitrosalicylic acid (DNS) method. The total Kjeldahl nitrogen (TKN) was estimated using the Kjeldahl nitrogen apparatus (Upadhyay and Sahu 2012) for the targeted AH biomass. Crude protein was determined from the TKN value (Upadhyay and Sahu 2012).

### 4.3.2 Phase II: Investigate the anaerobic digestion of pretreated AH with due emphasis on its biogas potential.

#### 4.3.2.1 Pretreatment method adopted

A batch hydrolysis study on AH by four types of chemical pretreatment was adopted in this research to check its suitability for the biomethane production. The dosages of each pretreatment considered in this study are given below,

    (a) $H_2SO_4$: 2,4,6,8, and 10%

    (b) NaOH: 2,4,6,8, and 10%

    (c) $H_2O_2$: 2,4,6,8, and 10%

    (d) Ethanol in 1% $H_2SO_4$: 25%, 50%,75%, and 100%

All the pretreatments were performed at two process temperatures, i.e., at 25ºC and 90ºC, by fixing solids loading (1:10) and process duration (24 hours) in duplicates. The AH with no chemical pretreatment was considered as control. The temperature domain selection was to check the difference in the solubilization at room temperature and an elevated temperature so that the maximum temperature range was covered for the future upscaling of the process.

*4.3.2.2 Study on material solubilization*

The residues were separated by 0.45μm pore size filter paper using pressure filter after the pretreatment. The filtrate was analyzed for soluble chemical oxygen demand (sCOD) using APHA 5220C method and total phenols (TPC) using the Folin-Ciocalteu method (Xie et al. 2018). The residues obtained were washed and dried at 60ºC, and further checked for TS, VS, and biomass composition for different pretreated AH. All the experiments were conducted in duplicates. The selection of the best pretreatment method among the adopted pretreatments and process temperature was done from the solubilization study and was employed for the digestion studies. The structural and functional transformations in the selected pretreated AH, when compared with the raw AH, was checked before anaerobic digestion studies. The raw and pretreated AH's morphological changes can be studied through scanning electron microscopy (*JOEL-JSM-6380LASEM*). Similarly, Fourier transform infrared (FT-IR) spectra were recorded for the biomass samples ranged from 400-4000 cm$^{-1}$ (*Bruker alpha FTIR spectrophotometer*, resolution: 4 cm$^{-1}$). The attenuated total reflection (ATR) technique was employed for the samples to obtain the peaks.

*4.3.2.3 Bioreactor operation and anaerobic digestion study*

A set of 12 single-stage lab-scale digestion reactors (Schott Duran bottles) were employed in this study. The digesters of 1000 mL capacity sealed by septa with a working volume of 600 mL were used for the biogas potential assays. Biogas assays were initiated by introducing the inoculum and the substrates in the reactors in appropriate amounts and by subsequently adding deionized water to the mixture if needed, to bring the total volume to approximately 600 mL. It can be noted that deionized water was used instead of tap water, to avoid the eventual presence of traces of unknown substances, which might alter the results. The inoculum quantity in each assay was maintained at 15 gVS/L, and the substrate addition was done based on the

substrate to inoculum ratio (S/I) value. S/I was fixed to 0.8 on volatile solids (VS) basis (Capson-Tojo et al. 2017; Haider et al. 2015). Blank assays containing only inoculum (S/I = 0) were also performed since the inoculum was not degassed prior to BMP assays. Following this step, the pH of the mixture was adjusted at 7.8±0.05 by adding small amounts of NaOH (1 M). Flushing of $N_2$ was done to ensure an inert atmosphere and closed with a gas-tight stopper with septa. Experiments were conducted in the mesophilic condition maintained at 35±2˚C, and manual shaking was done several times a day for all bottles to ensure proper mixing of substrate and inoculum (Pellera and Gidarakos 2017).

The process parameters include pH, volatile fatty acids (VFA), and alkalinity, whereas process outcomes include the biogas volume and biogas composition. The daily biogas volume was measured daily using the water displacement method, whereas the $CH_4$ and $CO_2$ percentages were quantified once in a week using Gas Chromatography (*GC, Model: Thermo-1110 using a packed column, id: 0.53 mm*) equipped with thermal conductivity detector (TCD) at a flow rate of 36 ml/min with nitrogen as a carrier gas. A temperature of 120°C, 150°C, and 150°C was maintained at the oven, injector, and detector, respectively. Biogas measurement was terminated as the volume obtained was less than 1% of the reactor's total working volume.

*4.3.2.4 Biodegradability index (BI)*

At standard temperature and pressure (STP), the theoretical methane potential (TMP) of both raw and pretreated AH samples were predicted from the elemental composition (C, H, O, N and S) of each sample using stoichiometric degradation equation (Eq. 4.1) developed by Buswell and Hatfield (Achinas and Euverink 2016; Buswell and Hatfield 1980). This Equation can be used for both organic municipal waste and lignocellulosic biomass since they depend upon the relative quantities of C, H, O, N and S.

$$C_aH_bO_cN_dS_e + \left(a - \frac{b}{4} - \frac{c}{2} + \frac{3d}{4} + \frac{e}{2}\right) H_2O \rightarrow \left(\frac{a}{2} + \frac{b}{8} - \frac{c}{4} - \frac{3d}{8} - \frac{e}{4}\right) CH_4 + \left(\frac{a}{2} - \frac{b}{8} + \frac{c}{4} + \frac{3d}{8} + \frac{e}{4}\right) CO_2 + d\ NH_3 + e\ H_2S \qquad (4.1)$$
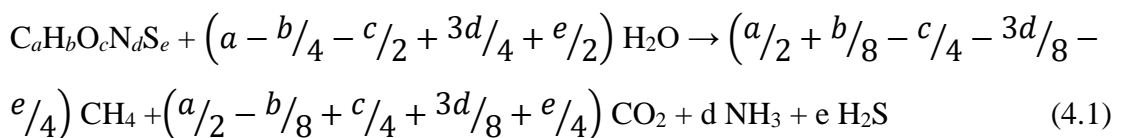
From the above stoichiometric Equation (4.1), TMP equation can be derived as shown in Eq. 4.2 below,

$$TMP\ (mL/gVS)_{STP} = 22.4 \text{ x } 1000 \text{ x } \frac{\left(\frac{a}{2} + \frac{b}{8} - \frac{c}{4} - \frac{3d}{8} - \frac{e}{4}\right)}{(12a + b + 16c + 14d + 32e)} \qquad (4.2)$$

This provides the information on maximum methane yield that can be achieved on the complete degradation of the biomass (Ali et al. 2018).

Specific Methane Potential (SMP) was obtained by converting the experimental cumulative methane yield after deducting the blank assay yield to STP conditions as given in Eq. (4.3) below,

BMP by experimental or Specific Methane Potential (SMP) =

$$\frac{Cumulative\ methane\ production_{STP}}{VS\ of\ sample\ added} \tag{4.3}$$

From these TMP and SMP values, the biodegradability index (BI) was estimated for raw and pretreated AH samples (Pellera and Gidarakos 2017) using the Eq. (4.4),

$$\text{Biodegradability index, BI (\%)} = \frac{SMP}{TMP} \times 100 \tag{4.4}$$

*4.3.2.5 Evaluation of model fitting*

In the present research, four kinetic models such as First-order exponential (FOE), Logistic function model (LFM), Transference/ Reaction curve function model, and Modified Gompertz model as listed in Eq. (4.5) - (4.8). The application of these models for the pretreatment aided anaerobic digestion from which kinetic parameters such as maximum biogas production potential (mL), maximal rate of biogas production (mL/day), and lag phase (λ, days) were determined. The FOE model assumes that hydrolysis is the rate-limiting step and follows a first-order decay rate (Edwiges et al. 2019). The other three exponential models assume that the biogas production rate is directly proportional to the microbial activity inside the anaerobic digester. Also, limitations in the substrate level do not influence microbial growth (Kainthola et al. 2019)

The experimental data obtained from the biogas potential assay was compared with kinetic analysis results through nonlinear regression using four kinetic models (Kainthola et al. 2019; Kumar et al. 2020).

(1) First-order exponential (FOE): $M = M_{max} \times [1 - exp(-kt)]$ (4.5)

(2) Logistic function model (LFM): $M = \dfrac{M_{max}}{1+exp([4\times R_{max}\times(\lambda-t)/P]+2)}$ (4.6)

(3) Transference/ Reaction curve function model: $M = M_{max} \times \Big\{1 - exp\Big[-\dfrac{R_{max}\times(\lambda-t)}{M_{max}}\Big]\Big\}$ (4.7)

(4) Modified Gompertz model: $M = M_{max} \times exp\left\{-exp\left[\frac{R_{max} \times e}{M_{max}}(\lambda - t) + 1\right]\right\}$

(4.8)

where,

M - cumulative biogas production (mL) at time t (days);

$M_{max}$ - maximum biogas production (mL);

k – kinetic rate constant (day$^{-1}$);

t- time in days;

$R_{max}$ - the maximum rate of biogas production (mL/day);

e - Euler's constant (e=2.718) and

λ - lag phase constant (days).

The model fit of experimental data, i.e., least-square nonlinear regression analysis, was performed using Microsoft's "Solver" tool (MS) Excel. This method targets the values $M_{max}$, $R_{max}$, and λ with the prime goal of minimizing the RSS. The predicted biogas potential from the nonlinear regression equations was plotted against the measured biogas potential to evaluate model fitness. The $R^2$ value and Residual Sum of Squares (RSS) value determine the model fitness of the kinetic study. The λ value reflects the minimum time required for the acclimatization of microbes present in the anaerobic digesters, which determines the digestion efficiency.

*4.3.2.6 Biomass composition and biodegradability index correlation*

A correlation between the biomass composition and biodegradability index is a requisite to indicate the anaerobic digestion performance and methane yield. To predict the biodegradability index of the biomass, statistical analysis was carried out by a simple linear regression to develop a model. A statistical linear equation was derived using statistical package for social sciences (SPSS) software (*IBM SPSS statistics 22*). The input variable considered for the analysis includes biomass compositional compounds, viz. Cellulose content (CC), Lignin content (LC), and Hemicellulose content (HC) for which the correlation was found to the output variable, i.e., BI. The model evaluation was done with the coefficient of determination ($R^2$ value), Residual Sum of Squares (RSS), and Analysis of Variance (ANOVA) for the input and output variables viz. biomass composition and BI.

*4.3.3 Phase III: To evaluate the effect of substrate mix ratio in batch mode anaerobic co-digester for biogas production.*

*4.3.3.1 Anaerobic digester configurations*

A series of potential biogas assay was experimentally performed in 1 L bench-scale amber-coloured anaerobic digesters at 35°C (mesophilic condition) in a batch mode operation. The operating factors assessed for this study of mix ratios, for the co-digestion of AH and food waste. Biogas test was performed in series with the different mix ratios (AH: FW) assay being performed first at a S/I ratio of 1, as mentioned in Table 4.1. Biogas produced from each bottle was collected, and measured by the water displacement method. Reference reactor is defined as the blanks containing only anaerobic sludge. The volume of biogas produced in the reference reactor is deducted from the volume of biogas produced by substrates to calculate the net biogas potential of substrate. All assays were performed in duplicates by providing intermediate manual shaking. Experiments were terminated when biogas yield is less (when the gas production drops below 1% of the total gas yield) within a week of digestion.

**Table 4.1 Conditions for co-digestion for biogas production**

| Reactor name | Mix ratio (based on VS) AH: FW | Operating conditions |
|---|---|---|
| M1 | 0:1 | |
| M2 | 1:3 | |
| M3 | 1:1 | a pH of 6.5-7.5 and S/I ratio of 1.0 |
| M4 | 3:1 | |
| M5 | 1:0 | |
| M6 | Blank | |

*4.3.3.2 Monitoring of the anaerobic digester*

The samples were drawn from the digesters using a 10mL syringe. The process parameters such as pH, VFA and alkalinity were considered for the digester monitor, as shown in Table 4.2. The process outcome was the biogas measurement was checked, as shown in Table 4.2. An immediate measurement of the pH was done, and samples were taken to check other parameters. For the analysis of VFA and alkalinity, samples were centrifuged at 8000 g for 10 mins, and the filtrate was taken for analysis.

**Table 4.2 Analytical methods for process parameters and process outcomes**

| Sl. No. | Parameter | Method of analysis | Sampling frequency |
|---|---|---|---|
| 1 | pH | Potentiometry (Electrode is dipped inside the sample to measure pH) | Once in three days |
| 3 | Volatile fatty acids (VFA) | Titration method using NaOH for VFA content Gas chromatography (GC - Trace 1110) for composition. | the initial and final day |
| 4 | Alkalinity | Acid-based titration method (Sample titrate against $H_2SO_4$, with Phenolphthalein indicator, colour change: pink to colourless) | The initial and final day |
| 5 | Biogas volume | Water displacement method | daily |

*4.3.4 Phase IV: To extract the lignin from AH and to synthesis novel lignin-based material for oil-water separation.*

*4.3.4.1 Isolation of lignin from AH*

Initially, the biomass composition such as Lignin (NREL/LAP), hemicellulose, and cellulose in AH was determined by the technical association of paper and pulp industry (TAPPI) method. Biomass compositional analysis includes determining the percentage of cellulose, hemicellulose, and lignin after removing extractives from the AH. Extractive free residues were obtained by sequential Soxhlet extraction using various solvents such as distilled water, ethanol, and n-hexane (NREL/TP-510-42619), each at a solid loading of 1:50 ratio for 4 hours. The extraction was done based on the slight modification in the method adopted (figure 4.2) in previous studies on sedge grass (Qu et al. 2017). Briefly, about 5g of extractive free AH of desired fibre length was soaked in a solution mixture (acetic acid (AA): formic acid (FA): distilled water) of 100mL in a ratio of 5:3:2 (v/v/v). The solution mixture with AH (1:20 of AH: Solution ratio) was heated at 60°C for 1 hr without agitation, and then, the temperature was elevated to 107°C for 3hrs under vigorous stirring. The solution mixture was allowed to cool then, filtered and the residues were repeatedly washed with the aqueous acetic acid of 0.5 N. Distillation of the filtrate was done at 118°C to recover the concentrated liquor. Lignin gets precipitated by water addition to the liquor, filtered and oven-dried at 40-50°C.
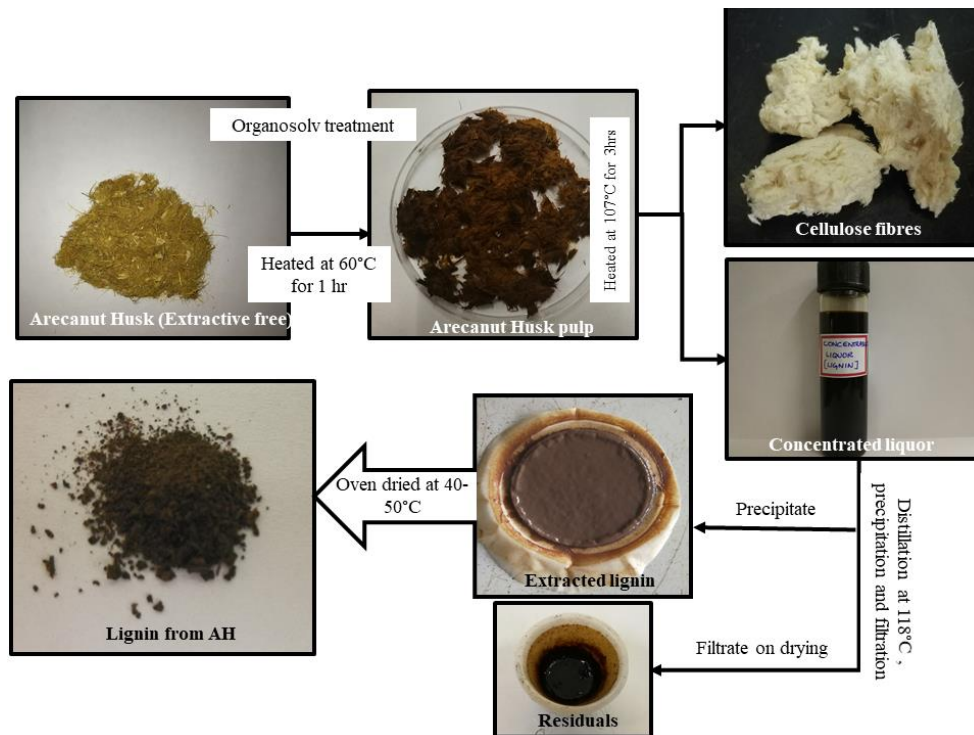
**Figure 4.2 Pictorial flow diagram of the extraction process of lignin from AH**

The lignin extraction was done for two-AH fibre size (a) less than 10 mm and (b) 10-20 mm to check the recovery efficiency varies according to the fibre size. The lignin yield and lignin recovery from AH were calculated from the measured extracted lignin as given in Eq. (4.9) and (4.10)

$$\text{Lignin yield (\%)} = \frac{\text{Weight of lignin extracted (mg)}}{\text{Weight of AH used in the extraction process (mg)}} \times 100 \qquad (4.9)$$

$$\text{Lignin recovery (\%)} = \frac{\text{Lignin Yield (\%wgt)}}{\text{Lignin content in AH(\%wgt)}} \times 100 \qquad (4.10)$$

Where, Lignin content = acid-soluble lignin+ acid-insoluble lignin (4.11)

### 4.3.4.2 Synthesis of Lignin based carbon foam (LCF)

The synthesis of lignin-based carbon foam (LCF) was performed rapidly, as stated below. Briefly, lignin, $ZnNO_3.6H_2O$ (acts as an oxidizing agent), and starch were added in 0.75:2:1 (w/w/w) ratio in a 100 mL beaker and heated at 180°C on a hotplate. The mixture gets liquified first and becomes a brownish gluey liquid. Further, a yellowish-brown foam was observed, which later forms a blackish foam-like material called

lignin-based carbon foam (LCF). The time expected for the whole reaction to complete is about 5 minutes.

### 4.3.4.3 Characterization of LS and LCF

The purity of the extracted lignin was confirmed by [1]H Nuclear magnetic resonance (NMR, *Variant 400 MHz*) analysis using DMSO-$d_6$ solvent. The morphological and structural characterisation of LS and LCF includes Field-emission scanning electron microscope (FESEM), Energy dispersive x-ray (EDAX) analysis, Fourier transform-infrared spectra (FTIR), and powder X-ray diffractometer (XRD). The morphological surface characteristics were observed by FESEM using *GeminiSEM 300-ZEISS* at an accelerating voltage of 3.00 kV. In addition, the pore size, pore volume and specific surface area analysis of LCF were done according to Brunauer–Emmett–Teller method (BET, *Belsorp Mini II*). N2 adsorption/desorption experiments at 77K help to determine the BET Specific surface area. The samples were degassed by holding at 90°C for 24 h before the experiments. At a relative pressure of 0.99, the calculation of total pore volume was done from $N_2$ adsorption data. The pore size of the LCF was determined by the Barrett-Joyner-Halenda (BJH) method. The chemical composition was investigated via EDAX (*METEK*) analysis from the FESEM technique. The FTIR was conducted for both LS and LCF using *Bruker alpha FTIR* spectrophotometer ranging from 400–4000 $cm^{-1}$ at a resolution of 4 $cm^{-1}$. The structural properties of the LS and LCF were evaluated by the XRD using a *Bruker D8 Advance Powder XRD* with Cu-Kα radiation (λ = 1.5418 Å). Measurements were obtained over a 2θ range of 10–80° with a goniometer speed of 2°/min. The thermal characteristics of LC and LCF were done using Thermogravimetric analysis (TGA, *Hitachi EXstar* TGA DTA 6300) placed on an alumina crucible with temperature ranging from 28°C to 600°C at a heating rate of 2°C/min under $N_2$ atmosphere. The contact angle made by the water droplet of volume 5µL on the LCF surface determined its surface wettability or hydrophobicity. It was obtained by a drop shape analyser (*KRUSS*) at room temperature. The bulk density of LCF was found according to *ASTM D8176-18* standard test method, and the flame test was carried out by holding the LCF in the spirit lamp flame of temperature ranging from 1100°C-1200°C for about 60 sec (Yu et al., 2019).

*4.3.4.4 Oil-water separation test using LCF*

The oil considered for evaluating LCF properties were 2T engine oil, diesel oil, Petrol oil, crude sunflower oil, and organic solvents such as toluene, petroleum ether, and n-hexane labelled with Sudan (III) dye. The adsorption performance of the LCF was done based on Standard Test Method (ASTM F716-99) (Bazargan et al. 2015). A known weight of the LCF was added to the beaker containing the oil-water mixture and taken out after the equilibrium state to measure the final weight. All experiments were performed in duplicates at 27±2°C, and then the average value was noted. The optimization of the contact time, initial oil concentration, and adsorbent dosage were done with the adsorption capacity response. The sorption capacity (M) of the LCF was calculated by using the Eq. (4) given below

$$M = \frac{m_f - m_i}{m_i} \times 1000 \qquad (4.12)$$

M - Oil sorption capacity (mg/g);

$m_f$ - the weight of saturated sorbent (weight of the oil plus sorbent) (g);

$m_i$ - the weight of dry sorbent (g)

*4.3.4.5 Studies on kinetics, isotherm and thermodynamics*

Adsorption kinetics defines the oil uptake rate at the solid-solution interface and provides possible reaction pathways and mechanisms. The kinetics of diesel oil sorption on LCF were analyzed using various kinetic models, as shown in Eq. (4.13) - Eq. (4.15). The correlation coefficients ($R_2$) show the fitness identification between model values and experimental data. Adsorption kinetics includes Lagergren pseudo-first-order, pseudo-second-order, and interparticle diffusion (Weber-Morris equation) models to analyze reaction pathways and mechanisms (Lv et al. 2018).

*Pseudo-first-order,* $ln(q_e - q_t) = lnq_e - k_1 t$ $\qquad (4.13)$

*Pseudo-second-order,* $\frac{t}{q_t} = \frac{1}{k_2 q_e^2} + \frac{t}{q_e}$ $\qquad (4.14)$

*Interparticle diffusion model,* $q_{t = k_p t^{0.5} + C}$ $\qquad (4.15)$

Where $q_t$ - amounts of adsorbate (g/g) at a time (t);

$q_e$ - amounts of adsorbate (g/g) at equilibrium;

$k_1$ (min$^{-1}$) - pseudo-first-order rate constant,

$k_2$ (g/g.min$^{-1}$); pseudo-second-order rate constant, and

$k_p$ - intraparticle diffusion rate constant (g/g. min$^{1/2}$).

For oil in the water system, diesel oil of different concentrations (10-100 g/L) was added to a 500 mL beaker at room temperature. A certain known amount of synthesized LCF was added into the beaker containing the oil-water emulsion. The LCF was allowed to adsorb oil for some time until saturation is reached. Later, the adsorbent was removed from the systems and finally weighed again. In this research, two-factor adsorption isotherms such as Freundlich, Langmuir, Temkin, Dubinin -Radushkevich (D-R), and Elovich models as shown in Eq. (4.16)- (4.23) were utilized to interpret the experimental data (Al Jaberi et al. 2020)

$$\textit{Freundlich isotherm, } ln\, q_e = lnK_F + \frac{1}{n}\, lnC_e \qquad (4.16)$$

$q_e$ - amounts of adsorbate (g/g) at equilibrium;

$C_e$ (g/L) - oil concentration at equilibrium;

$K_F$ (g/g) - Freundlich constant (related to the adsorption capacity)

The $K_F$ and the slope (1/n) define the relative adsorption capacity and surface heterogeneity or adsorption intensity. The n value depicts the degree of non-linearity between oil concentration and quantity of oil adsorbed. If n<1, it indicates the chemical adsorption; if n=1, it indicates the linear adsorption; if n>1, it indicates the physical adsorption.

$$\textit{Langmuir isotherm, } \frac{C_e}{q_e} = \frac{1}{(q_{max}K_l)} + \frac{C_e}{q_{max}} \qquad (4.17)$$

where, $q_e$ - amounts of adsorbate (g/g) at equilibrium;

$q_{max}$ – maximum capacity of adsorption (g/g) corresponding to complete monolayer surface adsorption;

$C_e$ (g/L) - oil concentration at equilibrium;

$k_L$ (L/g) - Langmuir constant (related to the adsorption energy);

The Langmuir isotherm assumes that sites of sorption have an affinity to the oil. An essential characteristic of the Langmuir isotherm is the separation factor ($R_L$) calculated as per Equation (10), which expresses the adsorption nature as irreversible ($R_L = 0$), favourable ($0 < R_L < 1$), linear ($R_L = 1$), or unfavourable ($R_L > 1$). It determines the affinity between oil and LCF.

$$R_L = \frac{1}{1+k_L C_0} \qquad (4.18)$$

$$\textit{Temkin isotherm, } q_e = BlnK_T + BlnC_e \qquad (4.19)$$

where, $q_e$ - amounts of adsorbate (g/g) at equilibrium;

$C_e$ (g/L) - oil concentration at equilibrium;

$K_T$ – Temkin isotherm constant;

B (J/mol) – heat of adsorption = RT/b;

R- gas constant (8.314J/mol. K);

T (K)- absolute temperature;

b (J/mol)- Temkin constant.

Temkin isotherm mainly governs the assumptions that heat of adsorption (free Energy) is a function of surface coverage.

*Dubinin -Radushkevich (D-R) isotherm,* $\ln q_e = \ln q_s + K_{DR}\varepsilon^2$ (4.20)

Where,

Polanyi's potential, $\varepsilon = \mathrm{RT}\ln\left(1 + \dfrac{1}{C_e}\right)$ (4.21)

$q_e$ - amounts of adsorbate (g/g) at equilibrium;

$C_e$ (g/L) - oil concentration at equilibrium;

$q_s$ - amounts of adsorbate (g/g) at saturation;

$K_{DR}$ – activity coefficient constant at free energy of sorption (E) per adsorbate;

R- gas constant (8.314J/mol. K);

T (K)- absolute temperature;

Mean free energy (kJ/mol), $E = \dfrac{-1}{\sqrt{-2K_{DR}}}$ (4.22)

For heterogeneous surfaces, the adsorption process follows the pore-filling mechanism and depends on the material's porosity. The D-R model is temperature-dependent and related to physical adsorption under the Vander Waal's force of multilayer.

*Elovich model,* $\ln\dfrac{q_e}{C_e} = \ln(K_e q_{max}) - \dfrac{q_e}{q_{max}}$ (4.23)

$q_e$ - amounts of adsorbate (g/g) at equilibrium;

$q_{max}$ – maximum capacity of adsorption (g/g) corresponding to complete monolayer surface adsorption;

$C_e$ (g/L) - oil concentration at equilibrium;

$K_E$ (L/g) – Elovich equilibrium constant;

The model assumes an exponential rise in the adsorption sites with a multilayer adsorption process based on the kinetic principle.

To evaluate the thermodynamics in oil adsorption experiments (Initial oil concentration=10g/L, LCF dosage=1g, and time 30mins) were carried out at four

70

temperatures conditions (298K, 303K, 308K, and 313K). The thermodynamic parameters such as spontaneity, the nature of adsorbate-adsorbent interactions and feasibility can be investigated using the thermodynamic variables such as standard enthalpy change ($\Delta H°$), standard entropy change ($\Delta S°$), and Gibbs free energy change ($\Delta G°$) to check the effect of temperature on the oil adsorption onto LCF. The mathematical equations used for the determination of the above-mentioned thermodynamic parameters is shown below in Eq. (4.24) -(4.26).

$$K_0 = {q_e}/{C_e} \tag{4.24}$$

$$\ln K_0 = \frac{\Delta S^0}{R} - \frac{\Delta H^0}{RT} \tag{4.25}$$

$$\Delta G_0 = -RT \ln K_0 \tag{4.26}$$

T= temperature in Kelvin (K)

R= Universal gas constant

The slope and intercept obtained from the $\ln K_0$ versus $1/T$ plot (linear form) refers to the enthalpy change and entropy change respectively.

*4.3.4.6 Reusability studies*

Based on adsorption-combustion cycles, a trial study was conducted to determine the reusability of the oil-filled LCF. The oil-filled LCF was burned directly in the air, and the burnt LCF was reused in the following cycle. Before and after each cycle, the weight of the carbon foam was measured.

# CHAPTER 5

## RESULTS AND DISCUSSIONS

### 5.1 Characterization of substrates and inoculum

The advantage of using AH as a substrate for biogas production is their cheaper availability throughout the year. Moreover, with an increasing emphasis on cost reduction of industrial processes and value addition to agro-industrial residues, utilization of AH as an energy source seems promising because of their higher energetic value. The characteristics of AH, FW and sludge inoculum used is depicted in Table 5.1 given below

**Table 5.1 Properties of the raw AH, FW and anaerobic sludge inoculum.**

| Parameters | AH | Food waste (FW) | Inoculum |
|---|---|---|---|
| TS (% wb[a]) | 99.94 | 19.47 | 2.35 |
| VS (% wb[b]) | 82.45 | 18.50 | 1.86 |
| VS/TS | 0.825 | 21.08 | 0.79 |
| pH | 6.5 | 6.2 | 7.3 |
| Ultimate analysis (db[b]): | | | |
| C (%) | 45.77 | 48.51 | 32.4 |
| H (%) | 6.31 | | 0.34 |
| S (%) | ND[c] | | ND[c] |
| N (%) | 0.36 | 1.63 | 3.89 |
| O (%) | 47.81 | | 24.56 |
| Ash (%) | 0.74 | | 34.17 |
| HHV (MJ/Kg) | 22.66 | | 10.60 |
| TKN (%) | 1.09 | | 3.18 |
| Crude protein (%) | 6.82 | | |
| TRS (mg/mL) | 0.38 | | - |

[a]wb: wet basis

[b]db: dry basis

[c]ND: Not detected

**5.2 Phase II: Investigate the anaerobic digestion of pretreated AH with due emphasis on its biogas potential**.

*5.2.1 Solubilization study and selection of best pretreatment method*

The solubilization effects at different dosages of the four pretreatments such as acidic ($H_2SO_4$), alkaline (NaOH), oxidative ($H_2O_2$), and organosolv (Ethanol+1% $H_2SO_4$) at two different temperature conditions (25ºC and 90ºC) were analyzed using various factors.
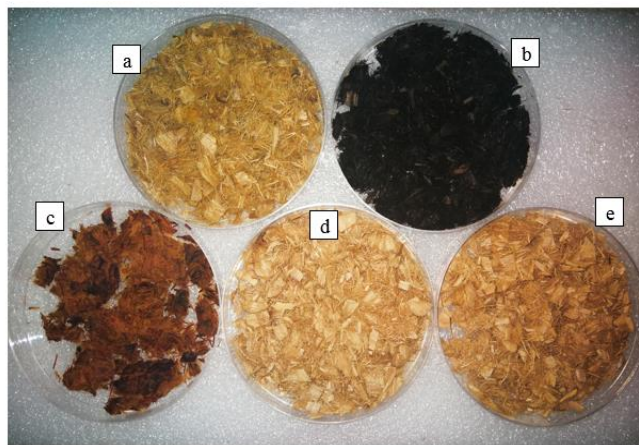


**Figure 5.1 AH after various pretreatment (a) Raw AH (b) Acidic pretreatment (c) Alkaline pretreatment (d) Oxidative pretreatment & (e) Organosolv pretreatment**

Figure 5.1 shows the photographic images of the pretreated AH and raw AH. As the colour can express the visual features in a better way, it can be seen that raw AH has a slightly yellowish colour. This is due to the presence of cellulose, lignin, hemicelluloses, and traces of pectin, protopectin, waxes, and tannins (Bhat and Raghavendra 2018). The colour change to dark (black) is predominantly due to hemicellulose degradation and lignin dissolution on acidic pretreatment. Alkaline pretreatment turned the yellow colour of raw AH into dark orangish-yellow and found little swollen than the raw AH. It indicates the rise in porosity, enhancing the enzyme accessibility and digestion of sugar (Lazim et al. 2014). For oxidative and organosolv pretreatment, the biomass turned to a lighter colour with no much visual changes.

Besides the differences in visual appearance, their compositional changes were also studied and discussed in the subsequent section.

*5.2.1.1 Variation in VS/TS ratio*

From Figure 5.2 (a) & (b), the variation in TS at temperatures 25⁰C and 90⁰C found to be in range 99.61%-99.95% and 99.09%- 99.93% respectively. This confirms that there is no effect of the pretreatment method, its dosage, and the TS reduction temperature. However, VS reduction is considered to be a reference for the material solubilization of pretreated AH. Also, VS/TS ratio is directly proportional to the biodegradability. In this study, the VS/TS ratio exclusively depends on the VS content since TS content variation is considerably low.

In all cases, acidic pretreatment has a low VS/TS ratio irrespective of dosage and temperature change, negatively influencing its biodegradability. An impressive result can be noticed in VS/TS change for the other three pretreatment methods, viz. alkaline, oxidative, and organosolv at both temperatures. In process pretreatment at 25⁰C, the VS/TS ratio was low for organosolv pretreatment (0.87-0.95), whereas the highest was shown for alkaline pretreatment (0.90-0.96). Contrarily, at a higher process temperature of 90⁰C, the VS/TS ratio content was low for alkaline pretreatment (0.81-0.95) and increased for organosolv pretreatment (0.91-0.98). It is clear that with the increase in process temperature, the VS/TS ratio reduced.

Further, for all pretreatment method, a gradual decrease in the VS/TS ratio was observed with respect to the dosage. This is due to organic matter hydrolysis of AH to the liquid phase on increasing dosage severity (Lopez Torres and Llorens 2008). However, the maximum deviation in VS/TS ratio at a particular dosage of oxidative and organosolv pretreatment with respect to alkaline pretreatment were ±4.91% (25°C) and ±9.52% (90°C). Thus, the percentage difference in VS/TS ratio at a particular dosage for all pretreatment method was found to be negligibly small since the deviations obtained were less than 10%. A similar trend is observed in the study conducted by Pellera et al. (2016). They confirm that pretreatment duration and temperature have no effects on the VS/TS ratio for the alkaline pretreatment of olive pomace. So, it can be concluded that in this study, the pretreatment methods adopted

does not seem to have initiated any significant effects regarding this parameter (VS/TS ratio).
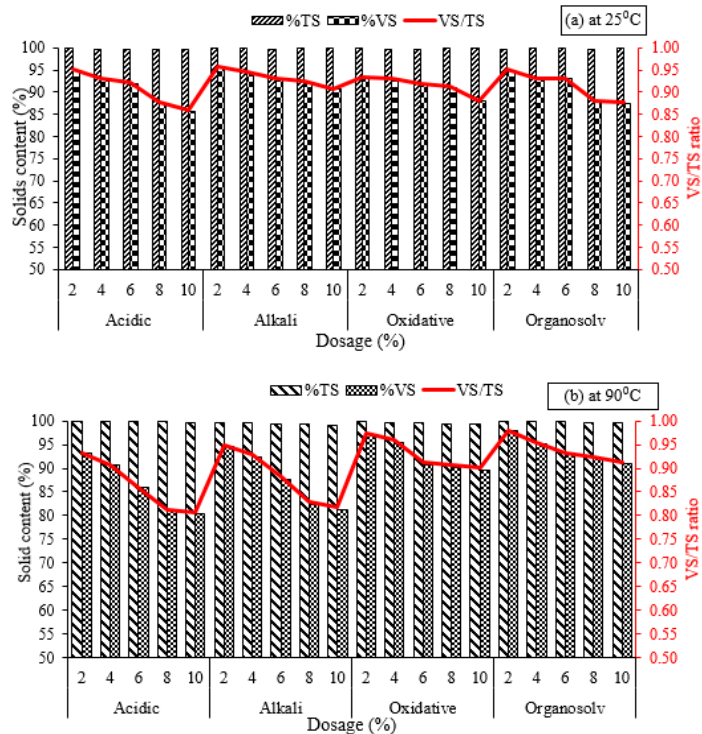


**Figure 5.2 Reduction in solid content and VS/TS ratio after various pretreatment at (a) 25⁰C (b) 90⁰C**

*5.2.1.2 Soluble COD (sCOD) and TPC variations after pretreatment*

The material solubilization of lignocellulosic biomass can be studied from sCOD and TPC release after the chemical pretreatments at different temperatures. These factors form the indicators of the degradation and lignin solubilization in the liquid phase. Figure 5.3 (a) shows sCOD values in the filtrate for different pretreatments at varying dosages. It was observed that alkaline pretreatment had a higher sCOD and TPC release than the other three pretreatments at both 25⁰C and 90⁰C. Similar results on alkaline pretreatment were also obtained by Michalska and Ledakowicz (Michalska and Ledakowicz 2013) on *Sorghum moench* grass species. At a higher process temperature (90⁰C), both sCOD and TPC release were higher than at the process temperature of 25⁰C. Hence, in this study, process temperature plays a significant role in the material solubilization of biomass, and similar conclusions were also reported by other researchers (Costa et al. 2014; Xie et al. 2011). Moreover, as the severity of dosage

increases, the solubilization increases for sCOD and TPC, facilitating all pretreatment hydrolysis process.

However, at 25ºC, only a slight linear increase in the release of sCOD was observed. At the elevated temperature of 90ºC, a drastic increase in the release was found for 6% of NaOH dosage. Later, it increases gradually. According to Kim et al. (Kim et al. 2018), thermal pretreatment alone has shown no effect on the solubilization study by sCOD. However, NaOH pretreatment on the spent coffee ground at a higher temperature have boosted the solubilization result. The present study results confirm the synergistic effect of temperature aided NaOH pretreatment on sCOD release (Costa et al. 2014; Shetty et al. 2016). For acidic and organosolv pretreatment, a moderate increase in the sCOD concentration can be noticed. The process temperature for ethanol pretreatment has no significant impacts on the sCOD release.

TPC is formed as a result of the degradation of lignin content in the biomass. Figure 5.3 (b) shows that the TPC release was highest for alkaline pretreatment. Within the alkaline pretreatment, higher temperature (90ºC) favoured more solubilization than at 25ºC for TPC, and the percentage increase in the TPC level was in the range of 18.67% to 51.89%. It is worth mentioning that process temperature and pretreatment dosage positively affects the solubilization process in alkaline pretreatment. This is due to the breakage of the chemical bonds, particularly ester and ether bonds in the lignocellulosic biomass matrix. Also, they are useful for the rupture of C-C bonds in the lignin molecules.
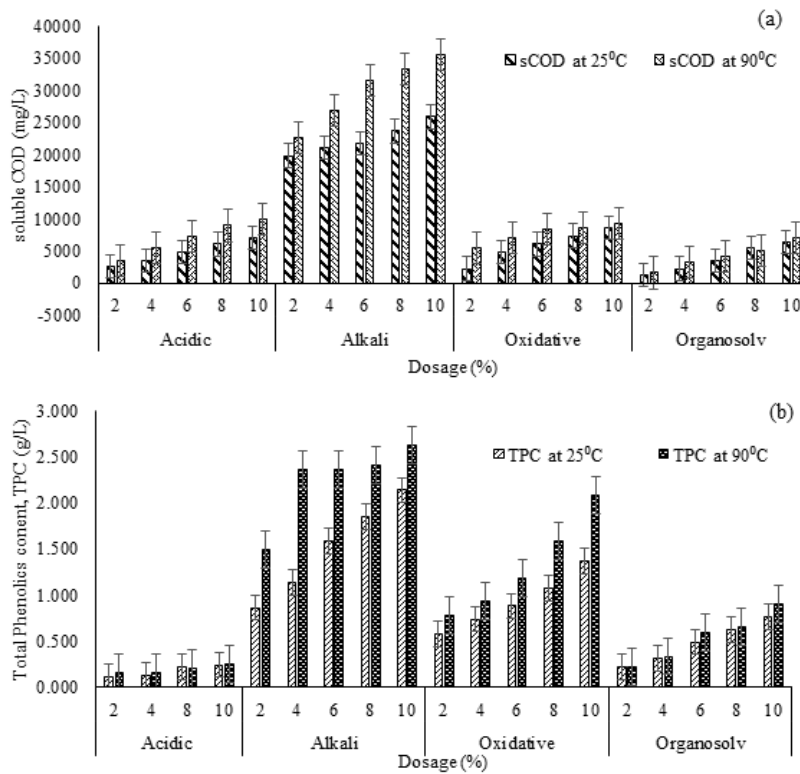
**Figure 5.3 Solubilization study for different pretreatment dosages at 25⁰C and 90⁰C (a) sCOD release (b) TPC release**

*5.2.1.3 Analysis of biomass compositional changes*

The percentage composition of lignin, hemicellulose, and cellulose in the raw AH was 22.1, 24.6, and 48.1% (%w/w), respectively. The removal percentages of cellulose, hemicellulose, and lignin in pretreated AH compared with the raw AH, are shown in Figure 5.4 (a) & (b). It is evident from figure 5.4 that the biomass composition tends to change with respect to pretreatment temperature. The organosolv pretreatment showed the minimum removal percentage for all the biomass composition compared to the other three pretreatments. However, the removal percentages of hemicellulose and lignin increased with increasing NaOH content, indicating that increasing alkalinity was to boost the removal percentage, especially lignin. The oxidative pretreatment also helps in similar lignin removal, which helps in accessing cellulosic content of the biomass. The OH- in NaOH can weaken the hydrogen bonding between cellulose and hemicellulose and break the bonding of ester and ether between lignin and polysaccharides. This results in the partial decomposition of cellulose, hemicellulose,

and lignin (Dai and Dong 2018). The cellulose was found to be removed in the sulphuric acid pretreatment. The 10% $H_2SO_4$ pretreatment had a minimum percentage of cellulose. However, the hemicellulose content showed a drastic decrease with increasing $H_2SO_4$ and NaOH content.
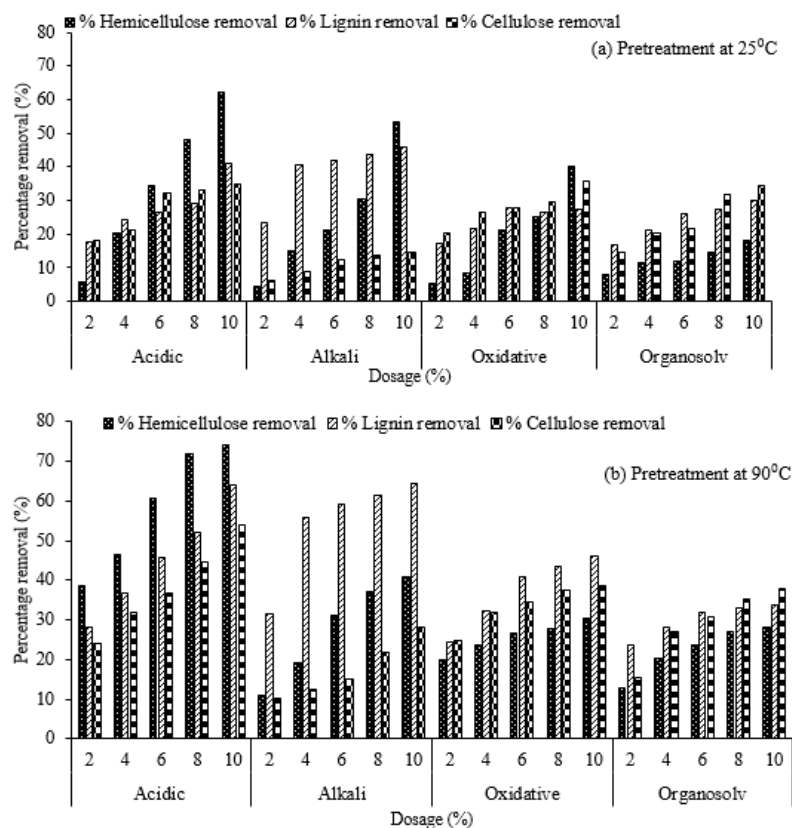


**Figure 5.4 Percentage removal of cellulose, hemicellulose, and lignin in the pretreated AH at (a) 25⁰C and (b) 90⁰C**

*5.2.1.4 MADM approach for pretreatment method selection*

The solubilization results obtained for the four different pretreatments at two temperature 25°C and 90°C were considered for TOPSIS technique as discussed in 3.5.1 to select the best pretreatment for AH. The matrix contains the attribute (column-wise) such as cellulose, hemicellulose, lignin, sCOD, and total phenolics corresponding to the alternatives (row-wise) and forms a 40×5 decision matrix as shown in table 5.2.

**Table 5.2 Decision matrix from the solubilization study of AH**

| Alternatives | | Hemicellulose (%) | Total lignin (%) | Cellulose (%) | sCOD | Total phenolics |
|---|---|---|---|---|---|---|
| | | | Decision matrix | | | |
| Acidic at 90 | 2 | 20.86 | 20.93 | 39.45 | 3520 | 0.11 |
| | 4 | 17.64 | 19.58 | 37.93 | 5440 | 0.13 |
| | 6 | 14.45 | 19.12 | 32.52 | 7360 | 0.17 |
| | 8 | 11.44 | 18.51 | 32.15 | 8960 | 0.23 |
| | 10 | 8.35 | 16.03 | 31.25 | 9920 | 0.24 |
| Alkali at 90 | 2 | 21.08 | 19.78 | 45.12 | 22720 | 0.86 |
| | 4 | 18.79 | 16.13 | 43.94 | 26880 | 1.14 |
| | 6 | 17.37 | 15.91 | 42.17 | 31680 | 1.58 |
| | 8 | 15.36 | 15.49 | 41.47 | 33280 | 1.85 |
| | 10 | 10.34 | 15.07 | 41.17 | 35520 | 2.14 |
| Oxidative at 90 | 2 | 20.96 | 21.00 | 38.23 | 5440 | 0.58 |
| | 4 | 20.23 | 20.10 | 35.37 | 7040 | 0.74 |
| | 6 | 17.42 | 18.78 | 34.71 | 8320 | 0.88 |
| | 8 | 16.53 | 19.12 | 33.79 | 8640 | 1.08 |
| | 10 | 13.26 | 18.89 | 30.86 | 9280 | 1.37 |
| Organosolv at 90 | 2 | 20.30 | 21.12 | 41.06 | 1600 | 0.22 |
| | 4 | 19.56 | 20.22 | 38.39 | 3200 | 0.32 |
| | 6 | 19.49 | 19.16 | 37.78 | 4160 | 0.49 |
| | 8 | 18.86 | 18.96 | 32.82 | 5120 | 0.63 |
| | 10 | 18.11 | 18.39 | 31.45 | 7040 | 0.77 |
| Acidic at 25 | 2 | 13.57 | 18.76 | 36.64 | 2560 | 0.16 |
| | 4 | 11.85 | 16.99 | 32.72 | 3520 | 0.17 |
| | 6 | 8.67 | 15.07 | 30.45 | 4800 | 0.19 |
| | 8 | 6.22 | 13.77 | 26.66 | 6080 | 0.21 |
| | 10 | 5.68 | 11.28 | 22.10 | 7040 | 0.26 |
| Alkali at 25 | 2 | 19.67 | 18.07 | 43.27 | 19840 | 1.49 |
| | 4 | 17.88 | 13.02 | 42.18 | 21120 | 2.36 |
| | 6 | 15.22 | 12.28 | 40.80 | 21760 | 2.37 |
| | 8 | 13.92 | 11.81 | 37.61 | 23680 | 2.41 |

| | 10 | 13.07 | 11.21 | 34.59 | 25920 | 2.63 |
|---|---|---|---|---|---|---|
| Oxidative | 2 | 17.68 | 19.55 | 36.22 | 2240 | 0.78 |
| at 25 | 4 | 16.87 | 17.88 | 32.85 | 4800 | 0.94 |
| | 6 | 16.24 | 16.08 | 31.61 | 6080 | 1.19 |
| | 8 | 15.97 | 15.54 | 30.05 | 7360 | 1.59 |
| | 10 | 15.36 | 15.01 | 29.63 | 8640 | 2.09 |
| Organosolv | 2 | 19.24 | 19.67 | 40.68 | 1280 | 0.22 |
| at 25 | 4 | 17.61 | 18.77 | 35.11 | 2240 | 0.34 |
| | 6 | 16.87 | 18.02 | 33.37 | 3520 | 0.60 |
| | 8 | 16.11 | 17.74 | 31.08 | 5440 | 0.66 |
| | 10 | 15.87 | 17.58 | 29.94 | 6400 | 0.91 |

The Eigenvalues for the weight determination was calculated from the Eigenvectors of relative importance matrix Eigenvalues using MATLAB code. The weights obtained for the corresponding attributes were 0.353, 0.198, 0.170, 0.174, and 0.104 respectively. The CI and CR values for the judgment set were calculated as 0.059 and 0.053, respectively, which is less than 0.1, showing a better consistency and reliability. The ranking of alternatives was following the suitability index value.

**Table 5.3 Ranking of various pretreatment method for AH**

| Pretreatment method | Dosage | $S_i^+$ | $S_i^-$ | TOPSIS scores | RANK |
|---|---|---|---|---|---|
| | 2 | 0.095539 | 0.057445 | 0.658713 | 13 |
| | 4 | 0.090924 | 0.048149 | 0.5777 | 20 |
| Acidic at 90 | 6 | 0.08885 | 0.037771 | 0.462881 | 32 |
| | 8 | 0.087717 | 0.03338 | 0.413927 | 34 |
| | 10 | 0.089898 | 0.030347 | 0.367916 | 36 |
| | 2 | 0.038769 | 0.088679 | 2.376082 | 5 |
| | 4 | 0.027696 | 0.093421 | 3.46646 | 3 |
| Alkali at 90 | 6 | 0.018152 | 0.102598 | 5.754697 | 1 |
| | 8 | 0.021299 | 0.104283 | 5.000451 | 2 |
| | 10 | 0.036398 | 0.106599 | 3.035269 | 4 |

| | | | | | |
|---|---|---|---|---|---|
| | 2 | 0.089849 | 0.057899 | 0.702305 | 11 |
| | 4 | 0.085794 | 0.055304 | 0.699915 | 12 |
| Oxidative at 90 | 6 | 0.083067 | 0.048425 | 0.631384 | 14 |
| | 8 | 0.08283 | 0.046026 | 0.601691 | 17 |
| | 10 | 0.084659 | 0.037578 | 0.481459 | 29 |
| | 2 | 0.100907 | 0.056627 | 0.61781 | 15 |
| | 4 | 0.096624 | 0.052794 | 0.599183 | 18 |
| Organosolv at 90 | 6 | 0.093848 | 0.052567 | 0.612698 | 16 |
| | 8 | 0.092356 | 0.048287 | 0.571122 | 22 |
| | 10 | 0.08752 | 0.047104 | 0.585308 | 19 |
| | 2 | 0.101888 | 0.034555 | 0.373703 | 35 |
| | 4 | 0.101723 | 0.026965 | 0.292044 | 37 |
| Acidic at 25 | 6 | 0.102734 | 0.019184 | 0.205917 | 38 |
| | 8 | 0.104478 | 0.015862 | 0.167684 | 40 |
| | 10 | 0.105097 | 0.016994 | 0.17869 | 39 |
| | 2 | 0.046883 | 0.079051 | 1.765163 | 9 |
| | 4 | 0.043996 | 0.078313 | 1.858308 | 7 |
| Alkali at 25 | 6 | 0.0455 | 0.074772 | 1.718122 | 10 |
| | 8 | 0.043798 | 0.076172 | 1.815351 | 8 |
| | 10 | 0.042061 | 0.080008 | 1.982185 | 6 |
| | 2 | 0.100071 | 0.045612 | 0.501414 | 25 |
| | 4 | 0.093862 | 0.04224 | 0.492267 | 26 |
| Oxidative at 25 | 6 | 0.090877 | 0.040971 | 0.491812 | 27 |
| | 8 | 0.087897 | 0.041234 | 0.510349 | 24 |
| | 10 | 0.084834 | 0.041759 | 0.534003 | 23 |
| | 2 | 0.102028 | 0.053301 | 0.575719 | 21 |
| | 4 | 0.100573 | 0.044522 | 0.48721 | 28 |
| Organosolv at 25 | 6 | 0.097523 | 0.041654 | 0.468769 | 31 |
| | 8 | 0.093187 | 0.039416 | 0.462393 | 33 |
| | 10 | 0.090945 | 0.039246 | 0.470783 | 30 |

The first five ranks (Table 5.3) were obtained for the 2, 4, 6, 8, and 10% dosages of alkaline pretreatment at 90°C and was selected for the further anaerobic digestion

studies. Additionally, the solubilization study shows that alkaline pretreatment at 90⁰C (selected pretreatment method) has facilitated a higher lignin removal from the AH. Lignin gets leached as phenols into the filtrate (Ariunbaatar et al. 2014) and reduced the recalcitrance of the residues. This shows the mass transfer of the recalcitrant material into the filtrate (solid phase to the liquid phase) without fragmenting hemicellulose and providing access to the cellulose (Jönsson and Martín 2015). The release of organic soluble compounds represented by the sCOD indicates the enhancement of AH biodegradability with alkaline pretreatment (Shetty et al. 2016). The NaOH aided pretreatment at 90⁰C was selected to be an effective method, and their morphological and chemical analysis was done to understand the swelling properties and other significant pretreatment effects. Later, digestion studies were carried out for the selected pretreatment aided AH by varying dosages and raw AH at the mesophilic condition to determine the best dosage of the chosen pretreatment for maximum biogas yield.

### 5.2.2 Analysis of morphological and chemical changes for selected pretreatment

The alkaline pretreatment of AH at a temperature of 90⁰C can be an efficient way to increase biogas potential. This can also be confirmed from the SEM (Figure 5.5 (a), (b), (c) & (d)) results obtained for raw and alkaline pretreated AH samples. The raw AH surface images show a compact and non-porous arrangement of binding materials such as lignin, pectin, hemicellulose, etc. (Julie Chandra et al. 2016) epidermis layer of biomass. The raw AH showed highly ordered fibrils with acute edges due to the trimming process and exhibited a rigid structure. The thorn-like structure on the intact surface depicts the trichomes, which can be phytoliths (silica storing bodies) (Ramesh et al. 2018). This structure confirms the inhibiting nature of the AH towards the hydrolysis process. On alkali pretreatment, a notable difference in the surface morphology can be identified. The surface appears to be deformed and swollen when compared with the raw AH. Further, the natural waxy layer in the raw AH surface was observed to be absent, which confirms the removal of waxes, pectin, and low weight components in the surface matrix. The intact epidermis gets broken, causing small pits-like pore on the surface, resulting in exposure to internal structures and thereby increasing the fibre porosity of the biomass. This increases the accessibility towards

inner cellulosic material for the effective bioconversions by reducing the recalcitrance. As per the structural architecture of AH's SEM images at prior and post pretreatment, alkaline pretreatment was found to be efficient, which beholds the possible reason for increased sugar release for the biodegradation process.
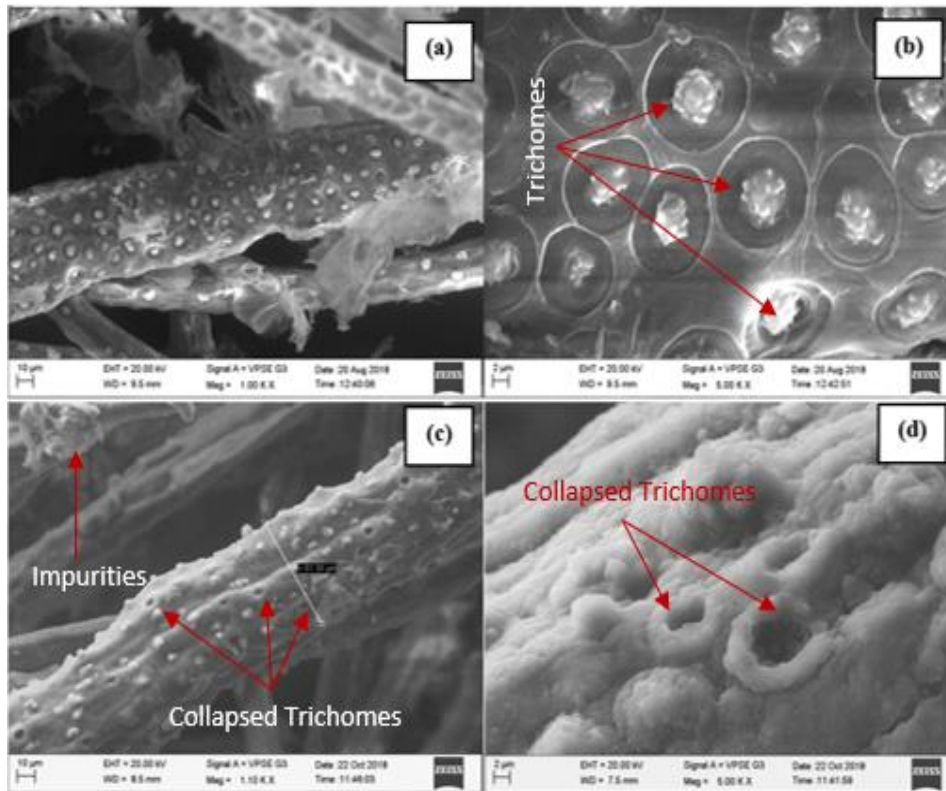


**Figure 5.5 SEM images for (a) Raw AH at 1000X (b) Raw AH at 5000X (c) Alkaline pretreated AH at 1100X (d) Alkaline pretreated AH at 5000X**

FTIR results portray the changes in physicochemical, conformational, and functional group characteristics of molecules in a biomass sample. The FTIR spectra (Figure 5.6) was taken for both raw and alkaline pretreated AH and compared with other literature to ascertain the changes in the biomass composition. As discussed previously, the AH fibres predominantly consists of mainly cellulose, hemicelluloses, and lignin. Alkanes, esters, aromatics, ketones, and alcohols, with different oxygen-containing functional groups, are the main functional groups present in these three organic matter forms (cellulose, hemicellulose, and lignin). The disappearance of some particular peaks in spectra indicates the removal of corresponding components after the alkaline pretreatments of the fibre as described below.
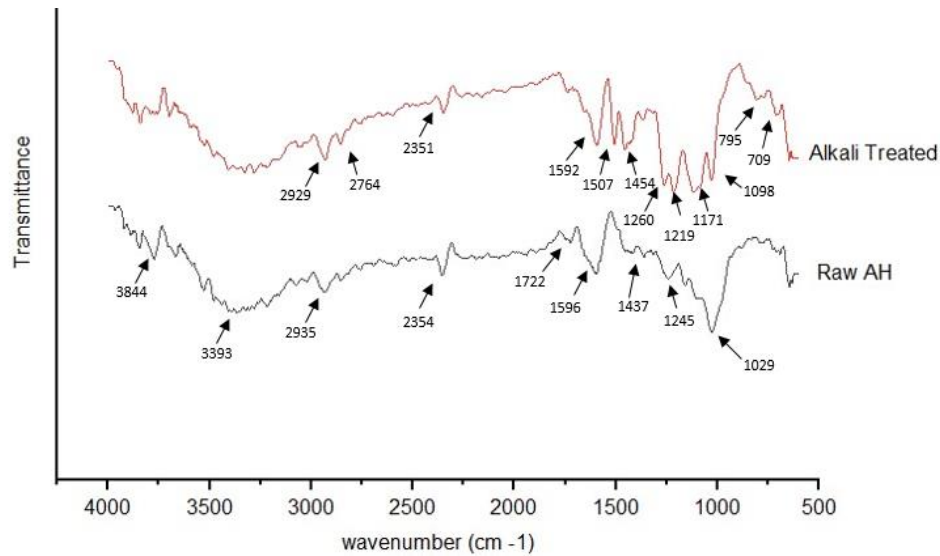
**Figure 5.6 FTIR spectra for raw and alkali-treated AH**

There are two main absorption regions observed for the two fibre samples, one at a low wavelength region from 700 to 1840 cm$^{-1}$ and the other at a high wavelength region between 2700 and 3700 cm$^{-1}$. The absorption bands in the range 3393–3404 cm$^{-1}$ and 2890–2980 cm$^{-1}$ found in the spectra of both the fibres represent the OH stretching vibrations of the hydrogen-bonded hydroxyl groups and the CH groups of cellulose respectively (Julie Chandra et al. 2016). The peaks at 1245 and 1596 cm$^{-1}$ found in the spectrum of raw fibre correspond to the conjugated carbonyl or carboxyl spectra of the atomic ring and aromatic ring stretching of lignin. The appearance of significant peak at 1722 cm$^{-1}$ in raw fibre is due to the acetic and uronic ester groups of the hemicelluloses or the ester linkages of the carboxylic group ferulic p-coumaric acids of lignin or hemicelluloses as reported in the literature (Julie Chandra et al. 2016). The peak at 2935 cm$^{-1}$ corresponds to C-OH bending, which confirms the presence of hemicellulose content. The main observation from the alkali pretreated AH is that these peaks are absent, removing lignin and partial removal of hemicellulose. The peak at 1219 cm$^{-1}$ represents the C-O, C-C stretching, and C-OH bending, which attributes to the xylan molecule. The peaks at 795, 1098, and 1219 cm$^{-1}$ are due to C-O-C stretching vibrations of the β-1, 4-glycosidic ring linkages between the D–glucose units cellulose which are more pronounced after pretreatment.

*5.2.3 Anaerobic digestion studies*

The process parameters involved in the study of the performance of anaerobic digestion were pH, VFA, and alkalinity, as mentioned in section *4.3.2.3*. The process outcomes include daily biogas volume with the biogas composition for different dosages of the selected pretreated AH.

*5.2.3.1 pH variations*

The evaluation of pH during the biogas yield assays can be seen in Figure 5.7 (a). The graphs reveal relatively stable conditions throughout the digestion period. Small fluctuations generally characterize the different assays for most of the experiment. A slightly decreasing trend towards the end can be noticed, whose values range between 6.1-7.5 for all samples. The dip occurred in the graph on the 9th and 21st days, which may be due to the accumulation of VFA. To maintain the pH, the buffering solution was added to bring into the favourable pH condition. The pH variations greatly influence the methanogens growth rate, and the optimal range is reported to be 6.5 -7.8. At a lower pH value (less than 6.6), microbial growth has been retarded and finally causes the lower biogas yield (Shetty et al. 2016). The pH cannot be an effective measure for the stability of an anaerobic process when there is a high buffering capacity. In such cases, other parameters have to be checked to ascertain the digester performance.

*5.2.3 2 Alkalinity variations*

Alkalinity is used to reflect the process performance directly to check the digester stability. The alkalinity of a steady system is between 1000mg and 5000mg $CaCO_3$/L. In this study, the alkalinity of all bioreactors containing various dosages of pretreated AH was found to be higher than raw AH at the beginning stage of AD. This can be mainly due to the addition of sodium hydroxide solution to those bioreactors during pretreatment (Figure 5.7 (b)). On days 0–9, the alkalinity of bioreactors with 2, 4, 6, 8, 10 % NaOH dosages decreased sharply by 70.5%, 72.5%, 73.4%, 67.2%, and 66.5%, respectively, and reached 1000mg $CaCO_3$/L which indicates that the process was unstable in this stage. Similarly, between days 9-21, the variation in the alkalinity ranged between 71.4%-73.5%. The maximum alkalinity was found on the day 12th and

24th day of the entire digestion period. The highest alkalinity values were obtained for 12th day were 4087 (2%), 4244 (4%), 4651 (6%), 3907 (8%) and 3995 (10%) respectively. Additionally, there was only a small difference in alkalinity among bioreactors at different NaOH dosages. Even though the concentration of NaOH solution used during pretreatment changed a lot; on the other hand, the alkalinity in the control bioreactor always increased from 347mg $CaCO_3$/L to 1674mg $CaCO_3$/L during days 0–27. The increase of alkalinity was normally due to the activity of the methanogenic bacteria, which could produce alkalinity in the form of $NH_3$, $CO_2$, and bicarbonates (Kumar et al. 2015c; Uma et al. 2018).

*5.2.3.3 VFA variations*

VFA production from pretreated AH and raw AH reached the maximum on day 9, as shown in Figure 5.7 (c). It was observed that pretreatment with NaOH caused microbial enzymes to degrade faster than raw AH. The bacteria produce acids faster by converting small organic molecules to volatile fatty acids when using pretreated AH (Singh and Trivedi 2013). The VFA concentration varied in 1500–3145mg/L for pretreated AH samples during anaerobic digestion, whereas the raw AH value ranged between 910-1620mg/L. When comparing both control and bioreactors fed with pretreated AH, the highest performance of VFA production was observed in a bioreactor having 4% NaOH dosage, and the lowest VFA concentration was observed in a bioreactor with raw AH. The average VFA concentration of each bioreactor during the period of AD was 2165.3mg/L (2%), 2471.5mg/L (4%), 2057.5mg/L (6%), 2083.3mg/L (8%), 1996.3mg/L (10%) and 1208mg/L (raw AH). The possible reason for the reduction in VFA may be due to the inhibition in the acetogenesis stage because of the high sodium concentration (Pellera et al. 2016).
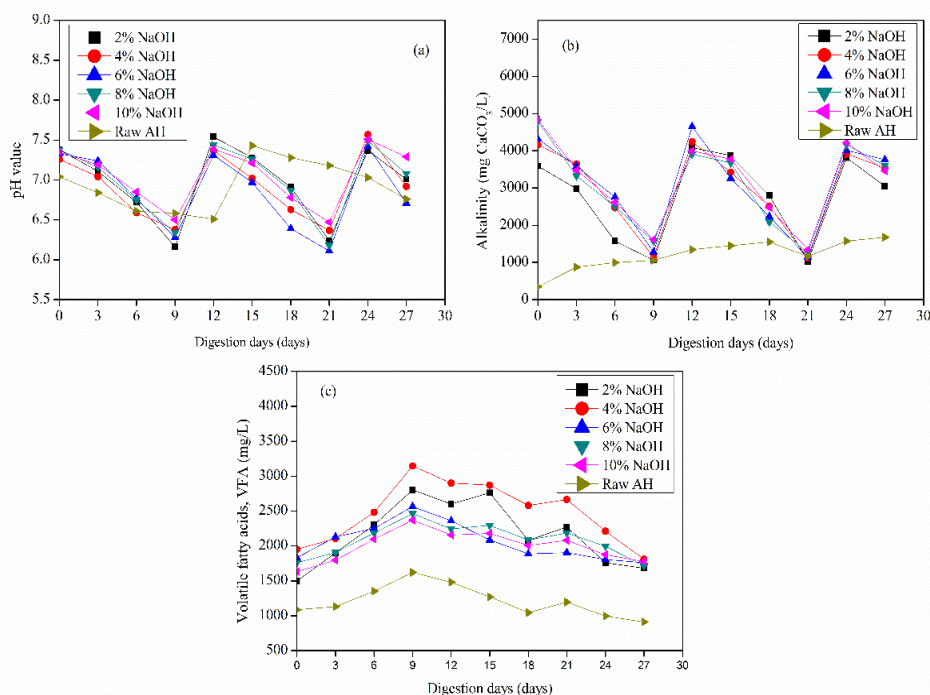
**Figure 5.7 Variation of process parameters (a) pH, (b) alkalinity and (c) VFA in the anaerobic digester for methane production**

*5.2.4 Biogas generation*

The time-course profile of cumulative biogas production can be observed in Figure 5.8. The untreated and pretreated AH were anaerobically digested for 27 days beyond that biogas was found nil in the reactors. Maximum biogas volume for all the pretreated AH was noticed between the 9th and 10th day. The biogas volume increased with the fermentative phase prolongation, evidenced by enhanced production of volatile acids such as acetic acid and methanoic acid (Chaiyapong and Chavalparit 2016). From the cumulative biogas curve, it can be observed that the biogas increases for the first 17 days, achieving 80% of the total yield. A biogas yield of 683.89mL/gVS was obtained for 4% pretreated AH was found to be the highest yield among the different pretreated AH. The lowest yield was obtained for the raw AH and was found to be 297.67 mL/gVS. The increase in biogas yield for each dosage of 2, 4, 6, 8, and 10% compared with the raw AH is 1.6, 2.3, 1.7, 1.7, and 1.5 times. The biogas compositions shown in Figure 5.9 depict the methane content in percentage, which helps determine the

88

biomethane yield (See Appendix A). Methane compositions (n=4) found stable in the range of 71.53%- 75.06% for pretreated AH and for raw as 62.31%. An increased methane yield shows the biodegradability of the pretreated AH in comparison with raw AH. The methane content values fall in line with the literature results (Uma et al. 2018).
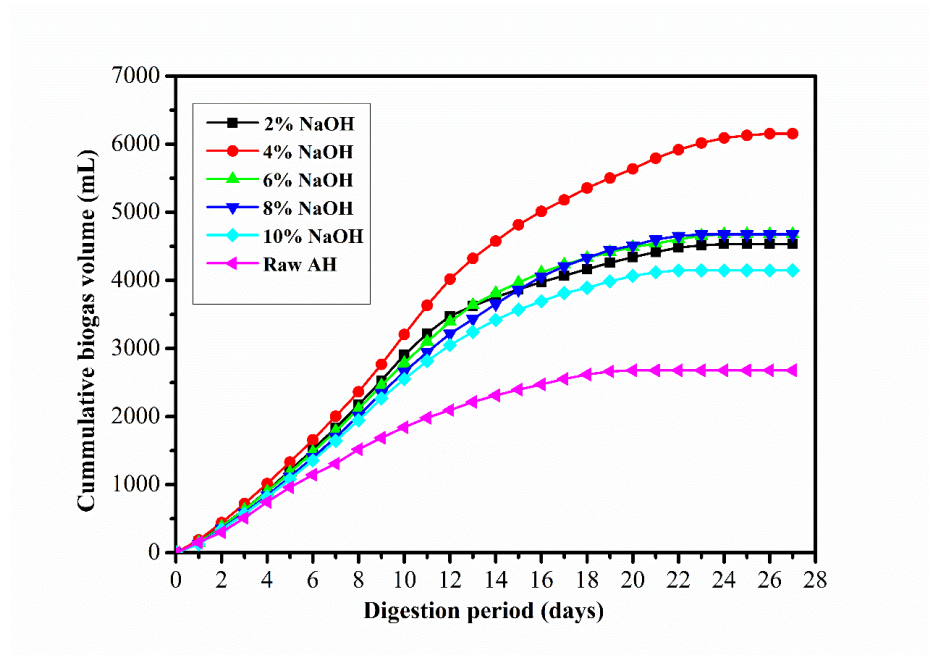


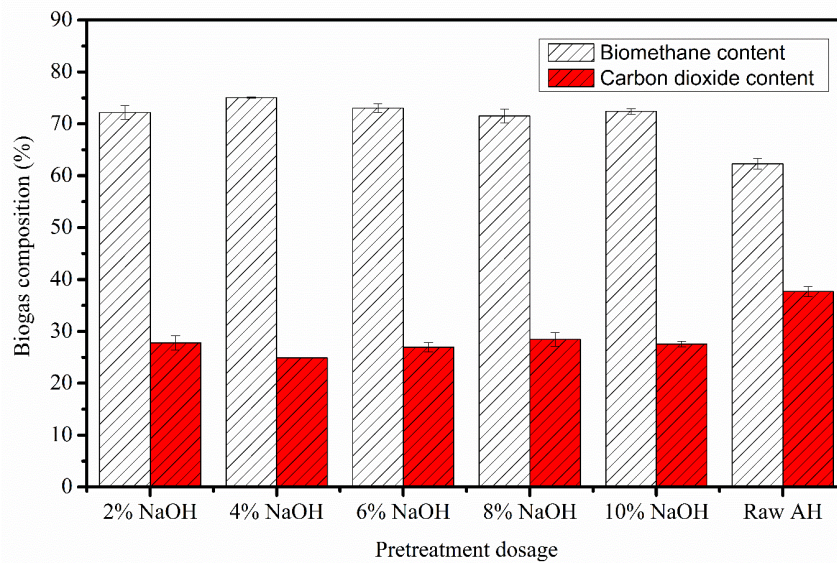**Figure 5.8 Cumulative biogas yield over the 27 days of the digestion period**



**Figure 5.9 Biogas compositions for different pretreated AH**

The result of the present study was found to be comparable with other studies done for the enhancement of biogas production from lignocellulosic biomass pretreated with NaOH. Monlau et al. (2012) investigated NaOH pretreatment effects for 24 h at 30, 55, 80°C on biogas production of sunflower stalks. They reported that the pretreatment of NaOH at 55°C increased the biogas production by 35%. They also confirmed that NaOH pretreatment yielded higher biomethane volume than $Ca(OH)_2$ and was very useful for high lignin-containing biomass for enhanced biomethane production (Monlau et al. 2012). Kaur and Phutela (Kaur and Phutela 2016a) studied enhancing paddy straw digestibility and biogas production through sodium hydroxide (NaOH) pretreatment. The paddy straw was pretreated with NaOH by soaking (24 h) in different concentrations of NaOH (2, 4, 6, 8, and 10%) and supplementing with microwave irradiations (30 min, 720 W, 180ºC). They found that 4% NaOH for 30 min microwave was the best pretreatment with a 54.7% increase in biogas production.

The present study results proved that pretreatment is necessary to enhance the biomethane production from agriculture biomass. The alkali pretreatment mechanism is the saponification of intermolecular ester bonds cross-linking xylan, hemicelluloses, and lignin (Kaur and Phutela 2016b). Moreover, alkali pretreatment aims to increase the porosity of material due to extensive swelling facilitated by cross-links removal. The data obtained from different pretreatment conditions unfold that the temperature aided lower alkali dosage breaks lignin more efficiently without degrading useful carbon sources (hemicellulose and cellulose). Also, it is proved that the diluted alkali pretreatment release more soluble sugar than concentrated alkali treatment.

The pretreatment is considered a crucial step, where it needs to be less expensive and effective enough to increase biomethane production. The current study would be practically ideal to use 4% NaOH pretreatment for the delignification of AH and further used for the biomethane production applications.

*5.2.5 Kinetic models for pretreatment aided anaerobic digestion*

Various attempts were made to fit the kinetic models, as explained in section 4.3.2.5 with the experimental data to have better model fitness for anaerobic digestion process (Raposo et al. 2011). In the present study, four kinetic models were used for modelling

the kinetic study of biogas potential assays. All the kinetic parameters involved in the digestion process were listed in Table 5.4 for all the four models adopted in this study. The curve fitting for various NaOH pretreatment aided biogas assays is depicted in figure 5.10.

Modified Gompertz equation ($R^2$= 0.99) and Logistic model ($R^2$= 0.99) were found to be the best fit model and can be suitably used to predict biogas productions. This can be concluded from the higher $R^2$ value (~1) and lowers RSS value, which is essential for the model selection for biogas rate predictions. As the $R^2$ value is more, the closeness between the daily predicted biogas value and daily experimental biogas value is more. However, a fascinating fact is that the $M_{max}$ value obtained from the Logistic function model (deviation percentage of ±1.65%) showed a close resemblance to the experimental values. The modified Gompertz model showed a maximum deviation of +4.39% concerning experimental data, which is also acceptable. According to Raposo et al. (Raposo et al. 2011), whether the adopted model is deemed valid for explaining the data, the deviations of the predicted values from actual values should be less than 10%. Even though the transference function and FOE model exhibited R2 values of 0.98, there was a deviation in the predicted biogas potential (Mmax) compared with the experimental biogas potential. The maximum variations in the transference function and FOE models were +30.00% and ±56.17%. This is due to the heterogeneous mixture of organic substances, whereas this model is best suited for the homogenous reaction mixtures (Samuel J. et al. 2017).

For LOE model, k value was found in the range of 0.038-0.063 day$^{-1}$, similar to the range of 0.039-0.130 day$^{-1}$ found in other literature (Kafle et al. 2013; Noonari et al. 2017). It is evident that, as the pretreatment severity increase, the k value tends to decrease. This can be well explained with the formation of complex compounds such as phenolics in the anaerobic digesters, which inhibit the biogas production. However, the obtained k-values were positive compared with the results of Dudek et al. (Dudek et al. 2019), which could be due to the bioavailability of cellulose, resulting in a faster rate of biomethane production.

The time consumed by the bacteria to adapt the anaerobic conditions and start the digestion process is accounted as the lag phase (λ) of the exponential growth functions.

The λ of the experimental anaerobic digestion process was found to be 2 days. Substrates that are highly fibres in nature or with higher cellulose content showed a specific lag phase of 1-5 days during which the hydrolysis of complex polymers occurs before the initiation of acetogenesis and methanogenesis stage. The λ value for the Modified Gompertz model (0.842-1.96) and logistic model (1.107-2.577) matched well with that of experimental data. As per literature, the λ values ranges from 0-17.92 days and 0-2.54 days refers to the short time of adaptation. The long lag phase duration for pretreated AH compared to AH may be due to LCFAs inhibition caused by higher lipid contents released after pretreatment. Thus, the Logistic and Modified Gompertz model was chosen as the best fit model for predicting the anaerobic digestion process by eliminating the other two models.

**Table 5.4 Kinetic parameters involved in various non-linear regression models for biogas assays.**

| Model | Parameter | Alkali AH- 2% | Alkali AH- 4% | Alkali AH - 6% | Alkali AH - 8% | Alkali AH - 10% | Raw AH |
|---|---|---|---|---|---|---|---|
| First-order exponential | $M_{max}$ | 5924.38 | 10342.51 | 6490.13 | 7010.59 | 5635.20 | 3188.20 |
| | k | 0.063 | 0.038 | 0.056 | 0.048 | 0.059 | 0.084 |
| | RSS | 1585264 | 2263252 | 1719583 | 1712792 | 1433225 | 350797 |
| | $R^2$ | 0.981 | 0.986 | 0.981 | 0.981 | 0.980 | 0.987 |
| Logistic | $M_{max}$ | 4459.23 | 6098.92 | 4647.08 | 4711.93 | 4142.97 | 2680.49 |
| | $R_{max}$ | 362.730 | 419.67 | 359.31 | 337.67 | 325.25 | 212.32 |
| | λ | 2.131 | 2.577 | 2.298 | 2.296 | 2.230 | 1.107 |
| | RSS | 315222 | 518053 | 239808 | 178022 | 208338 | 157715 |
| | $R^2$ | 0.996 | 0.996 | 0.997 | 0.997 | 0.997 | 0.993 |

| | | | | | | | |
|---|---|---|---|---|---|---|---|
| Transference function | $M_{max}$ | 5468.74 | 8793.68 | 5885.71 | 4769.95 | 5148.58 | 2992.58 |
| | $R_{max}$ | 438.63 | 460.03 | 424.59 | 305.38 | 391.52 | 322.44 |
| | $\lambda$ | 0.968 | 1.057 | 1.017 | 1.068 | 1.017 | 1.058 |
| | RSS | 1052207 | 1498246 | 1149531 | 677273 | 952944 | 164582 |
| | $R^2$ | 0.986 | 0.988 | 0.984 | 0.984 | 0.983 | 0.988 |
| Modified Gompertz | $M_{max}$ | 4611.59 | 6437.41 | 4823.33 | 4881.38 | 4287.30 | 2749.32 |
| | $R_{max}$ | 356.26 | 404.56 | 351.77 | 336.27 | 320.51 | 215.85 |
| | $\lambda$ | 1.684 | 1.963 | 1.802 | 0.891 | 1.772 | 0.842 |
| | RSS | 65116 | 79161 | 44875 | 74024 | 43519 | 44819 |
| | $R^2$ | 0.999 | 0.999 | 0.999 | 0.999 | 0.999 | 0.998 |
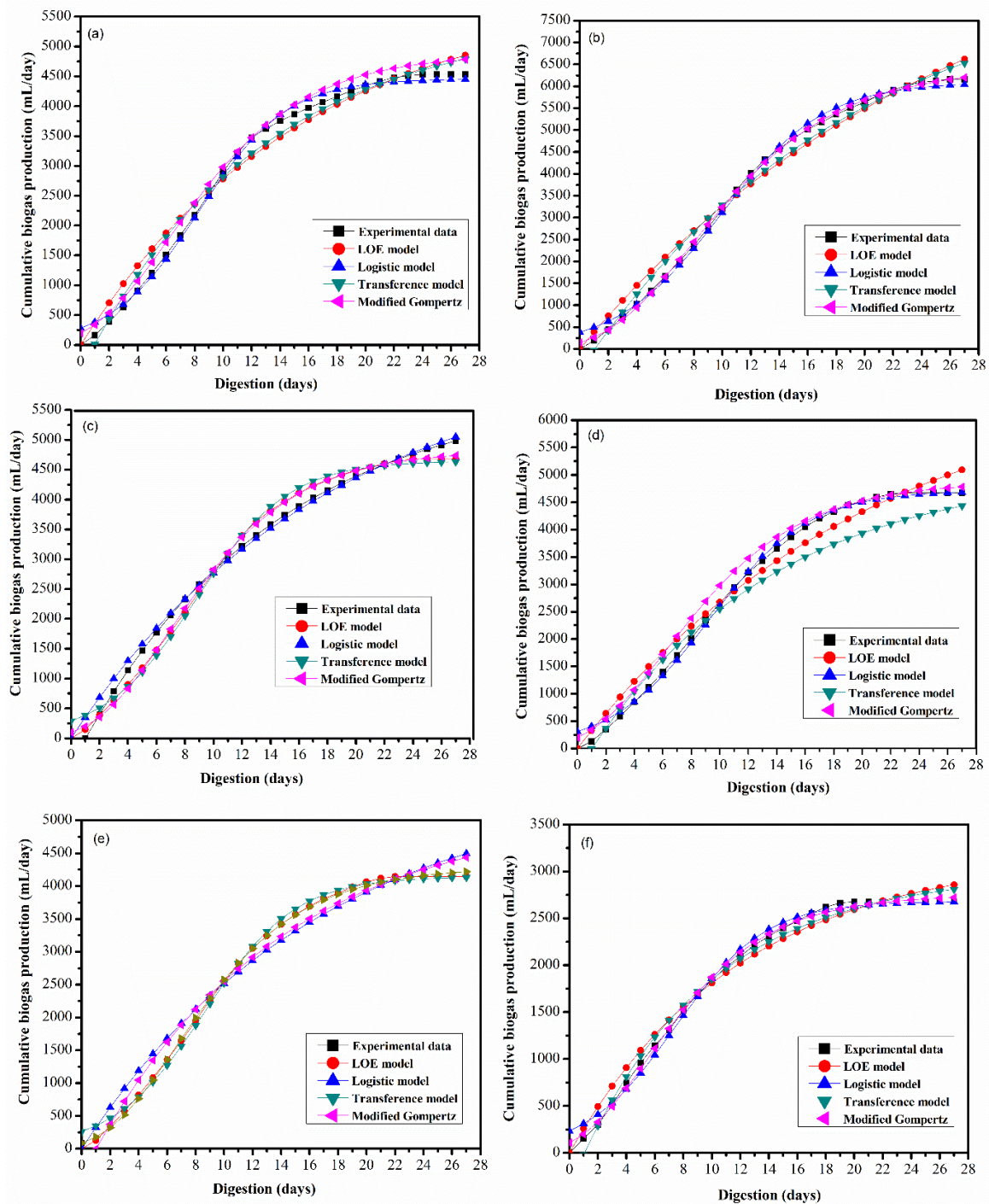
**Figure 5.10 Cumulative biogas production-time fit curve for adopted models on biogas assays of various pretreated AH (a) 2% NaOH loading (b) 4% NaOH loading (c) 6% NaOH loading (d) 8%NaOH loading (e) 10%NaOH loading and (f) Raw AH**

*5.2.6 Biodegradability index (BI)*

*5.2.6.1 Regression equation between biomass composition and BI*

As shown in Table 5.5, the TMP was higher than the SMP for all the biogas assays. Theoretical results are unlikely to agree with the experimental results because practically 100% organic matter degradation is impossible. So, the ideal conditions assumed by the model were not found in the real world. The model provides the biogas potential at its maximum by considering favourable conditions in the digester, i.e., neither non-degradable matter nor the energy demand of the microbes has prevailed. It is worth mentioning that both TMP and SMP were high for the 4% NaOH pretreatment aided AH than other pretreatments and raw AH. Ultimately, the present results reveal that as the pretreatment severities differ, effects on the degradability of the produced materials also tend to change. The highest BI was obtained for 4% NaOH pretreatment aided biogas assay, as shown in table 5.3.

**Table 5.5 Biodegradability index for raw and pretreated AH in biogas assay.**

| Pretreatment method | C[a] (%) | H[a] (%) | O[a] (%) | N[a] (%) | S[a] (%) | TMP (mLCH$_4$/gVS) | SMP (mLCH$_4$/gVS) | BI (%) |
|---|---|---|---|---|---|---|---|---|
| Raw AH | 49.42 | 8.25 | 59.40 | 0.57 | 0.00 | 408.92 | 225.16 | 55.06 |
| Alkali AH-2% | 58.00 | 12.36 | 54.69 | 0.32 | 0.00 | 553.58 | 380.97 | 68.82 |
| Alkali AH-4% | 60.86 | 14.76 | 54.20 | 0.29 | 0.00 | 607.12 | 517.29 | 85.20 |
| Alkali AH -6% | 58.66 | 13.39 | 55.11 | 0.39 | 0.00 | 570.08 | 393.24 | 68.98 |
| Alkali AH -8% | 59.53 | 11.56 | 52.14 | 0.11 | 0.00 | 559.37 | 392.91 | 70.24 |
| Alkali AH -10% | 57.46 | 10.84 | 53.71 | 0.33 | 0.00 | 531.26 | 348.36 | 65.57 |

Many researchers studied the correlation between methane yield and biomass composition. From the past studies, it is clear that lignin content (LC) has a negative correlation with the methane yield ($R^2$ value=0.92) for biomass such as sunflower stalks, grass, etc. under pretreatment (Dahunsi 2019). The LC plays a significant role

in methane production by restricting the access of microbes towards hemicellulose and cellulose. The holocellulose is biodegradable on their pure forms, whereas together with lignin, their biodegradability rate reduces. So, it is necessary to predict the biodegradability index (BI) as a function of biomass compositions (mainly, cellulose content (CC), hemicellulose content (HC), and lignin content (LC)) in percentage even if the actual test is not performed. In this research, a linear multiple regression equation is framed between the most crucial biomass components and BI using a better calibration statistic, as shown in equation (10) given below. To date, no attempt was made to find this relationship, which can predict the BI with a satisfactory resemblance to the actual data.

$$\text{Biodegradability index } = 53.35 + (5.79 \times \text{Hemicellulose content}) - (4.42 \times \text{lignin content}) - (0.38 \times \text{Cellulose content}) \qquad (5.1)$$

Table 5.6 depicts the ANOVA for the linear multiple regression equation. The Eq. (5.1) follows an $R^2$ value of 0.95, which shows better fitness of the model. The Probability value (p-value) of 0.027, which is less than 0.05, and Fischer value (F-value =12.087) greater than 4 confirms the significance of the regression equation. The actual BI and predicted BI using the linear multiple regression equation with their error percentages are shown in Table 5.7. The increase in the predicted values with respect to the actual value ranged between -3.93% to 3.97%. The negative symbol shows the decrease in the predicted BI values, whereas the positive symbol shows an increase in the predicted BI values. The predicted values were close enough to represent the actual values, so this linear multiple regression equation holds well for the analysis.

**Table 5.6 ANOVA table for the linear multiple regression equation**

| Model | Sum of Squares | df | Mean Square | F-value | p-value |
|---|---|---|---|---|---|
| Regression | 445.647 | 3 | 148.549 | 12.087 | .027[b] |
| Residual | 24.579 | 2 | 12.290 | | |
| Total | 470.226 | 5 | | | |

a. Dependent Variable: BI

b. Predictors: (Constant), CC, LC, HC

**Table 5.7 Actual and Predicted biodegradability index**

| Pretreatment dosage | Hemicellulose content, HC (%) | Lignin content, LC (%) | Cellulose content, CC (%) | Actual BI (%) | Predicted BI (%) | Error (%) |
|---|---|---|---|---|---|---|
| Alkali AH-2% | 19.67 | 18.07 | 43.27 | 68.82 | 70.93 | (-)3.06 |
| Alkali AH-4% | 17.88 | 13.02 | 42.18 | 85.20 | 83.30 | (+)2.24 |
| Alkali AH -6% | 15.22 | 12.28 | 40.80 | 68.98 | 71.69 | (-)3.93 |
| Alkali AH -8% | 13.92 | 11.81 | 37.61 | 70.24 | 67.45 | (+)3.97 |
| Alkali AH -10% | 13.07 | 11.21 | 34.59 | 65.57 | 66.33 | (-)1.16 |
| Raw AH | 22.10 | 24.63 | 48.12 | 55.06 | 54.15 | (+)1.65 |

*5.2.6.2 Method validation*

The $R^2$ value for the model's regression equation in predicting the BI values was 0.95. This shows the reliability in predicting the BI values by these models. Additionally, the deviation range is also within the range of 10%, which further confirms the suitability of these models in the BI value predictions. To ascertain the proper representation of the model for its intended use, method validation is carried out. If the predicted values achieve a close resemblance to the actual values, validation is achieved. The fractional errors determined should be in the range of 0.5-2 and theoretically can follow in the range of 0-2 (Thalla et al. 2010). From the charts (figure 5.11), it can be observed that most of the error points fall within 95% confidence interval.
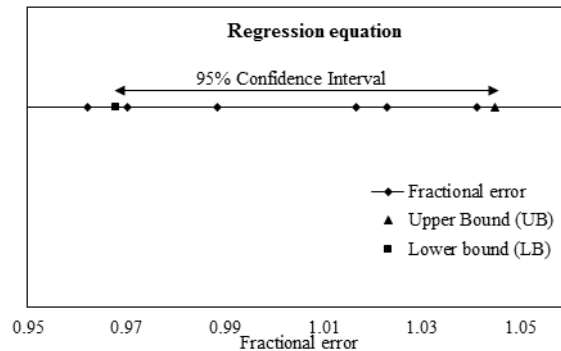
**Figure 5.11 Fractional error plot for linear multiple Regression equation developed.**

## 5.3 Phase III: To evaluate the effect of substrate mix ratio in batch mode anaerobic co-digester for biogas production.

### 5.3.1 Optimization of mix ratio

The process parameters involved in the study of the performance of anaerobic digestion were pH, VFA, and alkalinity, as mentioned in the materials and methodology section. The time-course profile of daily biogas volume and cumulative methane production can be observed in figure 5.12 & figure 5.13. The anaerobic digestion was carried out for 34 days with maximum biogas volume attained at the $3^{rd}$ -$6^{th}$ day for all the mix ratios. The volume of methane increased with the prolongation of the fermentative phase, evidenced by increased production of volatile organic acids such as acetic acid and formic acid (Chaiyapong and Chavalparit 2016). The maximum biogas yield of 321.12mL/gVS was obtained for the AH: FW 1:1 mix ratio. The biogas yields for AH: FW mix ratios with 1:0, 1:3, 1:1, 3:1, and 0:1 was 172. 35, 215.75, 321.12, 249.64, and 50.39 mL/g VS respectively. Also, for the same substrates, the co-digestion has enhanced the biogas yield than the mono-digestion. Similar results were also found by others (Rabii et al. 2019; Sayara and Sánchez 2019).
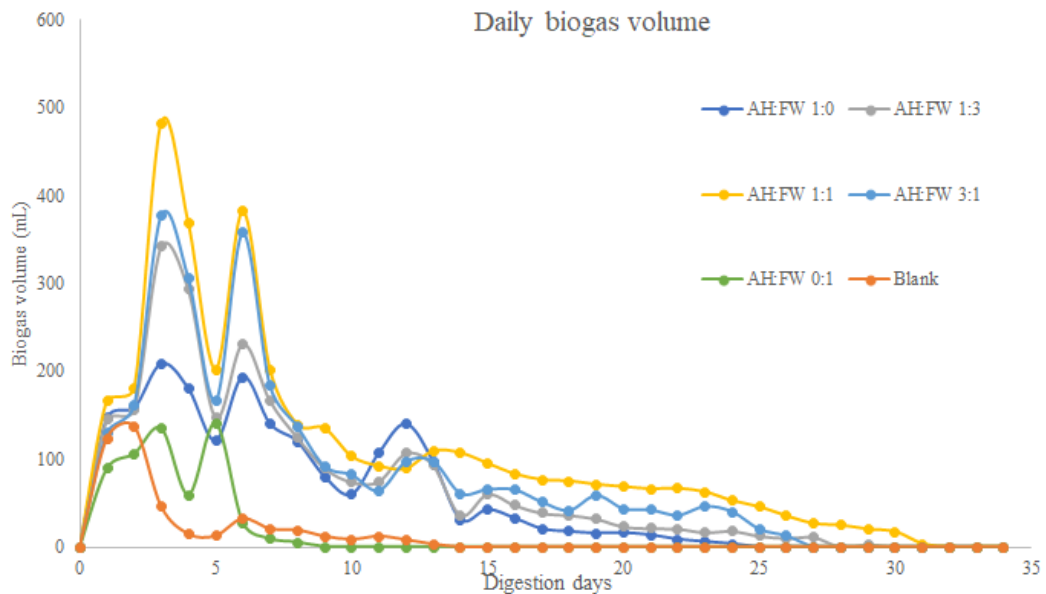
98

**Figure 5.12 Daily biogas volume over the 34 days of the digestion period**
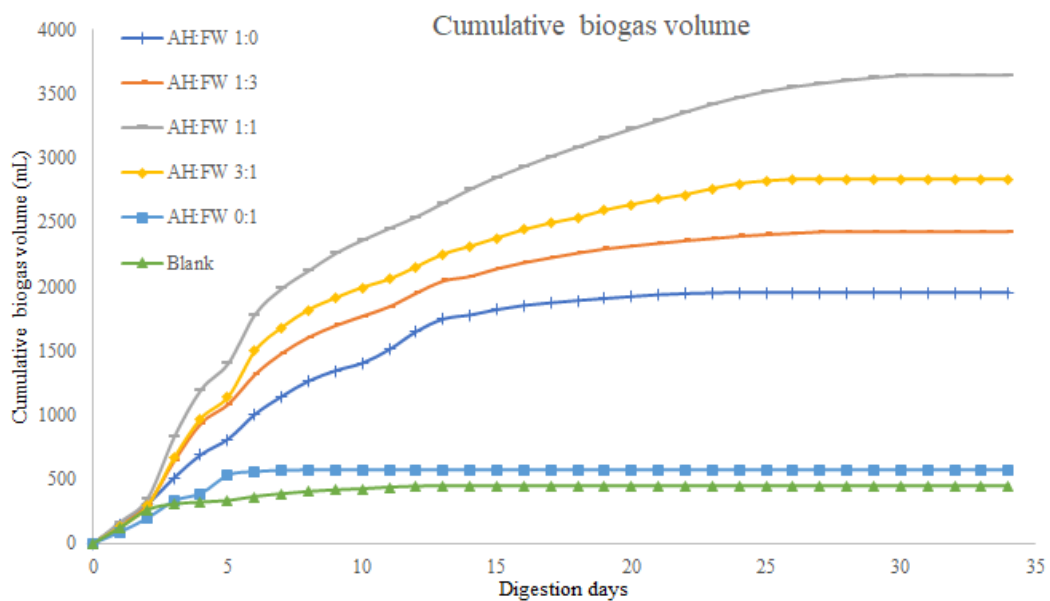


**Figure 5.13 Cumulative biogas yield over the 34 days of the digestion period**

*5.3.2 Variations in the process parameters*

The evaluation of pH during the biogas assays can be seen in figure 5.14. The graphs reveal relatively stable conditions throughout the digestion period. Small fluctuations generally characterize the data for the different assays for most of the experiment and a slightly increasing trend towards the end, whose values range between 6.5-7.9 for all

samples. The dip occurred in the graph on the 3$^{rd}$ and 6$^{th}$ days, which may be due to the accumulation of VFA. To maintain the pH, the buffering solution was added to bring into the favourable pH condition. The pH variations greatly influence the methanogens growth rate, and the optimal range is reported to be 6.5 -7.8. At lower pH value (less than 6.6), microbial growth has been retarded and finally causes the lower biomethane yield (Shetty et al. 2016). The pH cannot be an effective measure for the stability of an anaerobic process when there is a high buffering capacity.
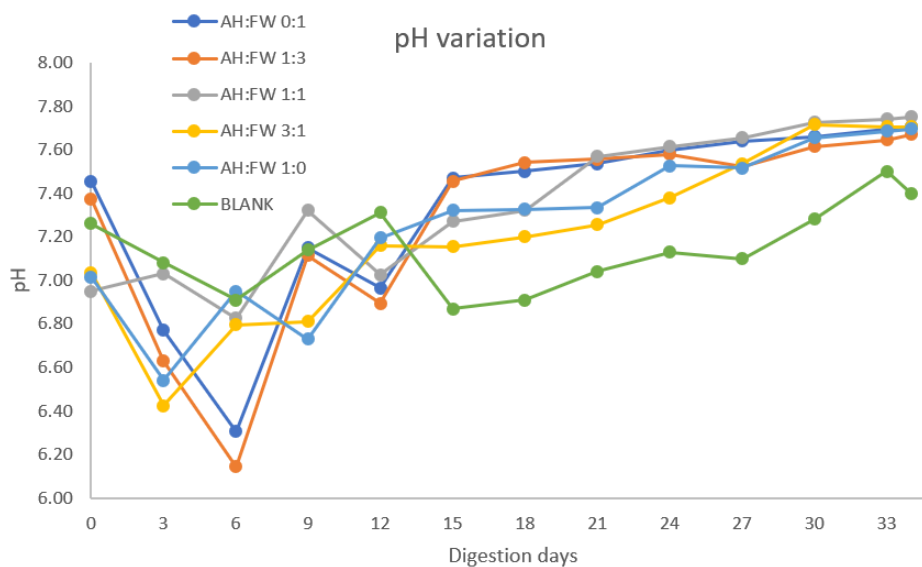


**Figure 5.14 pH variation over the 34 days of the digestion period**

As the batch mode study was conducted, alkalinity and VFA was determined at the initial and final stages of the anaerobic digestion. Alkalinity is used to reflect the process performance directly to check the digester stability. The alkalinity of a steady system is between 1000mg and 5000mg CaCO$_3$/L. (Kumar et al. 2015c, 2019; Uma et al. 2018). The initial and final alkalinity values were found to be in the range mentioned above, showing a steady performance for the batch mode co-digestion (Table 5.8). The bacteria produce acids faster by converting small organic molecules to volatile fatty acids when using pretreated AH (Singh and Trivedi 2013). The possible reason for the reduction in VFA may be due to the consumption of the VFA by the methanogens (Noonari et al. 2017). The VFA/Alkalinity ratio is a good indicator of digester health. In the current study, the initial VFA/Alkalinity ratios of all the bioreactors remained in between 0.3 and 0.4 except for the blank. This shows that the digesters are in good

health. According to previous literature, the optimum value for the VFA/Alkalinity ratio is considered to be less than 0.4 (Li et al. 2015b). At the final stage of the digestion period, this ratio was less than 0.1 for all digesters, which indicates the consumption of VFA by the methanogens (Yong et al. 2015).

**Table 5.8 performance of the digester at various mix ratios**

| AH: FW | 0:1 | 1:3 | 1:1 | 3:1 | 1:0 | Blank |
|---|---|---|---|---|---|---|
| iVFA | 968.00 | 1123.00 | 1400.00 | 997.00 | 764.00 | 441.00 |
| fVFA | 94.00 | 98.00 | 83.00 | 84.00 | 92.00 | 102.00 |
| iVFA/alkalinity | 0.37 | 0.40 | 0.30 | 0.32 | 0.38 | 0.44 |
| fVFA/alkalinity | 0.08 | 0.08 | 0.07 | 0.07 | 0.08 | 0.16 |

i- initial; f-final

## 5.4 Phase 3: To extract the lignin from AH and to synthesis novel lignin-based material for oil-water separation.

*5.4.1 Isolation of lignin from AH*

Lignin is a biopolymer consist of phenylpropane units branched by various groups (hydroxyl, phenolic hydroxyl, carboxyl, and epoxy) which are hydrophobic (Adcock et al. 2003). It is worth acknowledging that lignin remains undissolved in pure water, whereas it solubilizes completely in alcohol (Chen et al. 2018). The initial percentages mass content of cellulose, hemicellulose and lignin in the AH was 48.1, 24.6 and 22.1% (w/w). From the biomass composition, it is evident that AH contains high lignin content. The lignin extraction from AH was carried out using a mixture of formic acid/acetic acid/water by pulping. The retrieved lignin was washed for further material processing and was obtained as brown powders. The effect of fibre size on lignin extraction was considered in this study, and the fibre size was evaluated in two categories (a) size less than 10 mm and other (b) size between 10 mm and 20 mm. From figure 5.15 given below, it can be noticed that the highest yield of 15.79% (out of 22.1%) was obtained from this treatment process for the fibre size of less than 1cm. It can be concluded that as the size reduces, the lignin yield and recovery increase.

Similarly, This may be because reduced size can increase the access of the extraction solvents into the biomass (Tian et al. 2017). Finally, the present study showed 71% (w/w) of lignin recovery from the lignin source by this method. The extracted lignin (LS) was used to efficiently synthesize lignin-based carbon material to separate the oil and water mixture.
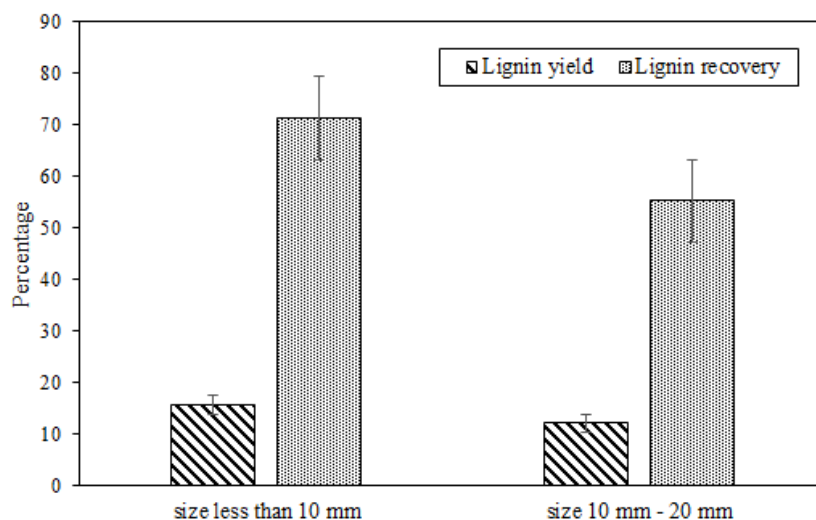


**Figure 5.15 Lignin yield and recovery percentage from AH of different size**

*5.4.2 Purity of extracted lignin*

The purity and chemical structure of the extracted lignin was analyzed from the $^1$H NMR spectra, as shown in figure 5.16 and summarised, as given in Table 5.9. The aliphatic moiety in lignin and aromatic protons present in the syringyl and guaiacyl units (monolignols) of lignin is depicted as the integrals of signals between 0.8-1.5 6.0 to 8.0 ppm, respectively. The peak at 3.82 ppm represents the methoxyl (-OCH$_3$) protons close to the syringyl: guaiacyl proportions. The signals integrals between 6.731-7.41 ppm revealed the aromatic protons of syringyl- propane units and guaiacyl-propane units confirm the presence of main monomers (monolignols) of lignin. Moreover, the syringyl monolignols were found more than the guaiacyl monolignol, referred from the more substantial peak at 6.8 relative to peak at 7.0 ppm (Rashid et al. 2018a). The signals at 2.500 refer to the solvent DMSO d$_6$ used for the analysis. From these analyses, it can be concluded qualitatively that the extracted material from AH is lignin.
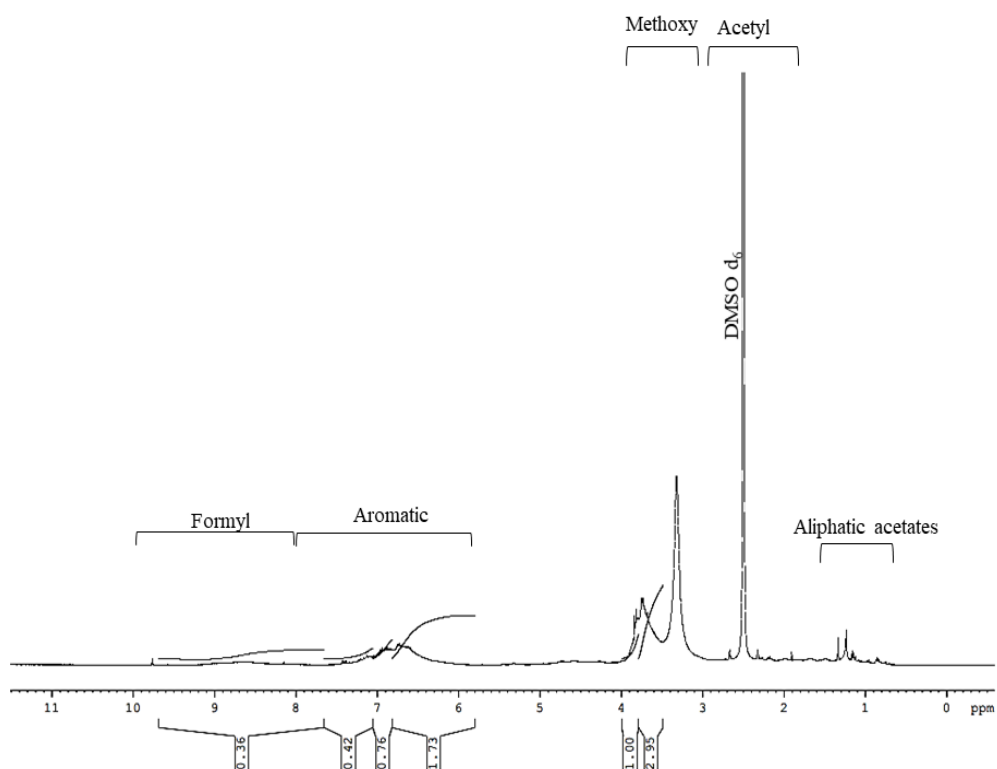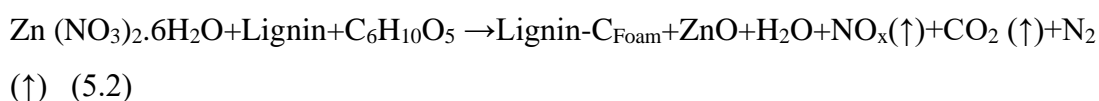
**Figure 5.16 NMR spectra for the extracted lignin**

**Table 5.9 $^1$H NMR spectra signal assignment of extracted lignin samples**

| Signal, δ (ppm) | Assignment |
|---|---|
| 0.8-1.5 | Aliphatic proton |
| 2.4-2.54 | H in aromatic and aliphatic acetates |
| 2.5 | DMSO solvent |
| 3.3-3.8 | Methoxyl proton |
| 6.73 | Aromatic proton in syringyl |
| 6.94 | Aromatic proton in guaiacyl |
| 6.73-7.41 | Aromatic proton in syringyl and guaiacyl |
| 8.0-9.5 | Formyl protons in cinnamaldehyde units and benzaldehyde units |

### 5.4.3 Synthesis of Lignin based carbon foam (LCF)

An ultralight and hydrophobic lignin impregnated carbon material was synthesized using the extracted lignin. The following characterizations confirm the material compositions and their nature. The lignin was immobilized into the carbon foam synthesized from the $Zn(NO_3)_2.6H_2O$ and starch through thermal treatment. The $Zn(NO_3)_2.6H_2O$ act as the oxidizing agent during the carbonation process. Initially, as the temperature raises $Zn(NO_3)_2.6H_2O$ gets liquified and form a gel-like formation which uniformly mixes starch and lignin at 180°C. The carbonization process can be visualized from the colour changes from brown to black with the expulsion of gases such as $NO_x$, $CO_2$, and $N_2$ etc. As the carbonization process continues, the lignin gets impregnated into the ZnO based carbon foam which acts as the template material. The reaction proposed for the above is given in Eq. (5.2) as follows,

$$Zn(NO_3)_2.6H_2O + Lignin + C_6H_{10}O_5 \rightarrow Lignin\text{-}C_{Foam} + ZnO + H_2O + NO_x(\uparrow) + CO_2(\uparrow) + N_2(\uparrow) \quad (5.2)$$

As the temperature elevates, the strong oxidizer $Zn(NO_3)_2.6H_2O$ decomposes and reacts with starch. The swollen starch particles get dehydrated and polymerize to form a carbon foam impregnated with lignin and ZnO particles. The LCF has a bulk density of about $0.0294 \ g/cm^3$, which is very light in weight and placed on a fragile leaf (Figure 5.17), which could retain it on the leaf without bending it. This helps the LCF float on the water's surface to efficiently remove the oils spread on the water surface.
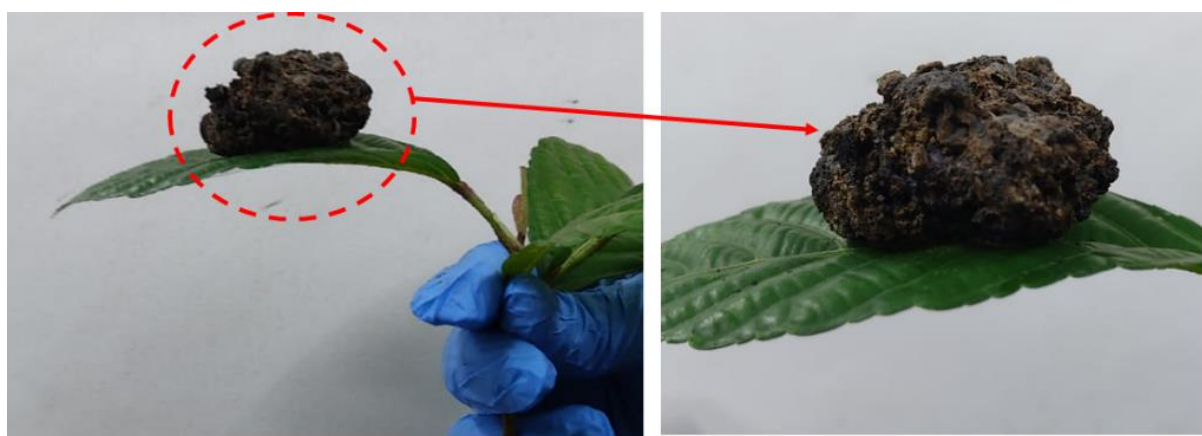


**Figure 5.17 Digital images of the LCF on a fragile leaf**

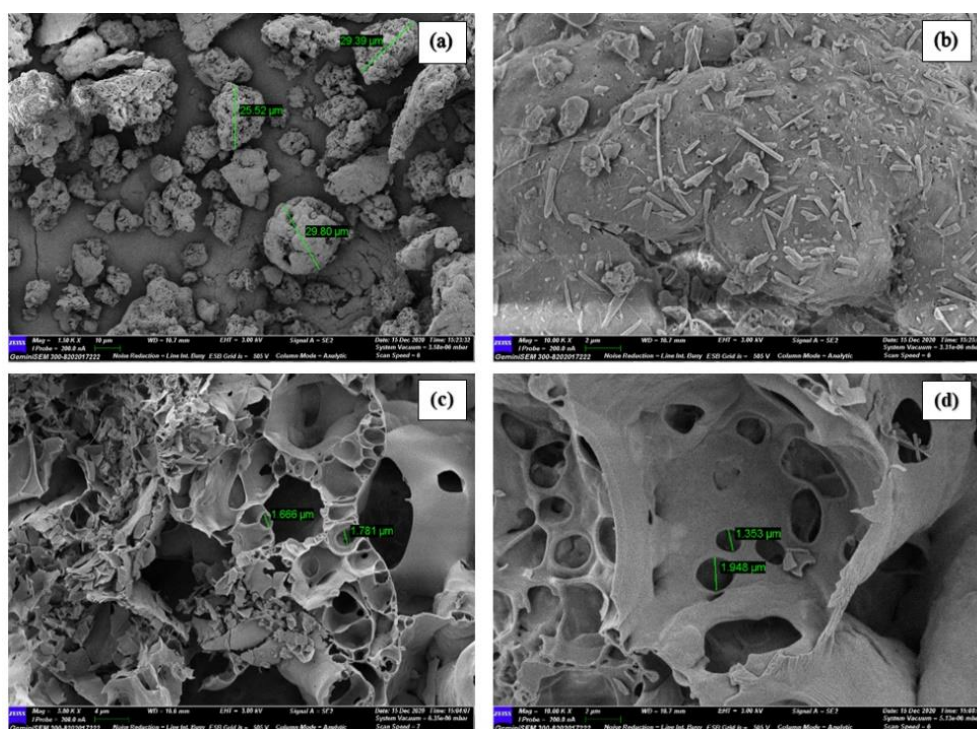*5.4.4 Morphological and structural studies on LS and LCF*



**Figure 5.18 Surface morphological characteristics of extracted lignin (a) at a 1500x magnification (b) at a 10,000x magnification and LCF (c) at a 5000x magnification (d) at a 10,000x magnification**

The surface morphologies of the extracted lignin (LS) and LCF were analyzed using FESEM images, as illustrated in figure 5.18. The obtained lignin (LS) particles show an irregular and less defined shape and form large conglomerates in the solid-state. The self-assembled agglomerate size ranges from 25μm-30μm. It was also found that the particles were unable to disperse in water which confirms the hydrophobicity of the lignin particle. In LCF, the surface is porous in nature with slender ligaments, and each cell is open and interconnected by a 3D network to adjoining cells.

Further, details on pores in LCF was obtained from the $N_2$ adsorption/desorption isotherm for LCF and Barret–Joyner–Halenda (BJH) plot for the pore size distribution of LCF. This isotherm represents Type III classification in isotherm at $p/p_0$ ranging from 0.0006 to 0.9908, forming a convex curve to $p/p_0$ axis (Kruk and Jaroniec 2001). A hysteresis loop in the plot exhibits the capillary condensation process at mesopores. Moreover, the gradually inclined adsorption curve (figure 5.19) depicts that the

mesopores/internal voids form irregular shape which can be confirmed from FESEM images (figure 5.18). The mean pore diameter, specific surface area, and pore volume values measured for LCF at $p/p_0$ =0.99 were 19.752 nm, 8.42 $m^2$/gm, and 0.0416 $cm^3$/g respectively. According to Achaw (2012), pore diameter between 10 nm-50 nm is considered mesopores, and they play a vital role in being ducts through which interiors of the carbon foam can be accessed. The BJH plot from desorption isotherm confirms the material to be mesoporous with a peak centred at 1.22 nm.

In comparison with the FESEM images, it can be summarized that the higher specific surface area attributes to the generation of mesopores within the LCF structure. The formation of these pores could be due to the expulsion of gases during the carbonization process at 180°C. Similarly, Priyanka and Saravanakumar (2018) and Wang, O'Connell, and Chan (2015) have observed similar results while preparing carbon foam from starch and sucrose. The mesoporosity confers the ability to adsorb diverse molecules in large quantities, making them suitable for the separation process.



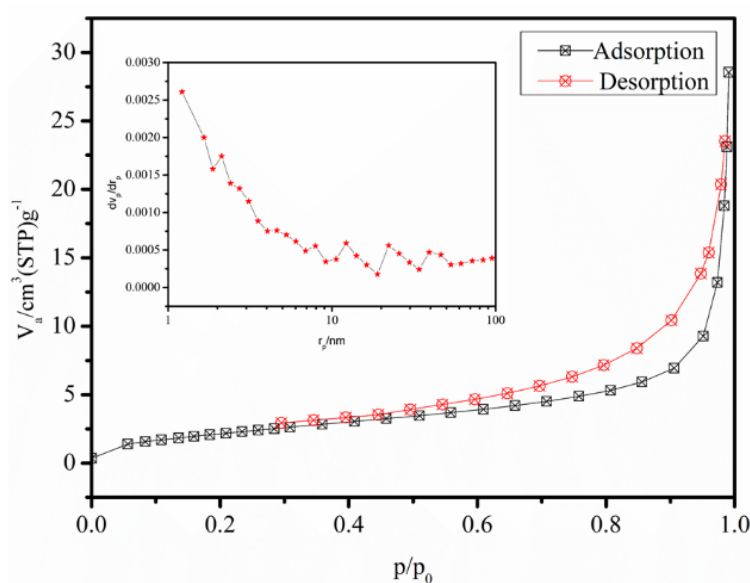**Figure 5.19 N$_2$ Adsorption-desorption isotherm for LCF at a temperature of 77K and saturated vapour pressure of 97.763kPa. Inset is the BJH plot for the pore size distribution of LCF evaluated from the isotherm analysis.**

From figure 5.20 (a), it can be noticed that extracted lignin particles pose the carbon (67.76%), oxygen (24.93%) and a trace amount of sulphur. These results are in line

106

with Aroua et al. (2009), which affirms the lignin particles after organosolv treatment of AH. The persistence of the ZnO and lignin particles embedded on the carbon foam can be confirmed from the presence of carbon, nitrogen, oxygen, and zinc from EDAX results as shown in figure 5.20 (b). The content of these elements was found to be 40.99% of carbon, 37.05% of zinc, 21.56% of oxygen and trace amounts of nitrogen in the LCF.
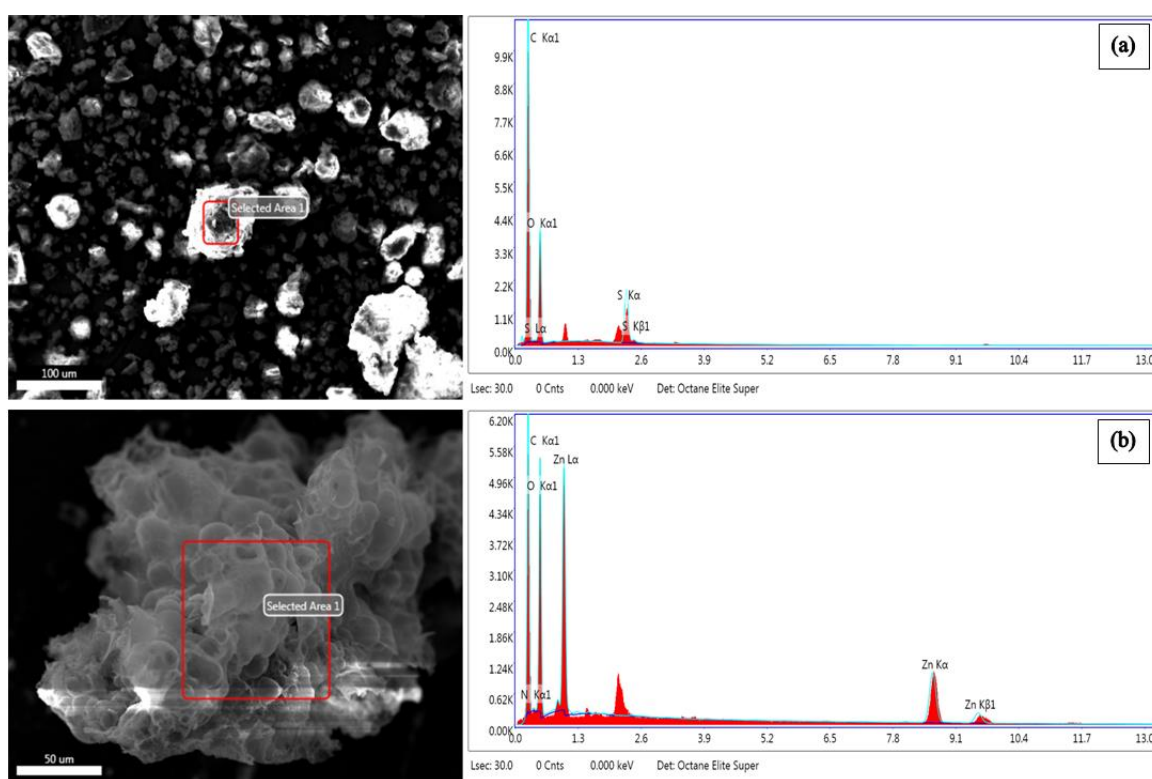


**Figure 5.20 EDAX spectra of sample (a) lignin extracted from AH (b) Lignin based-carbon foam (LCF)**

The extracted lignin (LS) X-ray diffraction pattern (figure 5.21) shows a broad peak indicating that it is amorphous and poses high cross-linking structure. The 3D polymer network of phenylpropane units does not have any order and stable molecular structure (Gupta et al. 2014; Wu et al. 2009). The XRD patterns of LCF shows the diffraction peaks at $2\theta = 22.51°$, $23.43°$, $31.78°$, and $33.87°$, as shown in figure 5.21. Out of these, the peaks at $31.78°$, and $33.87°$ (JPCDS card number: 00-036-1451) were allocated to planes (100) and (002) respectively. This plane specifies the hexagonal wurtzite crystal structure of ZnO with lattice parameters a= 3.25Å, b= 3,25Å, and c=5.21Å (Hussain

and Yakimova 2008; Molefe et al. 2015). Also, weak peaks found in the XRD pattern represents the amorphous nature of carbon in the LCF formed after carbonization. Moreover, the XRD curve width is observed to be greater than 0.5°. No structural information could be obtained for the carbon particle, ensuring that LCF (adsorbent material) is amorphous.
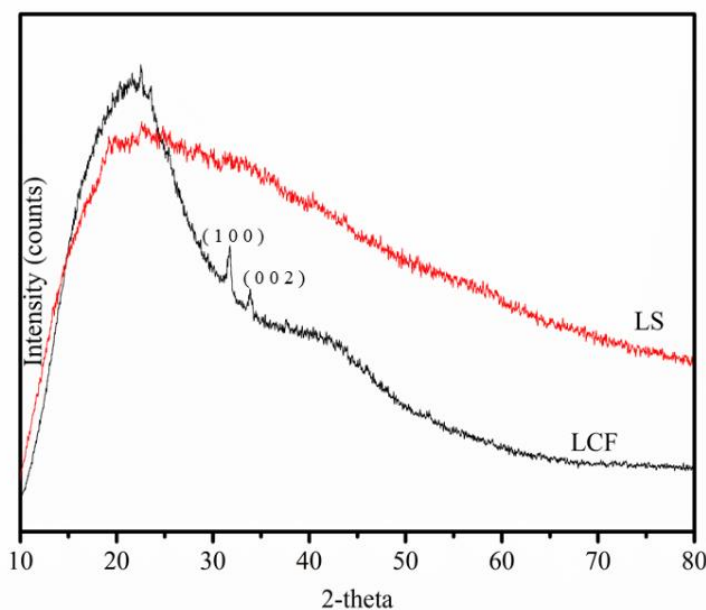


**Figure 5.21 Diffraction (XRD) pattern of LS and LCF**

The functional group determination of the lignin (LS) and lignin-based carbon foam (LCF) was done from the FTIR spectra (figure 5.22). Typically, the functional groups present in the lignin include carbonyl, carboxyl, hydroxyl, methoxyl, and aliphatic and aromatic C-H, which can be assessed from the FTIR spectra. The various peaks obtained for both LS and LCF and the corresponding assignments/ functional group are mentioned in detail in Table 5.10. A broad peak centred at 3338 (LCF) and 3408 $cm^{-1}$ (LS) is related to the stretching vibration of hydroxyl (-OH) groups. The signal at 2935 $cm^{-1}$ can be assigned to the C- H stretching of alkyl group present in lignin and lignin-based carbon foams. In the case of lignin (LS), high-intensity peaks ranging from 1500-1600 $cm^{-1}$ signifies the presence of aromatic lignin. The deformation in the C-H plane was due to syringyl monolignols at 1126 and 1094 $cm^{-1}$. The high intensities bands at 1512 and 1267 $cm^{-1}$ represent guaiacyl monolignols (Hamzah et al. 2020; Pereira et al. 2016).
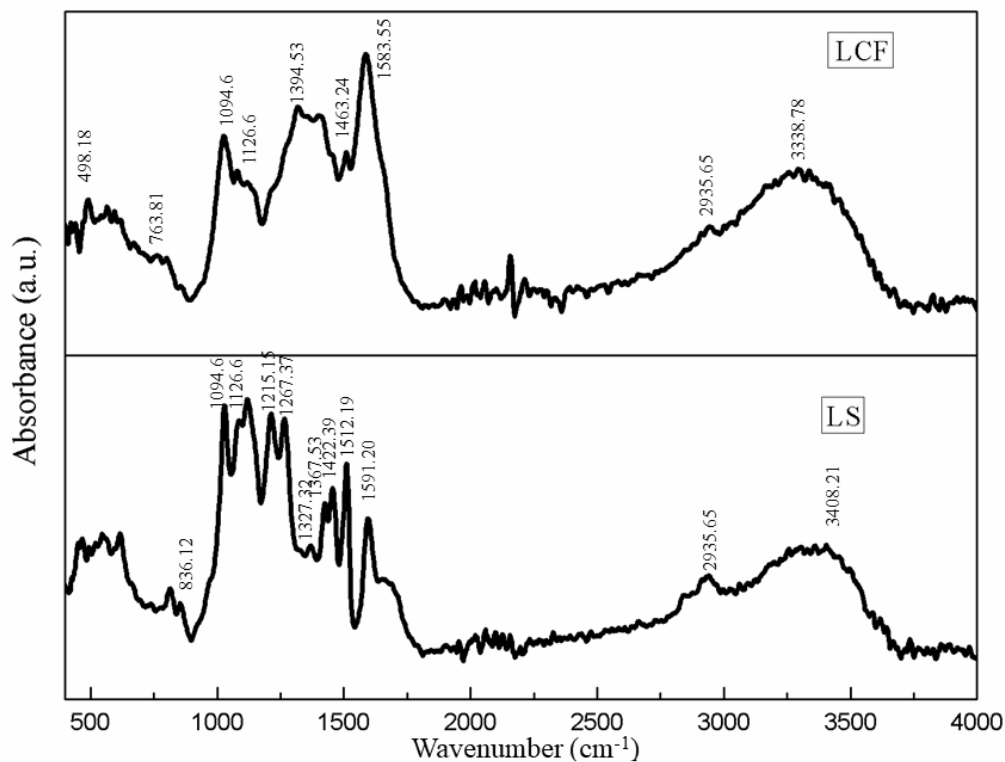
**Figure 5.22 FTIR spectra for the extracted lignin and LCF**

In the case of LCF, the peak at 763 $cm^{-1}$ represents the bending vibration of C-O in C-O-C group of starch. The peak at 498 $cm^{-1}$ attributes to the Zn-O stretching, which shows the presence of ZnO particles in the carbon foam (Fenoll et al. 2017). Also, the aromatic stretching vibrations at 1583 $cm^{-1}$ represents the presence of lignin in LCF. Similarly, the peak at 1126 $cm^{-1}$ attributes aromatic ring deformation in guaiacyl monolignols. The vibrations of carboxylic groups in the LCF is noted at the peak 1094 $cm^{-1}$ (Qu et al. 2017; Rao et al. 2020). Additionally, few lignin peaks are seen in the FTIR spectra of LCF, which confirms lignin in the LCF.

**Table 5.10 Attribution of FTIR spectra peaks**

| Lignin (LS) | | Lignin based carbon foam (LCF) | |
|---|---|---|---|
| Band position (cm$^{-1}$) | Assignment | Band position (cm$^{-1}$) | Assignment |
| 1589-1593 | Aromatic ring in guaiacyl and syringyl units | 1583 | C = C aromatic stretching |
| 1508-1512 | Aromatic ring in guaiacyl and syringyl units | 1463 | C - O vibration |
| 1417-1421 | C-H stretching in the guaiacyl and syringyl in plane | 1394 | C-H deformation |
| 1325-1327 | C-O stretching in syringyl units | 1126 | Vibration of C-O-C |
| 1267 | C-O stretching in guaiacyl units | 1094 | Vibrations of carboxylic groups |
| 1219-1226 | C-C, C-O and C=O stretching in guaiacyl units | 763 | C - O bending vibration |
| 1159-1161 | C=O stretching in ester grouping | 498 | Zn-O stretching bonds |
| 1126-1128 | Aromatic ring deformation in guaiacyl unit | | |
| 1091-1095 | C-O stretching in aliphatic ethers or secondary alcohols | | |
| 835-839 | Deformation out of C-H plane in guaiacyl and syringyl units | | |

*5.4.5 Thermal studies on LS and LCF*

The thermal studies on stability and degradation of organic compounds have been determined using TGA analysis under N$_2$ atmosphere. Herein, the TGA curve specifies the weight loss, whereas the DTG curve (figure 5.23) defines the corresponding weight loss rate with respect to temperature. Lignin structure is composed of aromatic rings with several branches, and the activity of chemical bonds lead the degradation in a wide

range of degradation temperature (100-800°C) (Yang et al. 2007). In the case of LS (figure 5.23 (a)), it can be noticed that lignin degradation can be divided into three stages. In the first stage, initial weight loss occurred between 28°C-80°C indicates the water evaporation. In the second stage, a steep curve can be found as the temperature rises from 120°C to 390°C, which attributes to the degradation of carbohydrate moieties in lignin sample and expulsion of volatile gases ($CO_2$, $CO$, and $CH_4$). At the final stage, degradation continues for a broad range of temperature (above 390°C). The degradation of volatile products (alcohols, phenolics, aldehyde, and acids) derived from lignin is characterized at this stage. About 32% of residues were still found unvolatized at 600°C, attribute to the formation of condensed aromatic structures which further forms char at elevated temperature. The thermal degradation of lignin material was initiated only after acquiring a certain quantity of heat. The max peak of DTG curve depicts the thermal stability characteristic of the material. The lignin extracted from AH had higher thermal stability (390°C), and in this region, pyrolytic decomposition is expected to happen. Watkins et al. (2015) reported that the $DTG_{max}$ values of lignin extracted from wheat straw, flax fibre, alfalfa, and pine straw were between 320°C-340°C.

Compared with this, the AH extracted lignin shows slightly higher thermal stability than the above mentioned lignins. The degradation includes the release of monomers, the disintegration of inter-unit linkages, and volatilize phenol derivatives. At an elevated temperature higher than 500°C, the disintegration of aromatic rings takes place and further form char (Sun et al. 2000; Tejado et al. 2007).
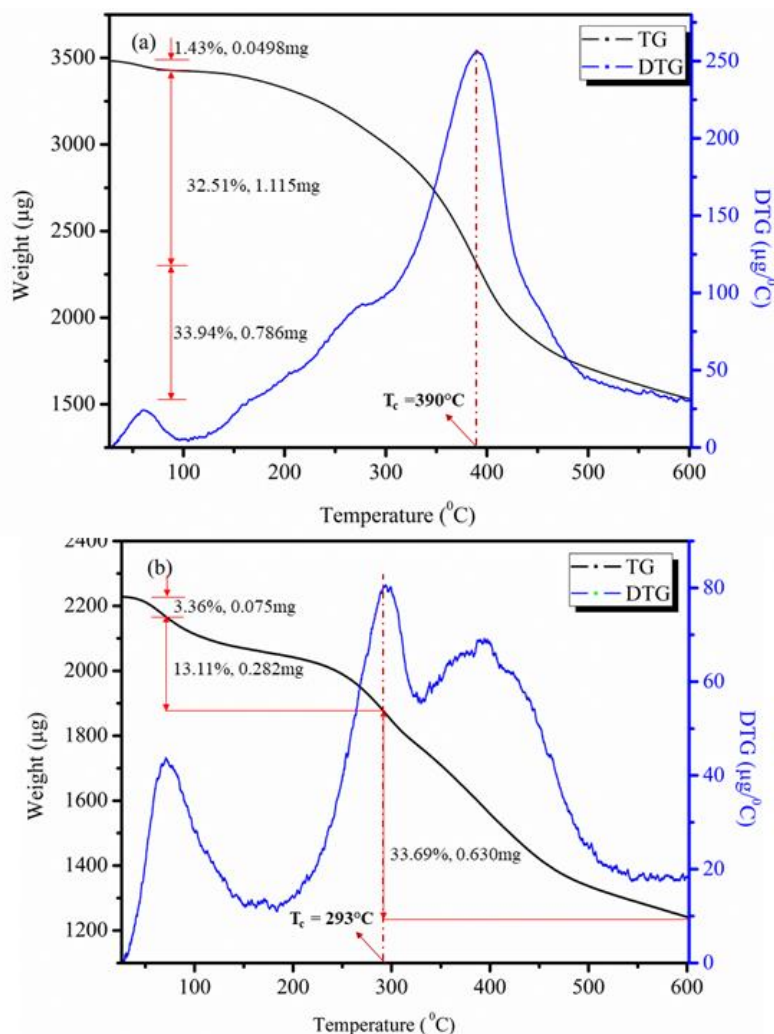
**Figure 5.23 TGA and DTG curve for the (a) extracted lignin and (b) LCF**

Similarly, the TGA and DTG curve for investigating the degradation process and thermal stability of LCF is depicted in figure 5.23 (b) as shown above. The curve portrays a three-stage degradation process from temperature 27°C to 600°C. The initial weight loss of 3.36% at $1^{st}$ stage of degradation implies the water loss in LCF. At the $2^{nd}$ stage of degradation (~80°C - 293°C), the functional group-containing oxygen present in starch-based ZnO embedded carbon foam gets degraded. The maximum weight loss (33.69%) was at the $3^{rd}$ stage of degradation (~293°C - 600°C) of LCF, representing the degradation of the lignin at a temperature above 390°C. The residuals presence of 49.83% indicates the presence of ZnO and high thermal stability of LCF (Ulfa et al. 2017).

*5.4.6 Adsorption studies on LCF*

The carbon foam embedded with the ZnO particles could interact with the lignin skeletons by π-π conjugation, making the material lightweight and excellent hydrophobic. LCF exhibits good potential for oil adsorption from the oil-water emulsions due to the outstanding properties such as highly porous structure, low density, low wettability and high thermal stability. During the oil distribution onto the surface of LCF, the air present in the mesopores is replaced by the oil due to hydrophobic interaction, capillary effect and Vander Waals forces. The LCF has a bulk density of about 0.0294 $g/cm^3$, which is very light in weight and placed on a fragile leaf (Figure 5.24 (a)), which could retain it without bending it. This helps the LCF float on the water's surface to efficiently remove the oils spread on the water surface. The digital images are shown below (Figure 5.24 (b)) prove that the synthesized LCF exhibits excellent hydrophobicity, which is demonstrated by placing a water droplet on the surface and allowing it to stay.

The tap water, distilled water and seawater droplet form an oval shape on the surface of the LCF. The fire-retarding property of the LCF can be evaluated by the flame test with the dominant orange flame of temperature ranging from 1100°C-1200°C, as shown in Figure 5.24 (c). As can be seen, the LCF showed a flame resistance on continuous exposure to the fire. The LCF found it hard to get ignited for about 40 secs, and the finally flame was self-quenched immediately, leaving behind large-area residue. Additionally, the LCF has shown a high electrical resistivity of 1.69 MΩ (Figure 5.24 (d)), making them suitable for electrical field applications.
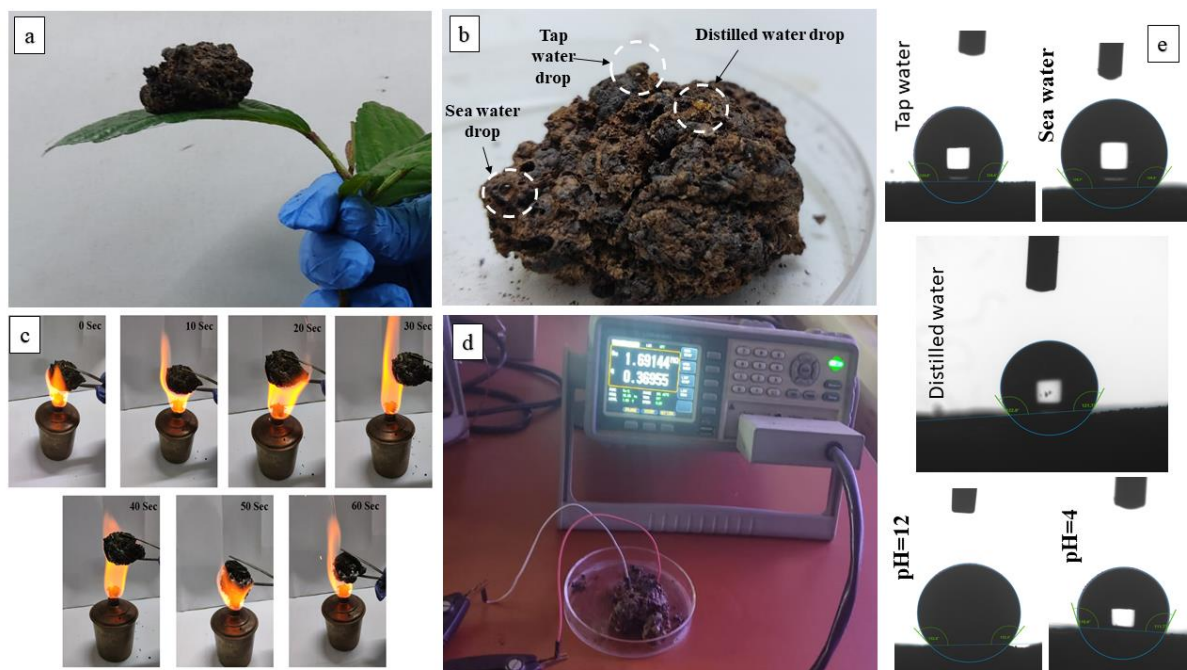
**Figure 5.24 (a) Digital images of the LCF on a fragile leaf (b) Digital images of the LCF with different water droplets on its surface (c) Flame (d) resistivity (e) Contact angle of various waterdrops on the surface of LCF**

The contact angle of the lignin-carbon foam for the different water-based solvents is shown in Figure 5.24 (e) above. When a water droplet is placed on the LCF surface, the intermolecular interactions between the liquid and solid phases will determine the spread of the drop. The contact angle formed between the droplet and the surface indicates the LCF wettability. The contact angle value greater than 90° represent hydrophobic or poor wettability feature. The contact angle for distilled water, tap water, seawater, solution of pH 4, and pH 12 was as follows 122°, 124°, 129°, 110°, and 132° respectively, which displays that LCF is highly hydrophobic.

*5.4.7 Adsorption studies*

The porous lignin-based carbon material was found to be an ideal material for the separation of oil in oil-water emulsions. The adsorption of a wide range of oils such as 2T engine oil, diesel oil, petrol oil, crude sunflower oil, and organic solvents such as toluene, petroleum ether, and n-hexane with different viscosity and density was carried out on the LCF. The series of photos given below, Figure 5.25, shows the adsorption progress of various oils on the LCF. The adsorption of diesel oil on the LCF was higher than the other oils, as depicted in Fig. 5.26. So, diesel oil was selected further to analyze

the rate and mechanism behind the adsorption process. Also, the retention of the adsorbed oil in the LCF was between 85%-99%. The selected oils, such as crude sunflower oil, petrol, diesel, 2T engine oil, n-hexane, toluene, and petroleum, show the contact angle approximately 0° (Figure 5.26). This confirms the super-oleophilicity of the LCF.

The following is the Supplementary information related to this article Video S2.
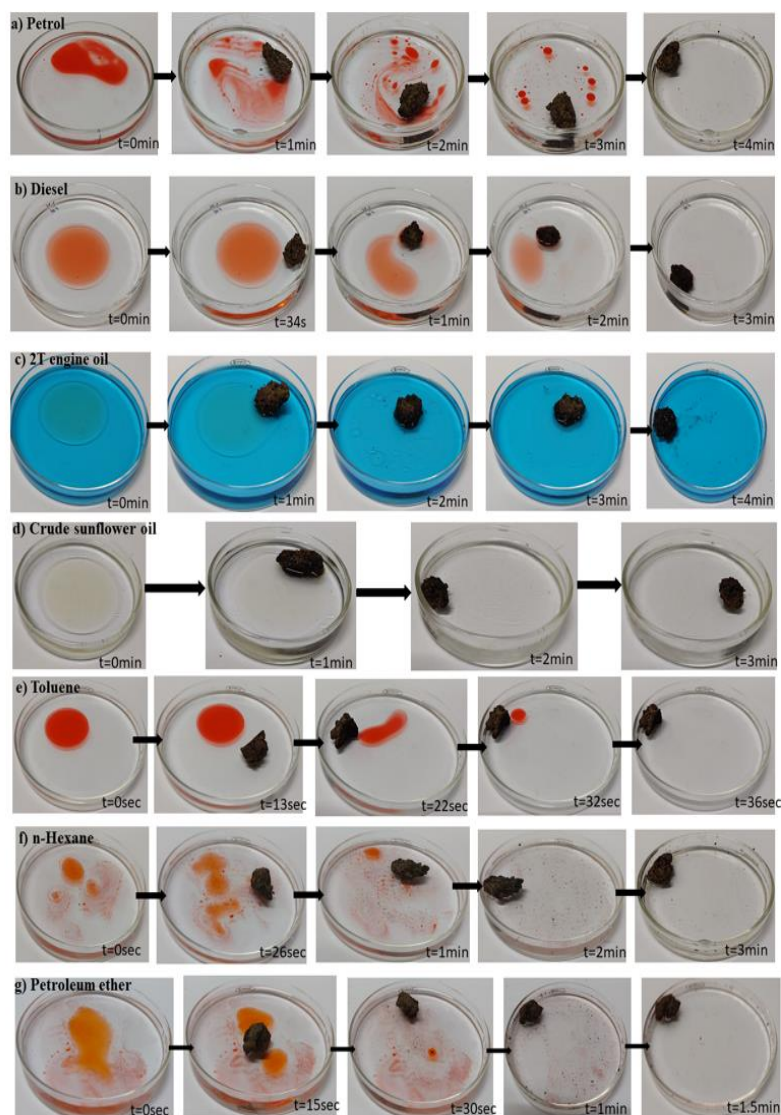


**Figure 5.25 Adsorption progress of various oils (a) petrol dyed with Sudan III in water (b) diesel dyed with Sudan III in water (c) 2T engine oil in water dyed with methyl blue (d) crude sunflower oil in water (e) toluene dyed with Sudan III in water (f) n-hexane dyed with Sudan III in water (g) petroleum ether dyed with Sudan III in the water on to the LCF**
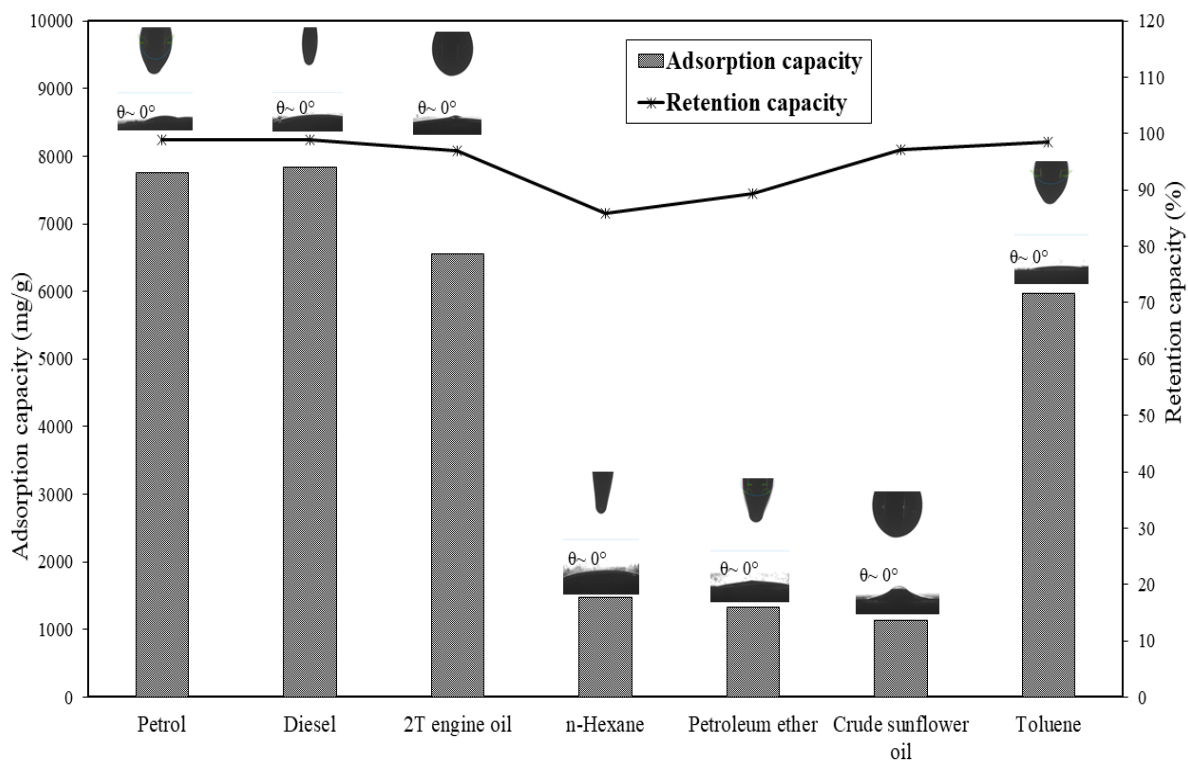
**Fig. 5.26 Adsorption capacity and retention capacity of various oils on to the LCF; Inset is the contact angle images of the different oils and solvents on LCF**

Additionally, a continuous oil-water separator was placed using a vacuum pump and syringe piston plugged with LCF (figure 5.27). Using this setup, continuous separation of diesel oil in water was carried out until no oil droplets were found in the water or clean and transparent water was obtained (figure 5.27). The result affirms that the LCF is capable of attaining the oil-water separation with high efficiency.

**Figure 5.27 (a) Schematic representation of the continuous oil-water separator setup using LCF (b) digital images of the actual setup in the laboratory (c) Clearwater remained in the piston after adsorption (d) separated diesel oil and water after adsorption by LCF**

*5.4.8 Factors affecting the adsorption process*

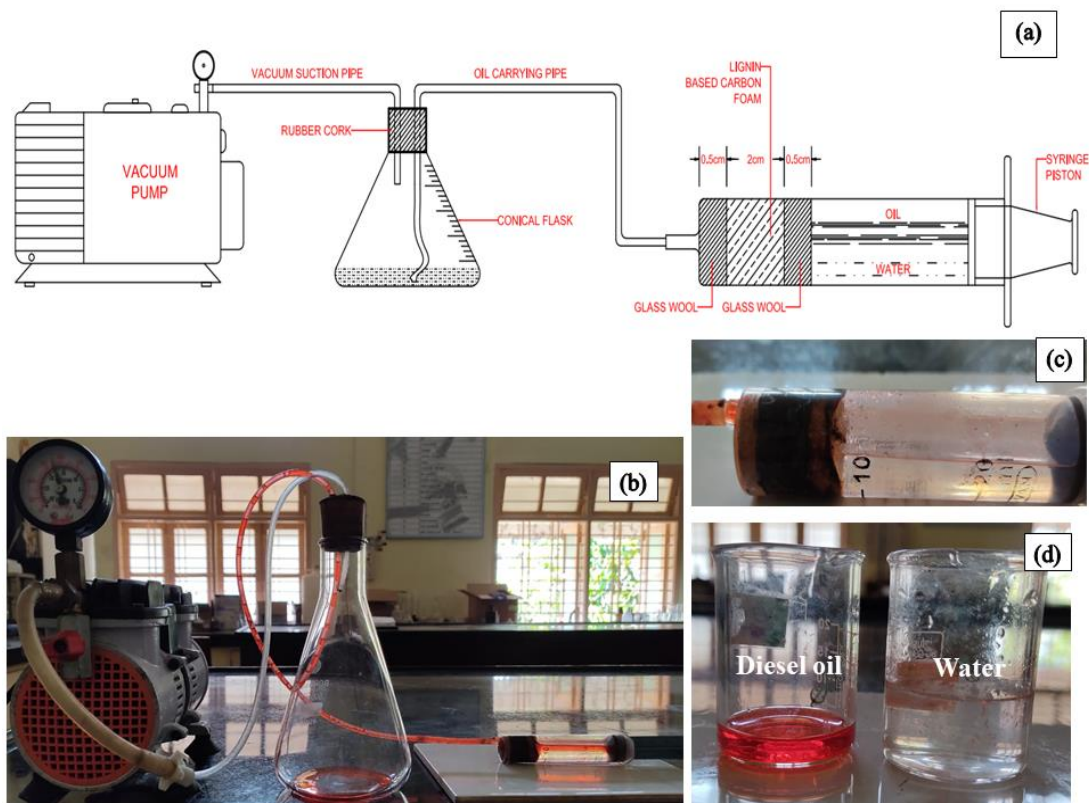The contact time, initial oil concentration, and adsorbent dosage form the fundamental factors governing the adsorption process (Figure 5.28). The optimization of the contact time is necessary to find the equilibrium contact time for maximal oil adsorption. The optimization was done by keeping the adsorbent dosage as 1.0g and initial oil concentration as 30g/L. A rapid oil uptake can be visible from 10 min to 30 min, and then it slows down till 180 mins, as shown in Figure 5.28 (a). Later, it attains an equilibrium condition after which the adsorption capacity becomes constant. This can be because of the saturation of active sites in the outer surface by the adsorbed oil, and no longer diffusion occurs (Khalifa et al. 2019).

Also, initial oil concentration strongly influences the kinetics and equilibrium behaviour of the adsorption process. The plot (Figure 5.28 (b)) depicts an increase in

the adsorption with the rise in initial oil concentration and then reaches a constant. The curve shows that the adsorption capacity rises abruptly with the initial oil concentration from 10g/L to 30g/L and then takes a gradual increase to reach a plateau. As the oil concentration increase, an improvement in oil distribution on the surface and interiors occur due to the gradient between the adsorbent particle and bulk solution. After 30g/L, no remarkable change is noticed in the adsorption, which confirms the proper consumption of vacant sites available in the adsorbent (Khalifa et al. 2019).

The impact of adsorbent dosage from 0.05g to 3.0g on diesel oil removal is depicted in Figure 5.28 (c). All other parameters, such as initial oil concentration and contact time, were kept constant at 10g/L and 10 min. Similarly, dosage optimization is also essential to attain maximum adsorption within a minimal dosage. A decrease in the adsorption can be seen with the increase in dosage, which claims that active sites remain unsaturated during the adsorption process (Lv et al. 2018).
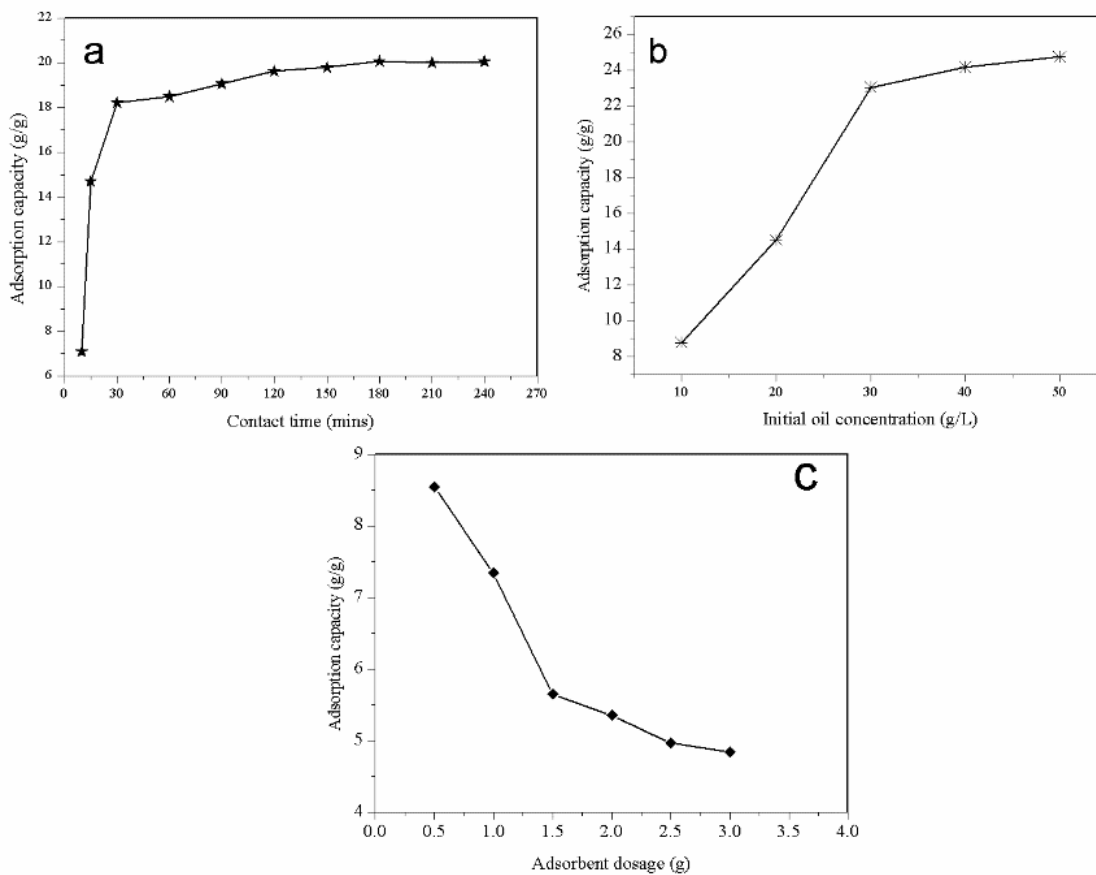


**Figure 5.28 Optimisation of factors (a) Contact time (b) Initial oil concentration & (c) Dosage**

### 5.4.9 Kinetics and isotherm study for diesel oil adsorption

The chemical or physical adsorption mechanism behind the adsorption process can be well addressed with kinetic modelling. The rate and mechanism behind the diesel oil adsorption process were analyzed by applying kinetic models such as pseudo-first-order, pseudo-second-order, and intra-particle diffusion model (Figure 5.29) to the experimental data of diesel oil adsorption by LCF. It was evident from the $R^2$ values that model fitness order follows: pseudo-second-order>pseudo-first order>intra-particle diffusion model for the diesel oil adsorption by LCF. The kinetic model parameters are enlisted in Table 5.11, given below. Figure 5.29 shows that the experimental data do not follow pseudo-first-order kinetics since the $R^2$ values attained are 0.855. The pseudo-second-order model best describes the diesel oil adsorption kinetics onto LCF. The pseudo-second-order model is based on the hypothesis of the chemisorption process of diesel oil on LCF. The mechanism followed is the transportation of oil from the reservoir to the LCF surface by valence forces through the exchange or sharing of electrons between adsorbate and adsorbent. The intra-particle diffusion model shows three complex steps in adsorption, i.e., two portions of linear and one portion of curved transition. The surface adsorption of diesel oil onto LCF by particle diffusion with a diffusion rate constant of $k_{p1}$ (value=4.731). The intermediate stage forms a curved portion that corresponds to the external border layer diffusion. The final linear stage represents the interior surface diffusion with the rate of constant $k_{p2}$ (value= 0.289). The value of $k_{p1}$ is greater than $k_{p2}$, which specifies that the internal pore diffusion is the rate-limiting step. The linear portion represents the macropore and mesopore diffusion of oil inside the LCF (Ewis et al. 2020).
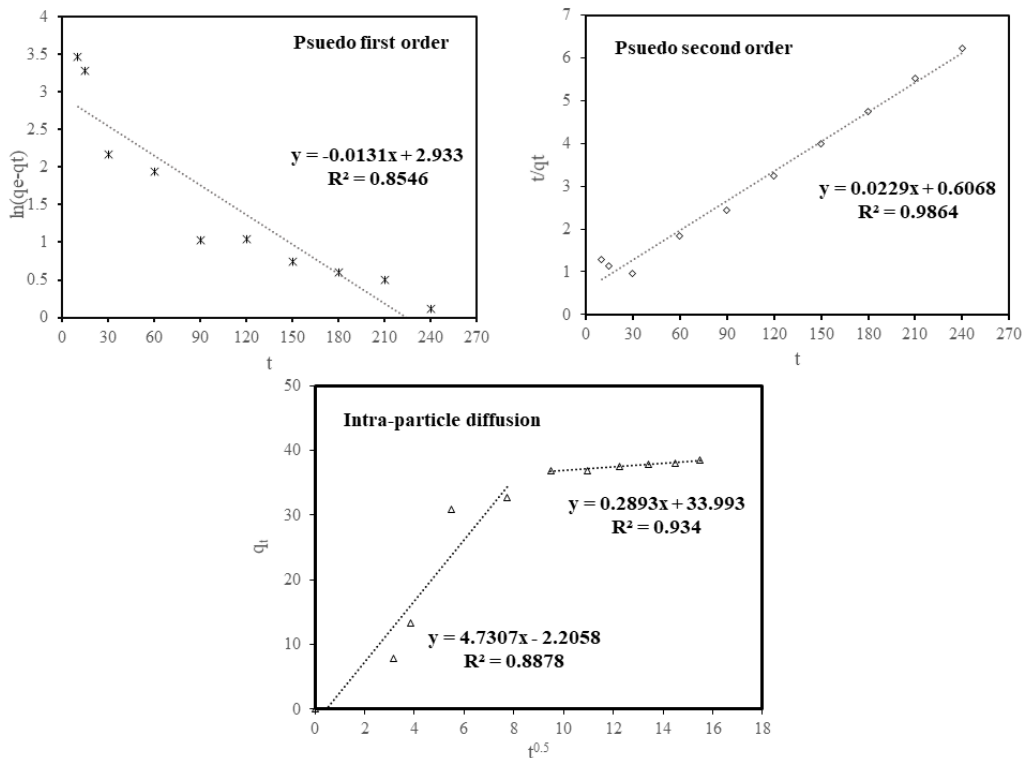
**Figure 5.29 Kinetic study on the adsorption of diesel oil onto the LCF**

Adsorption isotherms help understand the adsorption mechanism and quantify the adsorbate distribution between the solid and liquid phases at equilibrium. The fitness of each model to the experimental data can be determined by the regression correlation coefficient ($R^2$), as shown in Figure 5.30. From the study, it can be concluded that the Temkin>Freundlich >Langmuir>D-R>Elovich. The parameters evaluated by these adsorption isotherms are depicted in Table 5.11. It can be noted that the experimental data fitted best in Temkin isotherm ($R^2=0.955$) when compared with the other isotherms. The negative linear relationship between the heat of adsorption and surface coverage due to adsorbent-adsorbate interactions can be explicitly studied from the Temkin isotherm. The Temkin model plot provides a positive straight line with a $K_T$ value to be 0.151 and heat of adsorption, B value to be 15.254 J/mol. The positive energy value indicates that the adsorption process is endothermic (Inam et al. 2017).

Also, Freundlich isotherm shows a similar closeness to the experimental data with $R^2=0.947$. This makes it evident that the adsorption process is multi-layered and asymmetric. The n value portrays the heterogeneity in the adsorption process, i.e., if n≤1, then the adsorption mechanism is heterogenous and if n ≥1, then the adsorption is

homogenous. In this study, the n value obtained was 1.47, which is greater than 1, so the adsorption mechanism is expected to be homogenous. Moreover, the entrapment of oil in the LCF is accomplished by the pore filling along with the surface adsorption. The $K_f$ and $1/n$ values were 2.091 and 0.678, respectively, where $K_f$ was attributed to the adsorption capacity and n for adsorption intensity. Strong interaction between LCF and diesel oil can be inferred from the smaller $1/n$ (value= 0.678). For the Langmuir isotherm, the $q_{max}$ value and $K_L$ values were 69.44g/g and 0.0162 L/g. The $R_L$ value of 0.86, between 0 and 1, shows that the isotherm is favourable and feasible (Khalifa et al. 2019). The experimental data did not fit into D-R and Elovich isotherms, whose $R^2$ values were not close to 1.0. For this cause, the D-R and Elovich isotherm parameters cannot be applied to the present diesel oil adsorption study using LCF.

**Table 5.11 Kinetic and isotherm parameters for the diesel oil adsorption process onto LCF**

| Serial No. | Kinetics | Plot | Parameters |
|---|---|---|---|
| **Kinetic models** | | | |
| 1 | Pseudo-first order | $\ln q_e$-$q_t$ vs. t | $q_{e, cal}$= 18.78g/g $k_1$=0.0131 min$^{-1}$ $R^2$= 0.855 |
| 2 | Pseudo-second-order | $t/q_t$ vs. t | $q_{e, cal}$= 43.66 g/g $k_2$= $8.64 \times 10^{-4}$ min$^{-1}$ $R^2$= 0.986 |
| 3 | Interparticle diffusion | $q_t$ vs. $t^{0.5}$ | $k_{p1}$ = 4.731 $k_{p2}$ = 0.289 $C_1$=-2.206 $C_2$=33.993 |

| Serial No. | Isotherm | Plot | Parameters |
|---|---|---|---|
| **Isotherm models** | | | |
| 1 | Langmuir | $C_e/q_e$ vs. $C_e$ | $q_m$=69.44g/g $K_L$ = 0.016 L/g $R_L$= 0.860 $R^2$= 0.916 |
| 2 | Freundlich | $\ln q_e$ vs. $\ln C_e$ | n= 1.475 $K_F$= 2.091 $R^2$= 0.947 |
| 3 | Temkin | $q_e$ vs. $\ln C_e$ | B=15.254J/mol b=0.165J/mol |

| | | | $K_T$= 0.151 |
|---|---|---|---|
| | | | $R^2$=0.955 |
| 4 | Dubinin-Radushkevich | ln $q_e$ vs. $\mathcal{E}^2$ | $q_s$= 35.332g/g |
| | | | $K_{D-R}$= 25.939 |
| | | | E=0.139 |
| | | | $R^2$= 0.821 |
| 5 | Elovich | ln ($q_e/C_e$) vs. $q_e$ | $q_{max}$= 53.476g/g |
| | | | $K_E$= 0.0203L/g |
| | | | $R^2$= 0.6574 |
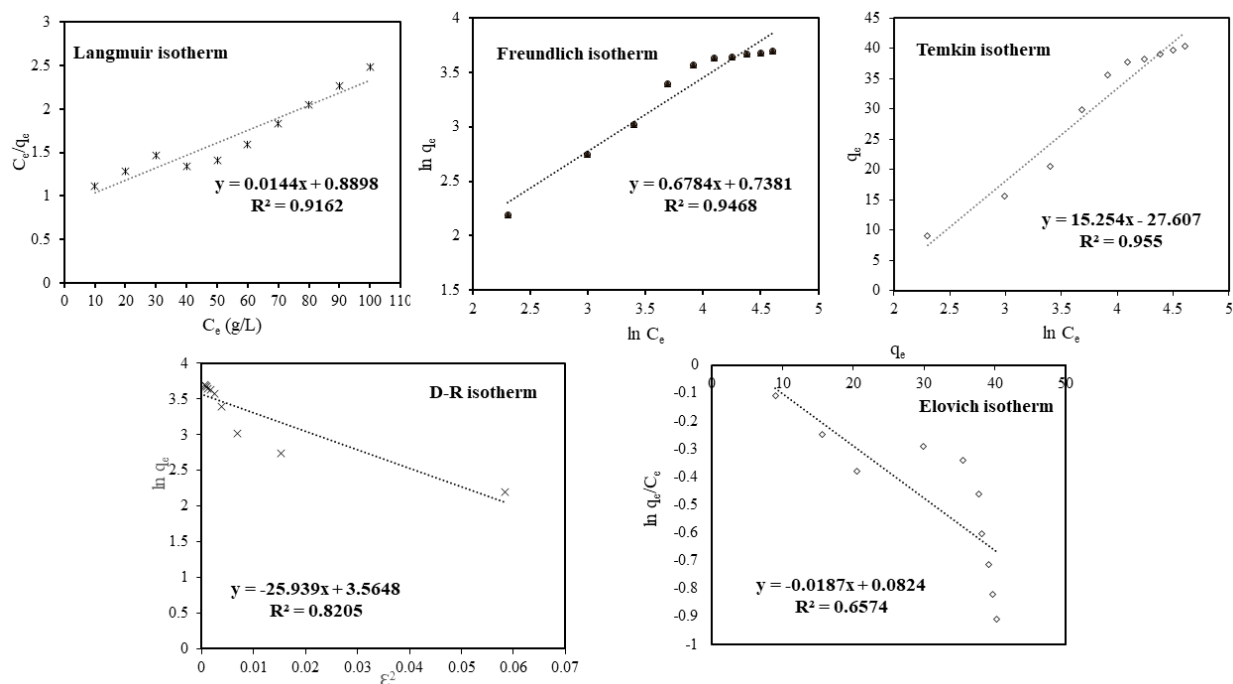


**Figure 5.30 Isotherm study of diesel oil on LCF**

The adsorption of oil on the LCF was checked w.r.t temperature (T). The test was performed at four temperatures, viz., 298K, 303K, 308K, and 313K. As the adsorption occurs spontaneously at a given temperature, it is permissible if the G° indicates a negative value. G° values were observed to be negative (-2592.76, -2732.27, -2850.45, -2973.84 J/mol) at 298K, 303K, 308K, and 313K respectively, from the graph plot of ln $K_d$ vs 1/T (Figure 5.31(a)). The value of G° decreased gradually as the temperature increases, indicating that adsorption was more favourable as the temperature increases (Figure 5.31(b)). Because of the endothermic aspect of the reaction, it was determined that $\Delta H^o$ was positive (+4926.46 J/mol), and the value of entropy change $\Delta S°$ (25.249 J/mol/K) was quite low. The positive value of $H^o$ indicated that the adsorbate species (oil) displaces the water molecules in order to bind to the binding sites, resulting in the

122

adsorption becoming endothermic. Exothermic processes are attributable to physical adsorption between the adsorbent and adsorbate, while endothermic processes are attributed to chemical adsorption mechanisms.
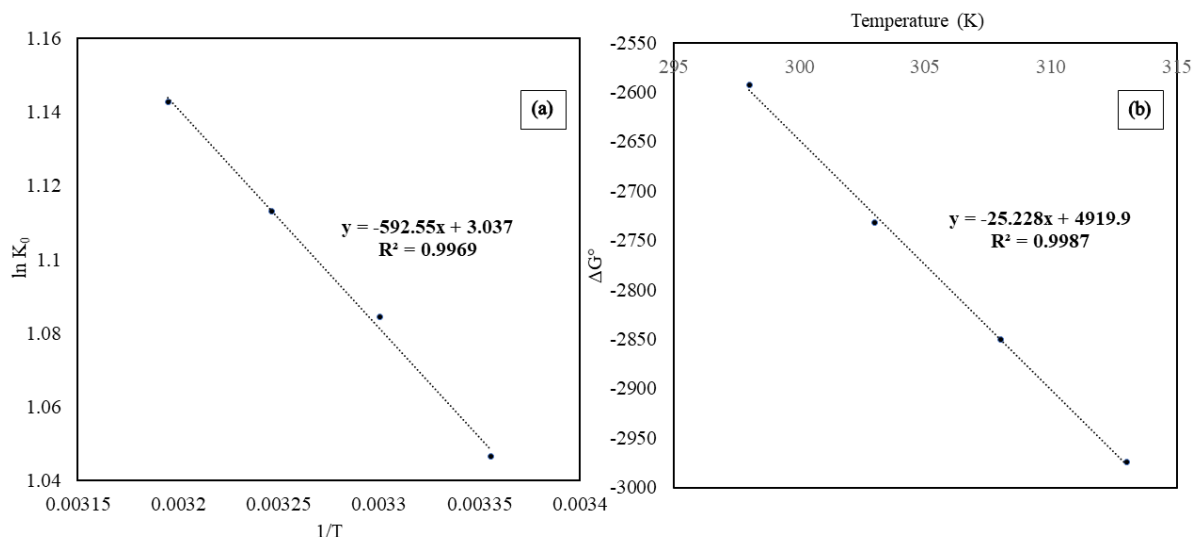


**Figure 5.31 Thermodynamic study of diesel oil on LCF (a) plot of ln $K_d$ versus 1/T and (b) plot of $\Delta G^o$ versus T**

*5.4.10 Reusability studies on LCF*

In the application of pollutant removal, large adsorption capacity and excellent reusability are two essential criteria. The LCF can readily separate the diesel oil that is floating on the surface of the water, and the LCF may then be reused by burning the diesel oil. The adsorption capacity of the LCF was tested up to five adsorption/burning cycles, as shown in Figure 5.32. By immediately exposing the LCF to the flame, and the adsorbed oil was removed. Approximately 93.7% of the original oil adsorption capacity is maintained after five adsorption/burning cycles. It suggests that the LCF can be utilised as a recyclable absorbent with a high level of sorption stability.

**Figure 5.32 Reusability studies: Adsorption capacity of LCF towards diesel oil after 5 adsorption/combustion cycle**

*5.4.11 Proposed adsorption mechanism*

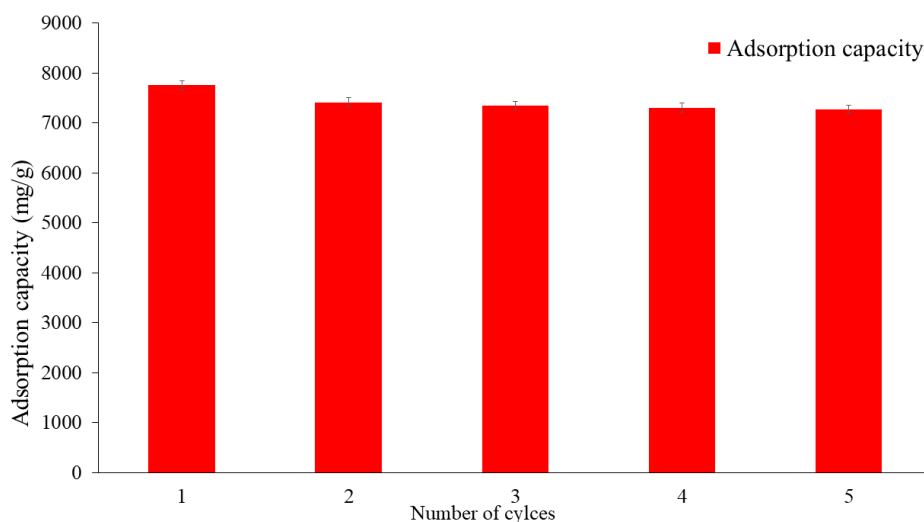The proposed mechanism (Figure 5.33 (b)) behind the spontaneous oil adsorption on LCF can be well explained by FESEM, BET and FT-IR analysis. The mesopores present in the LCF were initially captured by air before the adsorption. During the adsorption process, oil replaces the air and occupies the pore space forming oil-filled LCF. Moreover, diesel fuel is a mixture of hydrocarbons obtained from petroleum, and they are immiscible in water due to hydrophobicity. From the adsorption kinetics of LCF, it can be noted that the adsorption process follows a pseudo-second-order kinetic model, which specifies a chemisorption process. The LCF have some functional groups such as -COOH, -OH, C=C, etc. (Table 5.10), which can ensue in adsorption because of hydrogen bonding interaction. The diesel fuel underlay many functional groups such as paraffinic groups (-CH$_3$, -CH$_2$, -CH), naphthenic group (-CH-CH$_2$), olefinic group (-CH=CH$_2$), aromatic groups (C-CH), and ethanolic groups(-OH) (Jameel 2019). The H-bonding interactions happen between the oil molecule and the LCF in two categories (1) Dipole-dipole interactions and (2) Yoshida bonding. The H-donor present in hydroxyl groups of LCF interacts with the H-acceptors and aromatic rings in the oil, forming the dipole-dipole interactions and Yoshida bonding, respectively. The necessary evidence related to the adsorption mechanism can be delineated from the FTIR spectral changes before and after adsorption studies. The reduction in the OH peak intensities from 3000-4000 cm$^{-1}$ and 3528 cm$^{-1}$ after the oil adsorption (Figure

5.33 (a)) entitles the existence of dipole-dipole and Yoshida hydrogen bonding interactions. Also, the oxygen present in the carboxylic group, which acts as the electron donors, bonds with the aromatic rings (electron acceptors) in the oil at the interface of oil and LCF. The considerable reduction in the peak intensity of C-O can be noticed at the 1025 cm$^{-1}$ after the adsorption process exposes the n–π interaction (Ewis et al. 2020; Pan and Xing 2008).
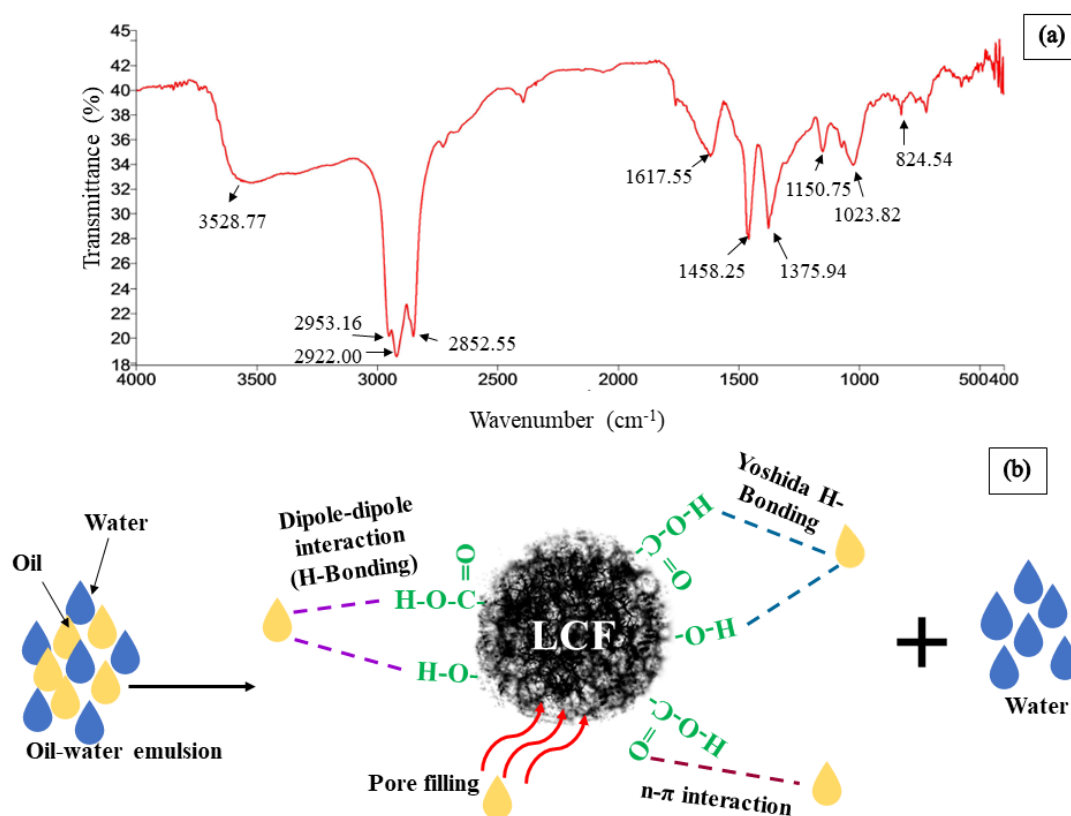


**Figure 5.33 Proposed mechanism for diesel oil adsorption by LCF**

A comparison table of LCF and other adsorbent materials previously published is depicted in table 5.11.

**Table 5.11 Comparison between the available foam materials for oil-water separation with the LCF**

| Material | Functionalized with | Wettability | Thermal stability | Sorption capacity | Reusability | Reference |
|---|---|---|---|---|---|---|
| Polyurethane (PU) foams | Graphite powder and magnetic nanostructures | 122° (WCA) and 0° (OCA) | Not reported | 30 g/g for Pump oil | more than 90% till 10 cycles | (Nandwana et al., 2020) |
| Lignin-formaldehyde (LPF) based carbon foams | Lignin | 149° (WCA) and 0° (OCA) | Not reported | 12 to 41 times higher than their own weight | more than 83% till 10 cycles | (J. Y. Qu et al., 2017) |
| Graphene foams | Graphene | 160° (WCA) and 0° (OCA) | Not reported | 165 times of its original weigh | more than 90% till 15 cycles | (Tabish et al., 2018) |
| Polystyrene (PS) foams | Magnetic ($Fe_3O_4$) particle | 138° (WCA) and 0° (OCA) | Sustains temperature up to 270°C | 17.83 and 16.21 times of its original weight | 10 reusable cycles via squeezing | (Yu et al., 2017) |
| Polyvinylidene fluoride (PVDF) foams | Expanded graphite | 159° (WCA) and 0° (OCA) | Not reported | 12 g/g for motor oil | 6 absorption/ desorption cycles | (Bentini et al., 2019) |

| | | | | | | |
|---|---|---|---|---|---|---|
| Polydimethylsiloxane (PDMS) foams | Sugar-templated | 120°-130° (WCA) and 0° (OCA) | Not reported | 498 wt% of its original weight | 20 reusable cycles via squeezing | (Choi et al., 2011) |
| Polyethylene foams | Waste packaging polymeric material | 96° (WCA) and 0° (OCA) | Not reported | 0.491–0.788 g/g | Not reported | (Patil et al., 2018) |
| Carbon foam | Cobalt based metal–organic framework (Co-MOF) nanosheets | 156° (WCA) and 0° (OCA) | Not reported | 85 to 200 times its own weight | 20 reusable cycles with no significant changes in sorption capacity | (Ge et al., 2019) |
| Thermoplastic polyurethane (TPU) | Carbon nanotubes | 135° (WCA) and 0° (OCA) | Not reported | 9 to 32 times its own weight | Poor adsorption capacity within 4 cycles | (Cao et al., 2018) |
| Lignin-carbon foam | Lignin-ZnO | 124° (WCA) and 0° (OCA) | Sustains temperature up to 390°C | 7.84g/g for diesel oil | with 93.7% capacity till 5 cycles | Present study |

# CHAPTER 6

## CONCLUSION

The following conclusions have arrived

❖ The pretreatment method's prioritization was done using the MADM technique to figure out the best out of all. The ranking done for each alternative from the suitability index value gives the priority list. The weight sets reduce the sensitivity of the weights, and the regression equation was obtained using DoE. Further, the calculated TOPSIS scores from the regression equation were used for the ranking. The best option obtained was the alkaline pretreatment both in terms of efficiency and economy. Similarly, the worst option was acidic pretreatment methods. It can be concluded that the model works well in prioritizing the pretreatment method for the sustainable conversion of lignocellulosic biomass to biogas.

❖ NaOH pretreatment effectively improved the hydrolysis of AH, as manifested by total phenols, COD and volatile solids solubilization, and the generally reduced lignin content of the pretreated materials. The maximum biogas yield was obtained for the 4% NaOH dosage at a temperature of 90ºC, and the yield was 2.3 times higher than the raw AH. A linear multiple regression equation was developed for the biodegradability index as a function of cellulose, hemicellulose and lignin with a reasonably high correlation having an $R^2$ value of 0.95. The Modified Gompertz model and logistic model fit better with the experimental results than the FOE and Transference function model.

❖ This research determined the feasibility of co-digestion of lignocellulosic biomass AH and food waste to produce biogas using an anaerobic batch mode digester at 35ºC. All the digestion tests were performed for 34 days, which required the complete digestion of the substrate mix. An AH: FW ratio of 1:1 gave higher biogas yield than other mix ratios confirm the husk usage as a substrate for fuel generation.

❖ The lignin extracted from AH was used as an additive for the facile synthesis of ultra-lightweight, excellent hydrophobic, and thermally stable lignin-carbon foam for oil spill clean-up. The water contact angle of LCF ranged from 110°~ 132°, making them water repellent. The rough surface texture and porous nature

(mesoporous) made the lignin-carbon foam exhibit hydrophobicity and instantaneously adsorbed a wide range of organic solvents and oils. The foam showed the highest adsorption for diesel oil (7842.71mg/g), and the least adsorption was for crude sunflower oil (1127.58mg/g). Also, this research proposes a model of continuous oil-water separation using LCF. The model can be possibly upscaled for extensive scale application in the field of oil-water separation. The synthesis of such oil-loving material from economical raw material is expected to be a good option for the clean-up of the oil spills.

❖ As a future recommendation, biogas production from the AH could be possibly up-scaled to a household level or small-scale industrial level for the given substrate. For the farmers who have arecanut plantations, the implementation of a small-scale biogas plant by co-digesting AH and FW would benefit them. An in-depth study on the microbial activities in the bioreactors for both pretreated and co-digested AH can help to correlate with the bigas production. Also, the effect of feeding frequency in the biogas production for the optimized substrate mix ratio (AH: FW) can be considered for the future study. In the case of adsorbent (LCF) used for oil-water separation, field-application study of the LCF could also be done.

# APPENDICES

## APPENDIX A

### Biogas composition data from Gas chromatography

### (a) 2% NaOH pretreatment of AH
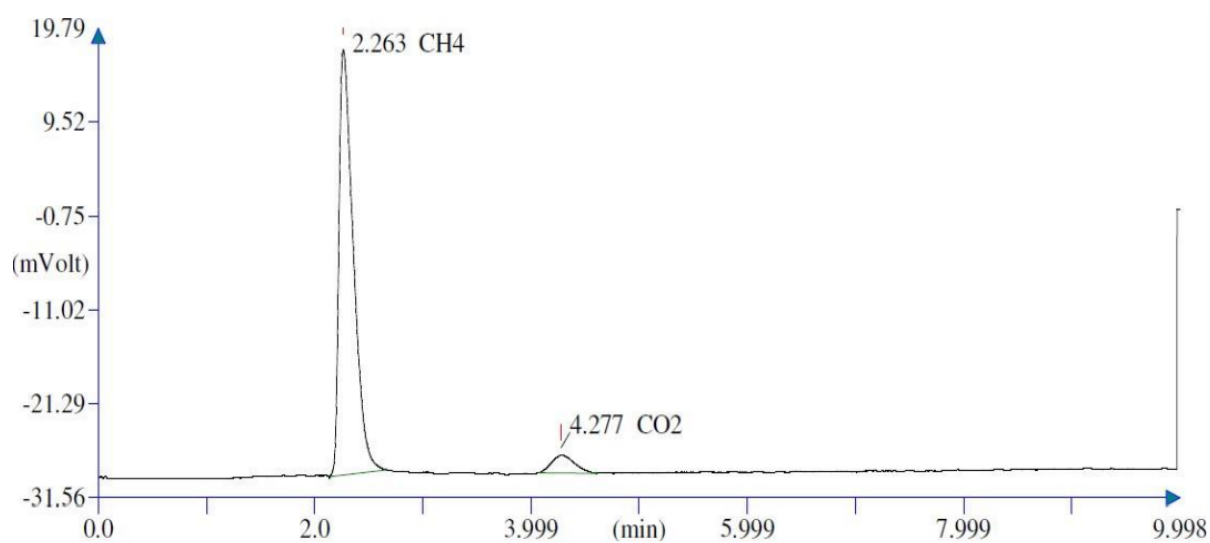


### (b) 4% NaOH pretreatment of AH

## (c) 6% NaOH pretreatment of AH



## (d) 8% NaOH pretreatment of AH

**(e) 10% NaOH pretreatment of AH**



**(f) Raw AH**

**REFERENCES**

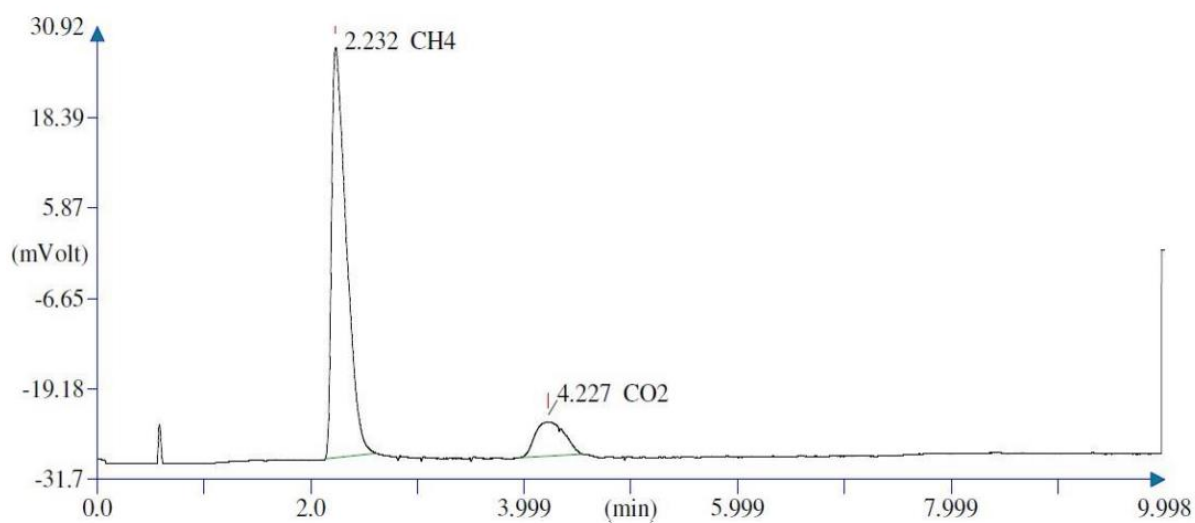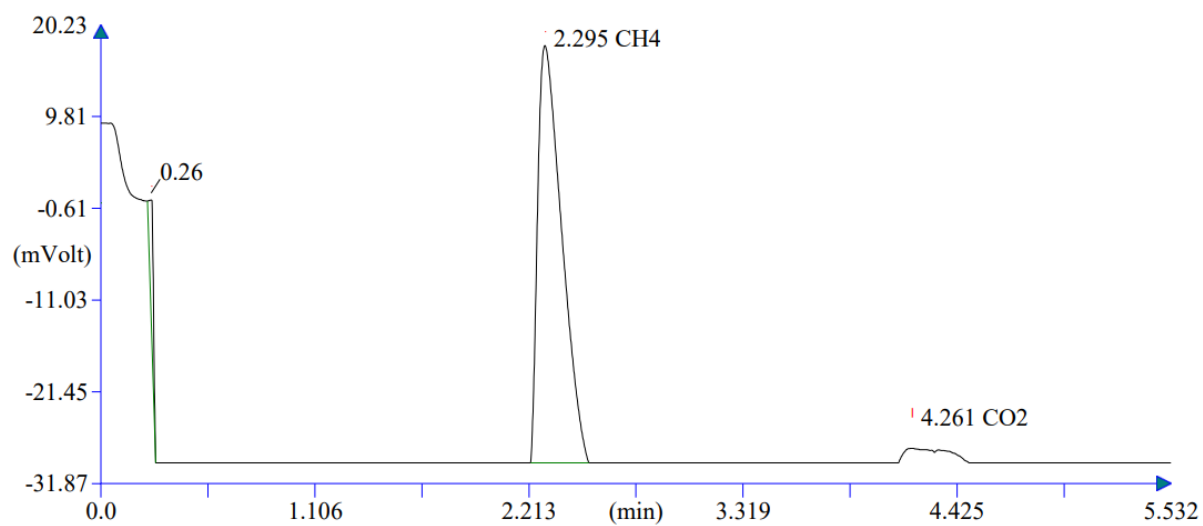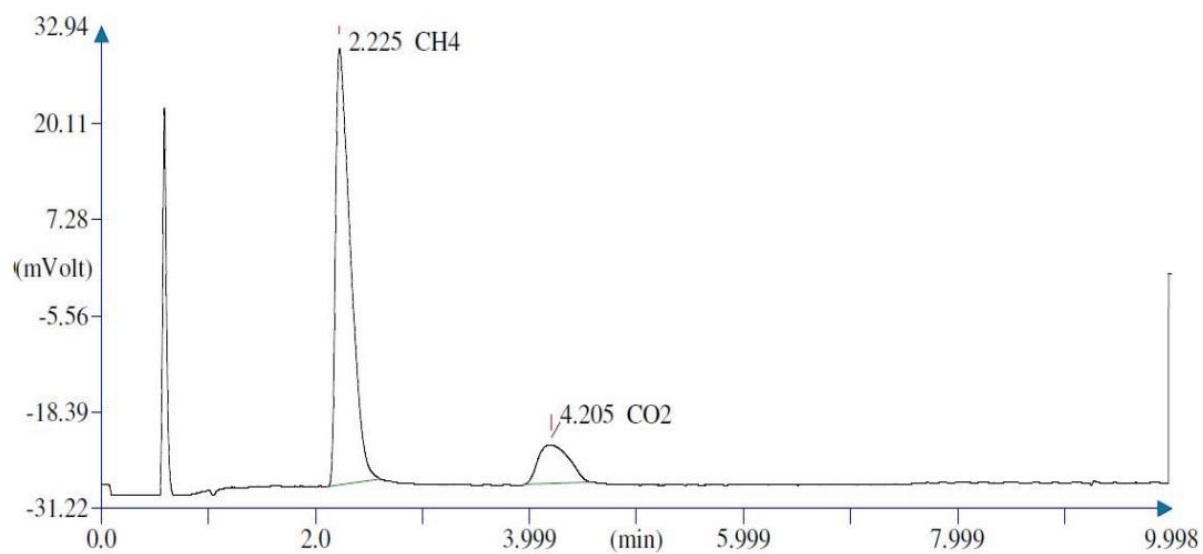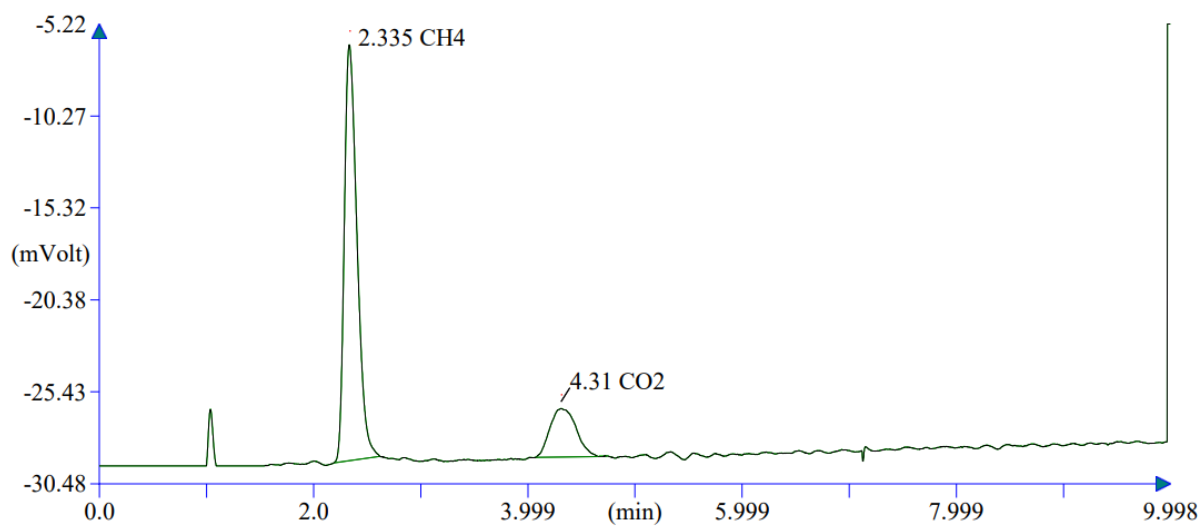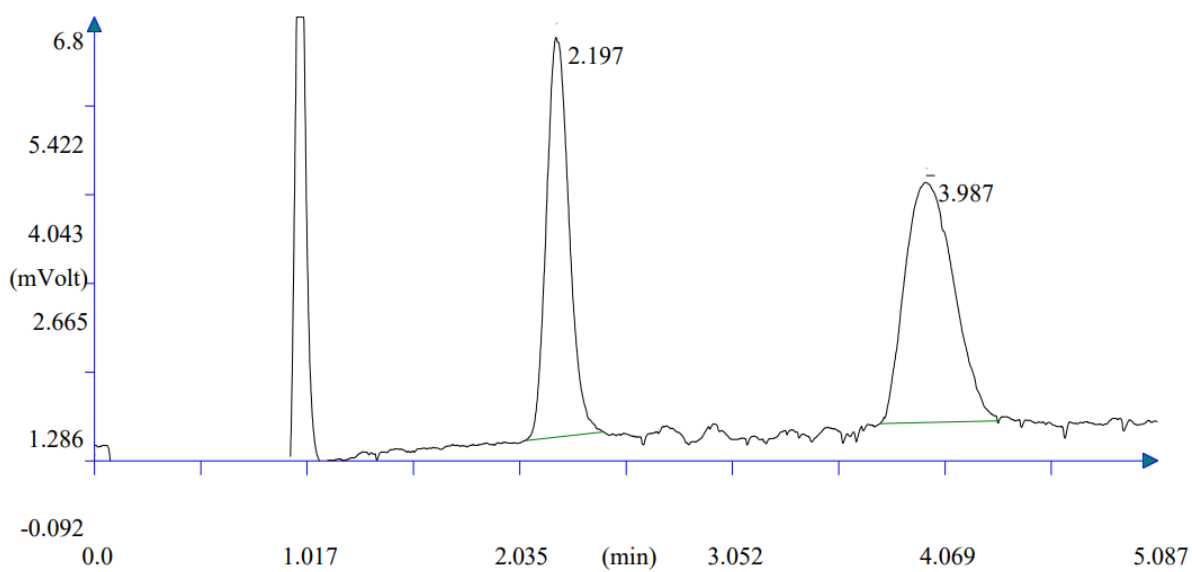Achaw, O.-W. (2012). "A study of the porosity of activated carbons using the scanning electron microscope." *Scan. Electron Microsc.*, 1–21.

Achinas, S., and Euverink, G. J. W. (2016). "Theoretical analysis of biogas potential prediction from agricultural waste." *Resour. Technol.*, 2(3), 143–147.

Achkar, J. H. El, Lendormi, T., Salameh, D., Louka, N., Maroun, R. G., Lanoisellé, J., and Hobaika, Z. (2018). "Influence of pretreatment conditions on lignocellulosic fractions and methane production from grape pomace." *Bioresour. Technol.*, 247, 881–889.

Adcock, T., Shah, V., Chen, M. J., and Meister, J. J. (2003). "Graft copolymers of lignin as hydrophobie agents for plastic (wood-filled) composites." *J. Appl. Polym. Sci.*, 89(5), 1266–1276.

Ahuja, D., Kaushik, A., and Singh, M. (2017). "Simultaneous extraction of lignin and cellulose anofibrils from waste jute bags using One Pot Pre-treatment." *Int. J. Biol. Macromol.*, 107, 1294–1301.

Alexandropoulou, M., Antonopoulou, G., Fragkou, E., Ntaikou, I., and Lyberatos, G. (2016). "Fungal pretreatment of willow sawdust and its combination with alkaline treatment for enhancing biogas production." *J. Environ. Manage.*, 203(2), 704–713.

Ali, S., Shah, T. A., Afzal, A., and Tabassum, R. (2018). "Exploring lignocellulosic biomass for bio-methane potential by anaerobic digestion and its economic feasibility." *Energy Environ.*, 29(5), 742–751.

Alvarado-morales, M., Tsapekos, P., Awais, M., Gulfraz, M., and Angelidaki, I. (2016). "TiO2/UV based photocatalytic pretreatment of wheat straw for biogas production." *Anaerobe*, 46(8), 155–161.

Ameri, A. A., Pourghasemi, H. R., and Cerda, A. (2018). "Erodibility prioritization of sub-watersheds using morphometric parameters analysis and its mapping: A comparison among TOPSIS, VIKOR, SAW, and CF multi-criteria decision making models." *Sci. Total Environ.*, 613–614, 1385–1400.

Amin, F. R., Khalid, H., Zhang, H., Rahman, S. u., Zhang, R., Liu, G., and Chen, C. (2017). "Pretreatment methods of lignocellulosic biomass for anaerobic digestion." *AMB Express*, 7(72), 1–12.

André, L., Pauss, A., and Ribeiro, T. (2018). "Solid anaerobic digestion : State-of-art , scienti fi c and technological hurdles." *Bioresour. Technol.*, 247(8), 1027–1037.

Appressi, L. (2014). "Biogas and bio-hydrogen : production and uses . A review." *Univ. Di Bol. Student Res. Man.*, 1–118.

Arni, S. Al. (2018). "Extraction and isolation methods for lignin separation from sugarcane bagasse : A review." *Ind. Crop. Prod.*, 115, 330–339.

Aroua, S., Lounis, A., Condom, S., and Semaoune, F. (2009). "Analysis of lignin isolated from alkaline leaching of Alfa grass." *Asian J. Chem.*, 21(3), 2293–2300.

Ashby, M. F. (2000). "Multi-objective optimization in material design and selection." *Acta Mater.*, 48, 359–369.

Astiaso, D., Sangiorgio, S., and Rosa, F. (2015). "Estimating the potential biomasses energy source of forest and agricultural residues in the Cinque Terre Italian National Park." *70th Conf. ATI Eng. Assoc. Estim.*, Elsevier B.V., 674–680.

Awasthi, S. K., Sarsaiya, S., Awasthi, M. K., Liu, T., Zhao, J., Kumar, S., and Zhang, Z. (2019). "Changes in global trends in food waste composting: Research challenges and opportunities." *Bioresour. Technol.*, 122555.

Ayeni, A. O., Adeeyo, O. A., Oresegun, O. M., and Oladimeji, E. (2015). "Compositional analysis of lignocellulosic materials: Evaluation of an economically viable method suitable for woody and non-woody biomass." *Am. J. Eng. Res.*, 4(4), 14–19.

Azubuike, C. C., Chikere, C. B., and Okpokwasili, G. C. (2016). "Bioremediation techniques–classification based on site of application: principles, advantages, limitations and prospects." *World J. Microbiol. Biotechnol.*, 32(11), 1–18.

Barua, V. B., Goud, V. V., and Kalamdhad, A. S. (2018). "Microbial Pretreatment of Water Hyacinth for Enhanced Hydrolysis followed by Biogas Production." *Renew.*

*Energy*, 126(10), 21–29.

Baruah, J., Nath, B. K., Sharma, R., Kumar, S., Deka, R. C., Baruah, D. C., and Kalita, E. (2018). "Recent Trends in the Pretreatment of Lignocellulosic Biomass for Value-Added Products." *Front. Energy Res.*, 6(December), 1–19.

Bazargan, A., Tan, J., and McKay, G. (2015). "Standardization of Oil Sorbent Performance Testing." *J. Test. Eval.*, 43(6), 20140227.

Beisl, S., Friedl, A., and Miltner, A. (2017). "Lignin from micro- To nanosize: Applications." *Int. J. Mol. Sci.*, 18(11).

Bertella, S., and Luterbacher, J. S. (2020). "Lignin Functionalization for the Production of Novel Materials." *Trends Chem.*, 2(5), 440–453.

Bhangale, P. P., Agrawal, V. P., and Saha, S. K. (2004). "Attribute based specification, comparison and selection of a robot." *Mech. Mach. Theory*, 39, 1345–1366.

Bhat, J. I., and Raghavendra, N. (2018). "An environmentally friendly approach towards mitigation of Al corrosion in hydrochloric acid by yellow colour ripe arecanut husk extract : Introducing potential and sustainable inhibitor for material protection." *J. Bio- Tribo-Corrosion*, 4(2), 1–12.

Borand, M. N., and Karaosmanoğlu, F. (2018). "Effects of organosolv pretreatment conditions for lignocellulosic biomass in biorefinery applications: A review." *J. Renew. Sustain. Energy*, 10, 033104.

British Petroleum Company. (2020). "Statistical Review of World Energy 2020." *London Br. Pet. Co.*, 69th editi, 68.

Brody, T. M., Bianca, P. Di, and Krysa, J. (2012). "Analysis of Inland Crude Oil Spill Threats, Vulnerabilities, and Emergency Response in the Midwest United States." *Risk Anal.*, 32(10), 1741–1749.

Broje, V., and Keller, A. A. (2006). "Improved mechanical oil spill recovery using an optimized geometry for the skimmer surface." *Environ. Sci. Technol.*, 40(24), 7914–7918.

Buswell, A. M., and Hatfield, W. D. (1980). "Dry anaerobic fermentation." *Biotechnol. Bioeng. Symp.*, 10, 43–65.

Capson-Tojo, G., Trably, E., Rouez, M., Crest, M., Steyer, J.-P., Delgenès, J.-P., and Escudié, R. (2017). "Dry anaerobic digestion of food waste and cardboard at different substrate loads, solid contents and co-digestion proportions." *Bioresour. Technol.*, 233, 166–175.

Carson, R. T., Mitchell, R. C., Hanemann, M., Kopp, R. J., Presser, S., and Ruud, P. A. (2003). "Contingent Valuation and Lost Passive Use: Damages from the Exxon Valdez Oil Spill." *Environ. Resour. Econ.*, 25(202), 257–286.

Carvajal, J. C., Gómez, Á., and Cardona, C. A. (2016). "Comparison of lignin extraction [1] J. C. Carvajal, Á. Gómez, and C. A. Cardona, 'Comparison of lignin extraction processes : Economic and environmental assessment,' Bioresour. Technol., vol. 214, pp. 468–476, 2016.processes : Economic and environmental a." *Bioresour. Technol.*, 214, 468–476.

Central electricity authority. (2020). *CEA annual report 2019-20. Gov. India, Minist. Power.*

Chaiyapong, P., and Chavalparit, O. (2016). "Enhancement of biogas production potential from Acacia leaf waste using alkaline pre-treatment and co-digestion." *J. Mater. Cycles Waste Manag.*, 18(3), 427–436.

Chakraborty, D., and Venkata Mohan, S. (2019). "Efficient resource valorization by co-digestion of food and vegetable waste using three stage integrated bioprocess." *Bioresour. Technol.*, 284(March), 373–380.

Chan, P. C., Toledo, R. A. De, and Shim, H. (2018). "Anaerobic co-digestion of food waste and domestic wastewater e Effect of intermittent feeding on short and long chain fatty acids accumulation." *Renew. Energy*, 124, 129–135.

Chen, C., Li, F., Zhang, Y., Wang, B., Fan, Y., Wang, X., and Sun, R. (2018). "Compressive, ultralight and fire-resistant lignin-modified graphene aerogels as recyclable absorbents for oil and organic solvents." *Chem. Eng. J.*, 350, 173–180.

Choong, Y. Y., Chou, K. W., and Norli, I. (2018). "Strategies for improving biogas production of palm oil mill effluent (POME) anaerobic digestion: A critical review." *Renew. Sustain. Energy Rev.*, 82(1), 2993–3006.

Cinelli, P., Anguillesi, I., and Lazzeri, A. (2013). "Green synthesis of flexible polyurethane foams from liquefied lignin." *Eur. Polym. J.*, 49(6), 1174–1184.

Cioabla, A. E., Ionel, I., Dumitrel, G.-A., and Popescu, F. (2012). "Comparative study on factors affecting anaerobic digestion of agricultural vegetal residues." *Biotechnol. Biofuels*, 5(39), 1–9.

Costa, A. G., Pinheiro, G. C., Pinheiro, F. G. C., Santos, A. B. Dos, Santaella, S. T., and Leitão, R. C. (2014). "The use of thermochemical pretreatments to improve the anaerobic biodegradability and biochemical methane potential of the sugarcane bagasse." *Chem. Eng. J.*, 248, 363–372.

Dahunsi, S. O. (2019). "Mechanical pretreatment of lignocelluloses for enhanced biogas production: Methane yield prediction from biomass structural components." *Bioresour. Technol.*, 280, 18–26.

Dai, B., and Dong, G. (2018). "Comparison of different pretreatments of rice straw substrate to improve biogas production." *Waste and Biomass Valorization*, 9, 1503–1512.

Deheri, C., and Acharya, S. K. (2021). "Effect of calcium peroxide and sodium hydroxide on hydrogen and methane generation during the co-digestion of food waste and cow dung." *J. Clean. Prod.*, 279, 123901.

Dell'Omo, P. P., and Spena, V. A. (2020). "Mechanical pretreatment of lignocellulosic biomass to improve biogas production: Comparison of results for giant reed and wheat straw." *Energy*, 203(2020), 117798.

Devatha, C. P., and Thalla, A. K. (2017). "Prioritizing cropping alternatives based on attribute specification and comparison using MADM models." *J. Saudi Soc. Agric. Sci.*

Dhanisetty, V. S. V., Verhagen, W. J. C., and Curran, R. (2017). "Multi-criteria

weighted decision making for operational maintenance processes." *J. Air Transp. Manag.*, 68(5), 152–164.

Dinh, P. V., Fujiwara, T., Phu, S. T. P., and Hoang, M. G. (2018). "Kinetic of biogas production in co-digestion of vegetable waste, horse dung, and sludge by batch reactors." *IOP Conf. Ser. Earth Environ. Sci.*, 1–9.

Dudek, M., Świechowski, K., Manczarski, P., Koziel, J. A., and Białowiec, A. (2019). "The effect of biochar addition on the biogas production kinetics from the anaerobic digestion of brewers' spent grain." *Energies*, 12(8), 1–22.

Dutra, E. D., Santos, F. A., Ribeiro, B., Alencar, A., Libanio, A., and Reis, S. (2018). "Alkaline hydrogen peroxide pretreatment of lignocellulosic biomass : status and perspectives." 225–234.

Edwiges, T., Bastos, J. A., Alino, J. H. L., D'avila, L., Frare, L. M., and Somer, J. G. (2019). "Comparison of various pretreatment techniques to enhance biodegradability of lignocellulosic biomass for methane production." *J. Environ. Chem. Eng.*, 7(6), 103495.

Elliott, A., and Mahmood, T. (2007). "Pretreatment technologies for advancing anaerobic digestion of pulp and paper biotreatment residues." *Water Res.*, 41(19), 4273–4286.

Elsayed, M., Blel, W., Soliman, M., Andres, Y., and Hassan, R. (2021). "Semi-continuous co-digestion of sludge, fallen leaves, and grass performance." *Energy*, 221, 119888.

Ethaib, S., Omar, R., Kamal, S. M. M., and Radiah, D. (2018). "Microwave-assisted pretreatment of lignocellulosic biomass : A review." *J. Eng. Sci. Technol.*, (Special issue on SOMCHE 2014 & RSCE 2014 Conference), 97–109.

Ewis, D., Benamor, A., Ba-Abbad, M. M., Nasser, M., El-Naas, M., and Qiblawey, H. (2020). "Removal of Oil Content from Oil-Water Emulsions Using Iron Oxide/Bentonite Nano Adsorbents." *J. Water Process Eng.*, 38(July), 101583.

Felix, L. C., Ede, J. D., Snell, D. A., Oliveira, T. M., Martinez-Rubi, Y., Simard, B.,

Luong, J. H. T., and Goss, G. G. (2016). "Physicochemical properties of functionalized carbon-based nanomaterials and their toxicity to fishes." *Carbon N. Y.*, 104, 78–89.

Fenoll, J., Garrido, I., Pastor-Belda, M., Campillo, N., Viñas, P., Yañez, M. J., Vela, N., and Navarro, S. (2017). "Solar detoxification of water polluted with fungicide residues using ZnO-coated magnetic particles." *Chem. Eng. J.*, 330(July), 71–81.

Ge, J., Zhao, H. Y., Zhu, H. W., Huang, J., Shi, L. A., and Yu, S. H. (2016). "Advanced sorbents for oil-spill cleanup: Recent advances and future perspectives." *Adv. Mater.*, 28(47), 10459–10490.

Gonzalez-estrella, J., Asato, C. M., Stone, J. J., and Gilcrease, P. C. (2017). "A review of anaerobic digestion of paper and paper board waste." *Rev. Environ. Sci. Bio/Technology*, 16(3), 569–590.

Guo, J., Wang, W., Liu, X., Lian, S., and Zheng, L. (2014). "Effects of thermal pre-treatment on anaerobic co-digestion of municipal biowastes at high organic loading rate." *Chemosphere*, 101, 66–70.

Gupta, A. K., Mohanty, S., and Nayak, S. K. (2014). "Synthesis, Characterization and Application of Lignin Nanoparticles (LNPs)." *Mater. Focus*, 3(6), 444–454.

Gupta, S., and Tai, N. H. (2016). "Carbon materials as oil sorbents: A review on the synthesis and performance." *J. Mater. Chem. A*, 4(5), 1550–1565.

Haider, M. R., Zeshan, Yousaf, S., Malik, R. N., and Visvanathan, C. (2015). "Effect of mixing ratio of food waste and rice husk co-digestion and substrate to inoculum ratio on biogas production." *Bioresour. Technol.*, 190, 451–457.

Hamzah, M. H., Bowra, S., and Cox, P. (2020). "Effects of ethanol concentration on organosolv lignin precipitation and aggregation from Miscanthus x giganteus." *Processes*, 8(7).

Harikishore Kumar Reddy, D., Vijayaraghavan, K., Kim, J. A., and Yun, Y. S. (2017). "Valorisation of post-sorption materials: Opportunities, strategies, and challenges." *Adv. Colloid Interface Sci.*, 242, 35–58.

Hendriks, A. T. W. M., and Zeeman, G. (2009). "Pretreatments to enhance the digestibility of lignocellulosic biomass." *Bioresour. Technol.*, 100, 10–18.

Hu, Y., Hao, X., Wang, J., and Cao, Y. (2016). "Enhancing anaerobic digestion of lignocellulosic materials in excess sludge by bioaugmentation and pre-treatment." *Waste Manag.*, 49, 55–63.

Hussain, S., and Yakimova, R. (2008). "Investigation of structural and optical properties of nanocrystalline ZnO." *Dep. Physics, Chem. Biol. Linkopings Univ.*

Inam, E., Etim, U. J., Akpabio, E. G., and Umoren, S. A. (2017). "Process optimization for the application of carbon from plantain peels in dye abstraction." *J. Taibah Univ. Sci.*, 11(1), 173–185.

Jaberi, F. Y. Al, Jabbar, S. M., and Jabbar, N. M. (2020). "Modeling of adsorption isotherms of oil content through the electrocoagulation treatment of real oily wastewater." *AIP Conf. Proc.*, 1–9.

Jain, S., Jain, S., Wolf, I. T., Lee, J., and Tong, Y. W. (2015). "A comprehensive review on operating parameters and different pretreatment methodologies for anaerobic digestion of municipal solid waste." *Renew. Sustain. Energy Rev.*, 52, 142–154.

Jameel, A. G. A. (2019). "A functional group approach for predicting fuel properties."

Jiao, J., Gai, Q. Y., Fu, Y.-J., Zu, Y.-G., Luo, M., Wang, W., Zhao, C.-J., Gu, C.-B., and Li, J. (2012). "Application of white-rot fungi treated Fructus forsythiae shell residue as a low-cost biosorbent to enrich forsythiaside and phillygenin." *Chem. Eng. Sci.*, 74, 244–255.

Jönsson, L. J., and Martín, C. (2015). "Pretreatment of lignocellulose : Formation of inhibitory by-products and strategies for minimizing their effects." *Bioresour. Technol.*, 199, 103–122.

Julie Chandra, C. S., George, N., and Narayanankutty, S. K. (2016). "Isolation and characterization of cellulose nanofibrils from arecanut husk fibre." *Carbohydr. Polym.*, 142, 158–166.

Kafle, G. K., Kim, S. H., and Sung, K. I. (2013). "Ensiling of fish industry waste for biogas production: A lab scale evaluation of biochemical methane potential (BMP) and kinetics." *Bioresour. Technol.*, 127, 326–336.

Kainthola, J., Kalamdhad, A. S., and Goud, V. V. (2019). "Enhanced methane production from anaerobic co-digestion of rice straw and hydrilla verticillata and its kinetic analysis." *Biomass and Bioenergy*, 125(04), 8–16.

Kalyani, D. C., Zamanzadeh, M., Müller, G., and Horn, S. J. (2017). "Biofuel production from birch wood by combining high solid loading simultaneous saccharification and fermentation and anaerobic digestion." *Appl. Energy*, 193, 210–219.

Karki, R., Chuenchart, W., Surendra, K. C., Shrestha, S., Raskin, L., Sung, S., Hashimoto, A., and Kumar Khanal, S. (2021). "Anaerobic co-digestion: Current status and perspectives." *Bioresour. Technol.*, 330(March), 125001.

Kaur, K., and Phutela, U. G. (2016a). "Enhancement of paddy straw digestibility and biogas production by sodium hydroxide-microwave pretreatment." *Renew. Energy*, 92, 178–184.

Kaur, K., and Phutela, U. G. (2016b). "Sodium carbonate pretreatment: an approach towards desilication of paddy straw and enhancement in biogas production." *Paddy Water Environ.*, 14, 113–121.

Khalifa, R. E., Omer, A. M., Tamer, T. M., Ali, A. A., Ammar, Y. A., and Eldin, M. M. S. (2019). "Efficient eco-friendly crude oil adsorptive chitosan derivatives: Kinetics, equilibrium and thermodynamic studies." *Desalin. Water Treat.*, 1–13.

Khatri, S., Wu, S., Kizito, S., Zhang, W., Li, J., and Dong, R. (2015). "Synergistic effect of alkaline pretreatment and Fe dosing on batch anaerobic digestion of maize straw." *Appl. Energy*, 158, 55–64.

Kim, D., Kim, J., and Lee, C. (2018). "Effect of mild-temperature thermo-alkaline pretreatment on the solubilization and anaerobic digestion of spent coffee grounds." *Energies*, 11(865), 1–14.

Krishania, M., Vijay, V. K., and Chandra, R. (2013). "Methane fermentation and kinetics of wheat straw pretreated substrates co-digested with cattle manure in batch assay." *Energy*, 57(08), 359–367.

Kruk, M., and Jaroniec, M. (2001). "Gas adsorption characterization of ordered organic-inorganic nanocomposite materials." *Chem. Mater.*, 13(10), 3169–3183.

Kumar, A., Kumar, N., Baredar, P., and Shukla, A. (2015a). "A review on biomass energy resources, potential, conversion and policy in India." *Renew. Sustain. Energy Rev.*, 45, 530–539.

Kumar, P., Vijay, V., Thalla, A. K., Dhar, H., and Kumar, S. (2015b). "Methane Production From Anaerobic Digestion of Oragnic Fraction in Municipal Solid Waste." *Proc. Int. Conf. Sustain. Energy Built Environ.*, (March), 677–682.

Kumar, P., Vijay, V., Thalla, A. K., Dhar, H., and Kumar, S. (2015c). "Methane production from anaerobic digestion of organic fraction in municipal solid waste." *Proc. Int. Conf. Sustain. Energy Built Environ.*, 677–682.

Kumar, S., Gandhi, P., Yadav, M., Paritosh, K., Pareek, N., and Vivekanand, V. (2019). "Weak alkaline treatment of wheat and pearl millet straw for enhanced biogas production and its economic analysis." *Renew. Energy*, 139(08), 753–764.

Kumar, V., Singh, J., Nadeem, M., Kumar, P., and Pathak, V. V. (2020). "Experimental and Kinetics Studies for Biogas Production Using Water Hyacinth (Eichhornia crassipes [Mart.] Solms) and Sugar Mill Effluent." *Waste and Biomass Valorization*, 11(1), 109–119.

Laghari, S. M., Isa, M. H., and Laghari, A. J. (2016). "Delignification of palm fiber by microwave assisted chemical pretreatment for improving energy efficiency." *Malaysian J. Sci.*, 35(1), 8–14.

Lazim, Y., Salit, S. M., Zainudin, E. S., Mustapha, M., and Jawaid, M. (2014). "Effect of alkali treatment on the physical, mechanical, and morphological properties of waste betel nut (Areca catechu) husk fibre." *BioResources*, 9(4), 7721–7736.

Li, C., Zhao, X., Wang, A., Huber, G. W., and Zhang, T. (2015a). "Catalytic

Transformation of Lignin for the Production of Chemicals and Fuels." *Chem. Rev.*, 115(21), 11559–11624.

Li, D., Liu, S., Mi, L., Li, Z., Yuan, Y., Yan, Z., and Liu, X. (2015b). "Effects of feedstock ratio and organic loading rate on the anaerobic mesophilic co-digestion of rice straw and cow manure." *Bioresour. Technol.*, 189, 319–326.

Li, J., Jha, A. K., and Bajracharya, T. R. (2014). "Dry Anaerobic Co-digestion of Cow Dung with Pig Manure for Methane Production." *Appl Biochem Biotechnol*, 173, 1537–1552.

Liew, L. N., Shi, J., and Li, Y. (2011). "Enhancing the solid-state anaerobic digestion of fallen leaves through simultaneous alkaline treatment." *Bioresour. Technol.*, 102, 8828–8834.

López González, L. M., Vervaeren, H., Pereda Reyes, I., Dumoulin, A., Romero Romero, O., and Dewulf, J. (2013). "Thermo-chemical pre-treatment to solubilize and improve anaerobic biodegradability of press mud." *Bioresour. Technol.*

Lopez Torres, M., and Llorens, M. del C. E. (2008). "Effect of alkaline pretreatment on anaerobic digestion of solid wastes." *Waste Manag.*, 28, 2229–2234.

Lv, N., Wang, X., Peng, S., Zhang, H., and Luo, L. (2018). "Study of the Kinetics and Equilibrium of the Adsorption of Oils onto Hydrophobic Jute Fiber Modified via the Sol-Gel Method." *Int. J. Environ. Res. Public Health*, 15(969), 1–14.

Mancini, G., Papirio, S., Lens, P. N. L., and Esposito, G. (2018). "Increased biogas production from wheat straw by chemical pretreatments." *Renew. Energy*, 119, 608–614.

Mata-alvarez, J., Dosta, J., Macé, S., and Astals, S. (2011). "Codigestion of solid wastes : A review of its uses and perspectives including modeling." 31(1), 99–111.

Matsakas, L., Gao, Q., Jansson, S., Rova, U., and Christakopoulos, P. (2017). "Green conversion of municipal solid wastes into fuels and chemicals." *Electron. J. Biotechnol.*, 26, 69–83.

Michalska, K., and Ledakowicz, S. (2013). "Alkali pre-treatment of Sorghum Moench

for biogas production." *Chem. Pap.*, 67(9), 1130–1137.

Michalska, K., and Ledakowicz, S. (2014). "Alkaline hydrogen peroxide pretreatment of energy crops for biogas production." *Chem. Pap.*, 68(7), 913–922.

Ministry of Agriculture & Farmers Welfare. (2019). *Horticultural Statistics at a Glance 2018*.

Misi, S. N., and Forster, C. F. (2001). "Batch co-digestion of multi-component agro-wastes." 80(April).

Molefe, F. V., Koao, L. F., Dejene, B. F., and Swart, H. C. (2015). "Phase formation of hexagonal wurtzite ZnO through decomposition of Zn(OH)2 at various growth temperatures using CBD method." *Opt. Mater. (Amst).*, 46, 292–298.

Molino, A., Nanna, F., Ding, Y., Bikson, B., and Braccio, G. (2013). "Biomethane production by anaerobic digestion of organic waste." *Fuel*, 103, 1003–1009.

Monlau, F., Barakat, A., Steyer, J. P., and Carrere, H. (2012). "Comparison of seven types of thermo-chemical pretreatments on the structural features and anaerobic digestion of sunflower stalks." *Bioresour. Technol.*, 120, 241–247.

Mousavi-nasab, S. H., and Sotoudeh-Anvari, A. (2018). "A new multi-criteria decision making approach for sustainable." *J. Clean. Prod.*, 182, 466–484.

Mustafa, A. M., Li, H., Radwan, A. A., Sheng, K., and Chen, X. (2018). "Effect of hydrothermal and Ca(OH)2 pretreatments on anaerobic digestion of sugarcane bagasse for biogas production." *Bioresour. Technol.*

Nagaraja, R., Gurumurthy, B. R., Shivanna, M. B., and Assistant, P. (2014). "BIO SOFTENING OF ARECANUT WASTE ARECA HUSK , LEAF AND LEAF SHEATH FOR VALUE ADDED COMPOST." 2(9), 105–112.

Noonari, A. A., Mahar, R. B., Sahito, A. R., and Brohi, K. . M. (2017). "Optimization of methane production from rice straw and buffalo dung by H2O2 and Ca(OH)2: pretreatments and its kinetics." *Waste and Biomass Valorization*, 10(4), 899–908.

Nozari, B., and Mirmohamadsadeghi, S. (2018). "Bioenergy production from sweet sorghum stalks via a biorefinery perspective." 3425–3438.

Ojala, J., Sirviö, J. A., and Liimatainen, H. (2018). "Preparation of cellulose nanocrystals from lignin-rich reject material for oil emulsification in an aqueous environment." *Cellulose*, 25(1), 293–304.

Oribayo, O., Feng, X., Rempel, G. L., and Pan, Q. (2017). "Synthesis of lignin-based polyurethane / graphene oxide foam and its application as an absorbent for oil spill clean-ups and recovery." 323, 191–202.

Pan, B., and Xing, B. (2008). "Adsorption mechanisms of organic chemicals on carbon nanotubes." *Environ. Sci. Technol.*, 42(24), 9005–9013.

Patowary, D., and Baruah, D. C. (2018). "Effect of combined chemical and thermal pretreatments on biogas production from lignocellulosic biomasses." *Ind. Crop. Prod.*, 124, 735–746.

Pellera, F., and Gidarakos, E. (2017). "Chemical pretreatment of lignocellulosic agroindustrial waste for methane production." *Waste Manag.*, 71(1), 689–703.

Pellera, F., Santori, S., Pomi, R., Polettini, A., and Gidarakos, E. (2016). "Effect of alkaline pretreatment on anaerobic digestion of olive mill solid waste." *Waste Manag.*, 58, 160–168.

Pereira, M., Beck, P. H., Muller, D. G., Moreira, J. B., Silva, J. S. da, and Durigon, A. M. M. (2016). "Extraction of Organosolv Lignin from Rice Husk under Reflux Conditions." *Biol. Chem. Res.*, (March 2018), 87–98.

Perendeci, N. A., Gökgöl, S., and Orhon, D. (2018). "Impact of alkaline H2O2 pretreatment on methane generation potential of greenhouse crop waste under anaerobic conditions." *Molecules*, 23(1794), 1–17.

Pérez-rodríguez, N., García-bernet, D., and Domínguez, J. M. (2016). "Effects of enzymatic hydrolysis and ultrasounds pretreatments on corn cob and vine trimming shoots for biogas production." *Bioresour. Technol.*, 221, 130–138.

Pohekar, S. D., and Ramachandran, M. (2004). "Application of multi-criteria decision making to sustainable energy planning — A review." *Renew. Sustain. Energy Rev.*, 8, 365–381.

Prasad, S., Singh, A., and Joshi, H. C. (2007). "Ethanol as an alternative fuel from agricultural , industrial and urban residues." *Resour. Conserv. Recycl.*, 50, 1–39.

Priyanka, M., and Saravanakumar, M. P. (2018). "Ultrahigh adsorption capacity of starch derived zinc based carbon foam for adsorption of toxic dyes and its preliminary investigation on oil-water separation." *J. Clean. Prod. J.*, 197, 511–524.

Qu, J., Han, Q., Gao, F., and Qiu, J. (2017). "Carbon foams produced from lignin-phenol-formaldehyde resin for oil/water separation." *New Carbon Mater.*, 32(1), 86–91.

Rabii, A., Aldin, S., Dahman, Y., and Elbeshbishy, E. (2019). "A review on anaerobic co-digestion with a focus on the microbial populations and the effect of multi-stage digester configuration." *Energies*, 12(6).

Ramesh, S., Sundararaju, P., Sara, K., Banu, P., and Karthikeyan, S. (2018). "Hydrothermal carbonization of arecanut husk biomass : fuel properties and sorption of metals." *Environ. Sci. Pollut. Res.*, 26(4), 3751–3761.

Rao, G. S., Nabipour, H., Zhang, P., Wang, X., Xing, W., Song, L., and Hu, Y. (2020). "Lightweight, hydrophobic and recyclable carbon foam derived from lignin–resorcinol–glyoxal resin for oil and solvent spill capture." *J. Mater. Res. Technol.*, 9(3), 4655–4664.

Rao, P. V., and Baral, S. S. (2011). "Attribute based specification, comparison and selection of feed stock for anaerobic digestion using MADM approach." *J. Hazard. Mater.*, 186, 2009–2016.

Rao, R. V., and Davim, J. P. (2008). "A decision-making framework model for material selection using a combined multiple attribute decision-making method." *Int. J. Adv. Manuf. Technol.*, 35(7–8), 751–760.

Raposo, F., Fernández-Cegrí, V., la Rubia, M. A. de, Borja, R., Béline, F., Cavinato, C., Demirer, G., Fernández, B., Fernández-Polanco, M., Frigon, J. C., Ganesh, R., Kaparaju, P., Koubova, J., Méndez, R., Menin, G., Peene, A., Scherer, P., Torrijos, M., Uellendahl, H., Wierinck, I., and Wilde, V. de. (2011). "Biochemical methane potential (BMP) of solid organic substrates: Evaluation of anaerobic biodegradability

using data from an international interlaboratory study." *J. Chem. Technol. Biotechnol.*, 86(8), 1088–1098.

Rashid, T., Gnanasundaram, N., Appusamy, A., and Fai, C. (2018a). "Enhanced lignin extraction from different species of oil palm biomass: Kinetics and optimization of extraction conditions." *Ind. Crop. Prod.*, 116, 122–136.

Rashid, T., Gnanasundaram, N., Appusamy, A., Kait, C. F., and Thanabalan, M. (2018b). "Enhanced lignin extraction from different species of oil palm biomass: Kinetics and optimization of extraction conditions." *Ind. Crops Prod.*, 116(February), 122–136.

Saaty, T. L. (2008). "Decision making with the analytic hierarchy process." *Int. J. Serv. Sci.*, 1(1), 83–98.

Sabaghi, M., Mascle, C., and Baptiste, P. (2015). "Application of DOE-TOPSIS Technique in Decision-Making Problems." *Int. Fed. Autom. Control*, 773–777.

Sadasivuni, S., Bhat, R., and Pallem, C. (2016). "Recycling potential of organic wastes of arecanut and cocoa in India : a short review." 2515(January).

Samuel J., Lohit Kumar S, G., and B, R. (2017). "Kinetic modeling of mixed culture process of anaerobic co-digestion of vegetable wastes with pistia stratiotes: A scientific attempt on biomethanationy." *J. Microb. Biochem. Technol.*, 09(01), 554–566.

Santos, O. S. H., Coelho, M., Silva, V. R., Mussel, W. N., and Yoshida, M. I. (2017). "Polyurethane foam impregnated with lignin as a filler for the removal of crude oil from contaminated water." *J. Hazard. Mater.*, 324, 406–413.

Sarbatly, R., Krishnaiah, D., and Kamin, Z. (2016). "A review of polymer nanofibres by electrospinning and their application in oil/water separation for cleaning up marine oil spills." *Mar. Pollut. Bull.*

Sayara, T., and Sánchez, A. (2019). "A review on anaerobic digestion of lignocellulosic wastes: Pretreatments and operational conditions." *Appl. Sci.*, 9(21).

Sen, P., and Yang, J.-B. (1998). "MCDM and tbe Nature of Decision Making in

Design." *Mult. Criteria Decis. Support Eng. Des. Springer, London*, 13–20.

Shetty, D. J., Kshirsagar, P., Tapadia-maheshwari, S., Lanjekar, V., Singh, S. K., and Dhakephalkar, P. K. (2016). "Alkali pretreatment at ambient temperature: a promising method to enhance biomethanation of rice straw." *Bioresour. Technol.*, 226(12), 80–88.

Singh, D. P., and Trivedi, R. K. (2013). "Acid and alkaline pretreatment of lignocellulosic biomass to produce ethanol as biofuel." *Int. J. ChemTech Res.*, 5(2), 727–734.

Song, Z., Yang, G., Liu, X., Yan, Z., Yuan, Y., and Liao, Y. (2014). "Comparison of seven chemical pretreatments of corn straw for improving methane yield by anaerobic digestion." *PLoS One*, 9(4), 1–8.

Stamatelatou, K., Antonopoulou, G., and Michailides, P. (2014). *Biomethane and biohydrogen production via anaerobic digestion/fermentation. Adv. Biorefineries Biomass Waste Supply Chain Exploit.*

Sun, R. C., Tomkinson, J., and Lloyd Jones, G. (2000). "Fractional characterization of ash-AQ lignin by successive extraction with organic solvents from oil palm EFB fibre." *Polym. Degrad. Stab.*, 68(1), 111–119.

Tan, R. R., Aviso, K. B., Huelgas, A. P., and Promentilla, M. A. B. (2013). "Fuzzy AHP approach to selection problems in process engineering involving quantitative and qualitative aspects." *Process Saf. Environ. Prot.*, 92(5), 467–475.

Tansel, Y. (2012). "An experimental design approach using TOPSIS method for the selection of computer-integrated manufacturing technologies." *Robot. Comput. Integr. Manuf.*, 28(2), 245–256.

Tansel Yusuf. (2014). "A TOPSIS based design of experiment approach to assess company ranking." *Appl. Math. Comput.*, 227, 630–647.

Tejado, A., Peña, C., Labidi, J., Echeverria, J. M., and Mondragon, I. (2007). "Physico-chemical characterization of lignins from different sources for use in phenol-formaldehyde resin synthesis." *Bioresour. Technol.*, 98(8), 1655–1663.

Thalla, A. K., Bhargava, R., and Kumar, P. (2010). "Nitrification kinetics of activated sludge-biofilm system: A mathematical model." *Bioresour. Technol.*, 101(15), 5827–5835.

Tian, D., Hu, J., Bao, J., Chandra, R. P., Saddler, J. N., and Lu, C. (2017). "Lignin valorization: Lignin nanoparticles as high-value bio-additive for multifunctional nanocomposites." *Biotechnol. Biofuels*, 10(1), 1–11.

Tsapekos, P., Kougias, P. G., Frison, A., Raga, R., and Angelidaki, I. (2016). "Improving methane production from digested manure biofibers by mechanical and thermal alkaline pretreatment." *Bioresour. Technol.*, 216(9), 545–552.

Ulfa, M., Setiawan, L. P., and Setyaningrum, A. (2017). "Synthesis and characterization of Carbon Foam from Gelatin (CFG)." *Orient. J. Chem.*, 33(2), 829–834.

Uma, S., Thalla, A. K., and Devatha, C. P. (2018). "Co-digestion of Food Waste and Switchgrass for Biogas Potential: Effects of Process Parameters." *Waste and Biomass Valorization*, 1–13.

Upadhyay, A. K., and Sahu, R. (2012). "Determination of Total Nitrogen in Soil and Plant." *CAFT Adv. Agro-technologies Improv. Soil, Plant Atmos. Syst.*, 18–19.

Vasco-correa, J., Khanal, S., Manandhar, A., and Shah, A. (2018). "Anaerobic digestion for bioenergy production: Global status, environmental and techno-economic implications, and government policies." *Bioresour. Technol.*, 247, 1015–1026.

Vasmara, C., Cianchetta, S., Marchetti, R., and Galletti, S. (2017). "Biogas production from wheat straw pre-treated with hydrolytic enzymes or sodium hydroxide." *Environ. Eng. Manag. J.*, 16(8), 1827–1835.

Veluchamy, C., and Kalamdhad, A. S. (2017). "Influence of pretreatment techniques on anaerobic digestion of pulp and paper mill sludge : A review." *Bioresour. Technol.*, 245(6), 1206–1219.

Venturin, B., Frumi Camargo, A., Scapini, T., Mulinari, J., Bonatto, C., Bazoti, S.,

Pereira Siqueira, D., Maria Colla, L., Alves, S. L., Paulo Bender, J., Luís Radis Steinmetz, R., Kunz, A., Fongaro, G., and Treichel, H. (2018). "Effect of pretreatments on corn stalk chemical properties for biogas production purposes." *Bioresour. Technol.*, 266, 116–124.

Wang, C., O'Connell, M. J., and Chan, C. K. (2015). "Facile one-pot synthesis of highly porous carbon foams for high-performance supercapacitors using template-free direct pyrolysis." *ACS Appl. Mater. Interfaces*, 7(16), 8952–8960.

Wang, P., Meng, P., Zhai, J., and Zhu, Z. (2013). "A hybrid method using experiment design and grey relational analysis for multiple criteria decision making problems." *Knowledge-Based Syst.*, 53, 100–107.

Ward-Doria, M., Arzuaga-Garrido, J., Ojeda, K. A., and Sánchez, E. (2016). "Production of biogas from acid and alkaline pretreated cocoa pod husk (Theobroma cacao l.)." *Int. J. ChemTech Res.*, 9(11), 252–260.

Ware, A., and Power, N. (2017). "Modelling methane production kinetics of complex poultry slaughterhouse wastes using sigmoidal growth functions." *Renew. Energy*, 104, 50–59.

Watkins, D., Nuruddin, M., Hosur, M., Tcherbi-Narteh, A., and Jeelani, S. (2015). "Extraction and characterization of lignin from different biomass resources." *J. Mater. Res. Technol.*, 4(1), 26–32.

Wu, R. L., Wang, X. L., Li, F., Li, H. Z., and Wang, Y. Z. (2009). "Green composite films prepared from cellulose, starch and lignin in room-temperature ionic liquid." *Bioresour. Technol.*, 100(9), 2569–2574.

Xie, S., Frost, J. P., Lawlor, P. G., Wu, G., and Zhan, X. (2011). "Effects of thermo-chemical pre-treatment of grass silage on methane production by anaerobic digestion." *Bioresour. Technol.*, 102(2011), 8748–8755.

Xie, Y., Hu, Q., Feng, G., Jiang, X., Hu, J., He, M., Hu, G., Zhao, S., Liang, Y., Ruan, Z., and Peng, N. (2018). "Biodetoxification of Phenolic Inhibitors from Lignocellulose Pretreatment using Kurthia huakuii LAM0618T and Subsequent Lactic Acid Fermentation." *Molecules*, 23(2626), 1–17.

Yang, H., Yan, R., Chen, H., Lee, D. H., and Zheng, C. (2007). "Characteristics of hemicellulose, cellulose and lignin pyrolysis." *Fuel*, 86(12–13), 1781–1788.

Yong, Z., Dong, Y., Zhang, X., and Tan, T. (2015). "Anaerobic co-digestion of food waste and straw for biogas production." *Renew. Energy*, 78, 527–530.

Yu, Q., Sun, C., Liu, R., Yellezuome, D., Zhu, X., Bai, R., Liu, M., and Sun, M. (2021). "Anaerobic co-digestion of corn stover and chicken manure using continuous stirred tank reactor: The effect of biochar addition and urea pretreatment." *Bioresour. Technol.*, 319(August 2020), 124197.

Yunqin, L., Dehan, W., Shaoquan, W., and Chunmin, W. (2010). "Alkali pretreatment enhances biogas production in the anaerobic digestion of pulp and paper sludge." *Waste Manag. Res.*, 170, 366–373.

Zakzeski, J., Bruijnincx, P. C. A., Jongerius, A. L., and Weckhuysen, B. M. (2010). "The catalytic valorization of lignin for the production of renewable chemicals." *Chem. Rev.*, 110(6), 3552–3599.

Zaman, U. K. U., Rivette, M., Siadat, A., and Mousavi, S. M. (2018). "Integrated product-process design : Material and manufacturing process selection for additive manufacturing using multi-criteria decision making." *Robot. Comput. Integr. Manuf.*, 51, 169–180.

Zan, F., and Hao, T. (2020). "Sulfate in anaerobic co-digester accelerates methane production from food waste and waste activated sludge." *Bioresour. Technol.*, 298(September 2019), 122536.

Zhang, J., Loh, K. C., Lee, J., Wang, C. H., Dai, Y., and Wah Tong, Y. (2017). "Three-stage anaerobic co-digestion of food waste and horse manure." *Sci. Rep.*, 7(1), 1–10.

Zhang, N., Qi, Y., Zhang, Y., Luo, J., Cui, P., and Jiang, W. (2020). "A review on oil/water mixture separation material." *Ind. Eng. Chem. Res.*, 59(33), 14546–14568.

Zhang, W., Zhang, L., and Li, A. (2015). "Anaerobic co-digestion of food waste with MSW incineration plant fresh leachate : process performance and synergistic effects."

*Chem. Eng. J.*, 259, 795–805.

Zheng, Y., Zhao, J., Xu, F., and Li, Y. (2014). "Pretreatment of lignocellulosic biomass for enhanced biogas production." *Prog. Energy Combust. Sci.*, 42(6), 35–53.

Zieminski, K., Romanowska, I., Kowalska-wentel, M., and Cyran, M. (2014). "Effects of hydrothermal pretreatment of sugar beet pulp for methane production." *Bioresour. Technol.*, 166, 187–193.

NATIONAL INSTITUTE OF TECHNOLOGY KARNATAKA, SURATHKAL

----------------------------------------------------------------

**List of Publications based on PhD Research Work**

| S. No. | Title of the paper | **Authors** (in the same order as in the paper. Underline the Research Scholar's name) | **Name of the Journal/ Conference/ Symposium, Vol., No., Pages** | **Month & Year of Publication** | **Category \*** |
|---|---|---|---|---|---|
| 1 | Synthesis and characterization of robust ultralight-weight, excellent hydrophobic, fire retardant biomass-derived lignin-carbon foam for the oil-water separation | Adhirashree Vannarath, Arun Kumar Thalla | Journal of cleaner production, Vol 325, 129263 (**Elsevier**)) | November 2021 | 1 |
| 2 | Evaluation, ranking, and selection of pretreatment methods for the conversion of biomass to biogas using multi-criteria decision-making approach | Adhirashree Vannarath, Arun Kumar Thalla | Environment Systems and Decisions, 40, 510–525. (**Springer**) | November 2019 | 1 |
| 3 | Experimental investigations on the effects of chemical pretreatment on Arecanut husk (*Areca catechu*) for biogas production: Its solubilization, digestion, and kinetics | Adhirashree Vannarath, Arun Kumar Thalla | Biomass and Bioenergy (**Elsevier**) (Resubmitted to the Journal) | - | 1 |
| 4 | Effect of feedstock mix ratio on anaerobic co-digestion of arecanut husk with food waste for enhanced production of biogas | Adhirashree Vannarath, Arun Kumar Thalla | Environmental science and pollution research (**Springer**) (communicated) | **-** | 1 |
| 5 | Batch mode anaerobic co-digestion of food waste and arecanut husk for enhanced biogas production | Adhirashree Vannarath, Arun Kumar Thalla | 8th International engineering symposium (IES) 2019, Kumamoto University, Japan. | March 13-15, 2019 | 3 |
| 6 | Bifurcation of lignocellulosic biomass (*Areca catechu*) using alkaline pretreatment: An efficient method | Adhirashree Vannarath, Arun Kumar Thalla | HERAKLION 2019 7th International Conference on Sustainable Solid Waste Management, Greece | 26-29 June 2019 | 3 |

| 7 | Efficient bioconversion of lignocellulosic biomass into biohydrogen and biomethane: Impacts of diverse microbial community and the reactor configurations', | Adhirashree Vannarath, Arun Kumar Thalla | NCCE-NITK, NITK Surathkal. | 30-31 Jan 2020 | 3 |
|---|---|---|---|---|---|

\* Category: 1: Journal paper, full paper reviewed 2: Journal paper, Abstract reviewed 3: Conference/Symposium paper, full paper reviewed 4: Conference/Symposium paper, abstract reviewed 5: others (including papers in Workshops, NITK Research Bulletins, Short notes etc.)

04/01/2022

**Adhirashree V**

Research Scholar

Name & Signature, with Date

10/01/2022

**Dr. Arun Kumar Thalla**

Research Guide

Name & Signature, with Date